



**Politecnico
di Torino**

Tufts
UNIVERSITY

Politecnico di Torino

Corso di Laurea Magistrale in Ingegneria Biomedica

A.a. 2020/2021

Sessione di Laurea Ottobre 2021

**Dual-slope method for near-
infrared spectroscopy (NIRS):
in vivo applications to skeletal
muscles and brain**

Relatore:

Prof. Valentina Agostini

Candidata:

Martina Bottoni

Supervisor esterni:

Prof. Sergio Fantini

Prof. Angelo Sassaroli

Co-supervisor esterni:

Giles Blaney

Cristianne Fernandez

Abstract

Near-Infrared Spectroscopy (NIRS) is a non-invasive, portable, and cost-effective technique that is widely used in the biomedical field to investigate the hemodynamics and oxygenation levels of a variety of biological tissues. To achieve a penetration depth of centimeters, NIRS employs wavelengths in the near-infrared spectral region (typically 650-900 nm). However, non-invasive measurements performed with NIRS are affected by two common problems: (1) the strong sensitivity to hemodynamic contributions from superficial layers, which may confound the measurements of targeted hemodynamics in deeper tissue; (2) artifacts originating from instrumental effects and from subject movements, which may limit practical applicability and clinical use. Over time, different instrumental and methodological approaches have been proposed to address these problems and increasingly sophisticated systems have been introduced, moving from single distance (SD) to multi distances (MD) techniques, which are based on data collected at a single or multiple source-detector separations, respectively. A specific MD method, termed Dual Slope (DS) was proposed in the literature and recently further developed in our laboratory. Previous studies have shown the potential enhancement offered by the DS technique, compared to existing SD and MD methods, to the sensitivity to deep versus superficial tissue, and to minimize instrumental and motion artifacts. These works also demonstrated the implementation of DS methods combining frequency-domain (FD-NIRS), at two discrete wavelengths (690 and 830 nm), and broadband continuous-wave (CW-NIRS) over a wide range of wavelengths (~ 650-1000 nm), to generate quantitative absorption spectra of biological tissues for measuring the chromophores concentration.

This thesis is devoted to a further characterization of the DS technique of layered media, and its application to human subjects for measuring the hemodynamics in skeletal muscle and brain. First, a theoretical study based on diffusion theory was performed to characterize the sensitivity region of the DS data in two-layer media, demonstrating the importance and influence of the optical properties, mainly scattering, of the upper (surface) layers. Second, measurements were conducted on three healthy volunteers using two different protocols: one involving venous and arterial occlusions in skeletal muscles to measure muscle blood flow and oxygen consumption, and one involving brain activation with the Stroop Color and Word Test to measure associated pre-frontal cortical changes in the oxy- and deoxyhemoglobin concentrations. *In vivo* measurements results showed the different information content of SD and DS data, highlighting the higher specificity provided by the novel approach on deeper tissue (i.e., muscle and brain) versus superficial tissue (i.e., adipose layer and scalp). In summary, this research shows the practical applicability and the potential for research and diagnostics of the new DS NIRS method, paving the way for new *in vivo* applications.

List of Contents

<i>Abstract</i>	1
<i>List of Figures</i>	4
<i>List of Tables</i>	7
<i>Introduction</i>	8
1. Near-Infrared Spectroscopy (NIRS)	10
1.1 Principles of NIRS.....	10
1.2 Tissue optical properties.....	12
1.3 Comparison with other methods.....	16
1.4 Mathematical model.....	18
1.5 Instrumentation.....	22
1.5.1 Sources	22
1.5.2 Optical fibers	22
1.5.3 Detectors.....	23
1.6 Techniques	24
1.6.1 TD-NIRS	24
1.6.2 FD-NIRS.....	25
1.6.3 CW-NIRS.....	27
2. Dual Slope technique	29
2.1 The probe	33
2.2 Mathematical model.....	36
2.2.1 Absolute optical properties.....	36
2.2.2 Relative optical properties.....	39
2.3 Simulations.....	42
3. Measurements on skeletal muscles	46
3.1 Introduction	46
3.2 Materials and Methods	48
3.2.1 Protocol	48
3.2.2 Instrument	51
3.2.3 Total hemoglobin concentration and tissue oxygen saturation.....	52
3.2.4 Muscle blood flow and oxygen consumption	52
3.3 Results	54
3.3.1 Absolute measurements.....	54
3.3.2 Relative measurements	58
3.4 Discussion	63
4. Measurements on brain	64
4.1 Introduction	64
4.2 Materials and Methods	68

4.2.1 Protocol	68
4.2.2 Instrument	71
4.2.3 Signal processing	72
4.3 Results	73
4.3.1 Behavioral response	73
4.3.2 Hemodynamic response	76
4.4 Discussion	86
<i>Conclusion</i>	<i>88</i>
<i>Acknowledgements</i>	<i>89</i>
<i>Bibliography</i>	<i>90</i>

List of Figures

Figure 1: Banana shape pathlength NIRS signal at multiple source-detector separations.....	11
Figure 2: Light propagation through a medium	13
Figure 3: Absorption spectra for different chromophores present in human tissue	14
Figure 4: Representation of input and output intensity signals recovered with TD-NIRS	25
Figure 5: Representation of input and output intensity signals recovered with FD-NIRS	26
Figure 6: Representation of input and output intensity signals recovered with CW-NIRS	28
Figure 7: Sensitivity maps to a localized absorption perturbation for each method	31
Figure 8: Scheme of the dual slope probe geometry combining CW and FD spectroscopy....	34
Figure 9: Device and instrumentation scheme to achieve absolute absorption spectra	34
Figure 10: Flow-chart to achieve absolute absorption spectra and absorbers concentration ...	38
Figure 11: Parametric simulation by changing one parameter at a time	44
Figure 12: Parametric simulation by changing one parameter at a time	44
Figure 13: Scheme of the probe and cuff pressure placement on the calf muscle	49
Figure 14: Venous and arterial occlusion test (VAOT) protocol scheme	50
Figure 15: Representative absolute concentration time traces for each subject.....	55
Figure 16: Absolute absorption coefficient (μ_a) recovered on each subject.....	55

Figure 17: Tissue oxygenation parameters time traces recovered on each subject..... 56

Figure 18: Absolute hemoglobin concentration time traces zoom during AO, recovered on each subject..... 57

Figure 19: Representative time traces for subject 1 of relative hemoglobin concentrations ... 59

Figure 20: Histogram showing muscle oxygen consumption (mVO₂)..... 60

Figure 21: Representative time traces of total hemoglobin concentration..... 61

Figure 22: Histogram showing muscle blood flow (mBF) 62

Figure 23: Scheme of cerebral hemodynamic response during neural activity 64

Figure 24: Illustration of the pathlength (in red) and penetration depth through the different layers of the head [32]. 66

Figure 25: Scheme of the probe placement and keyboard configuration responses 69

Figure 26: fNIRS block design protocol using FD 70

Figure 27: Temporal distribution of single trials within each section..... 73

Figure 28: Representative behavioral responses of subject 1 for averaged sections with the same task 74

Figure 29: Representative behavioral responses of subject 2 for averaged sections with the same task 75

Figure 30: Representative oxy- and deoxyhemoglobin concentrations changes, recovered from Dual Slope intensity (DSI) 77

Figure 31: Representative oxy- and deoxyhemoglobin concentrations changes, recovered from Dual Slope phase ($DS\Phi$)	77
Figure 32: Representative oxy- and deoxyhemoglobin concentrations changes recovered from SDI and DSI	79
Figure 33: Representative oxy- and deoxyhemoglobin concentrations changes recovered from $SD\Phi$ and $DS\Phi$	80
Figure 34: Representative oxy- and deoxyhemoglobin concentrations changes recovered from SDI and DSI	81
Figure 35: Representative oxy- and deoxyhemoglobin concentrations changes recovered from $SD\Phi$ and $DS\Phi$	82
Figure 36: Representative oxy- and deoxyhemoglobin concentrations changes peaks with standard deviations.....	83
Figure 37: Representative oxy- and deoxyhemoglobin concentrations changes peaks with standard deviations.....	83
Figure 38: Representative oxy- and deoxyhemoglobin concentrations changes peaks with standard deviations.....	84
Figure 39: Representative oxy- and deoxyhemoglobin concentrations changes peaks with standard deviations.....	85

List of Tables

Table 1: Characteristics of different imaging techniques.....	17
Table 2: Characteristics of NIRS techniques	28
Table 3: Two layers model and recovered parameters.....	43
Table 4: Subjects' demographic information and thickness of forearm and calf tissues.	48

Introduction

Near Infrared Spectroscopy (NIRS) is a non-invasive, cost-effective and portable imaging tool, widely used in the biomedical research field to investigate tissue oxygenation and hemodynamic responses in real time. By illuminating a sample of tissue with a source positioned a few centimeters away from a detector, it's possible to collect optical signals resulting from the interaction between light and tissue. The information achieved allows one to measure tissue optical properties and to quantify specific absorbing components present in the tissue, defining their spatio-temporal distribution. To achieve a penetration depth of a few centimeters with a good quality signal, NIRS employs wavelengths in the near-infrared spectral region (typically 650-900 nm).

However, apart from the limited spatial resolution (\sim cm), NIRS measurements are affected by two common problems: (1) the strong sensitivity to hemodynamic contributions from superficial layers, which may confound the measurements of targeted hemodynamics in deeper tissue; (2) artifacts originating from instrumental effects and from subject movements, which may limit practical applicability and clinical use. Over time, several solutions have been investigated, working on both instrumental and methodological points of view. Among these, specific geometries and optodes arrangements have been proposed, passing from traditional single distance approaches to more sophisticated multi distance methods. A specific configuration recently developed in our laboratory, defined Dual Slope (DS), have shown the potential enhancement in sensitivity to deep versus superficial tissue, also minimizing instrumental and motion artifacts.

The aim of this study is to further characterize the novel method from a theoretical and practical point of view. First of all, a simulation study based on diffusion theory was performed to characterize the sensitivity region of the DS data in a two-layer media model, getting closer to real tissues properties, compared to commonly used homogeneous model. Then, *in vivo* measurements on healthy subjects were carried out to assess their capability to measure the oxygenation levels and hemodynamic response of skeletal muscles and brain.

The work is divided into four chapters:

- Chapter 1 introduces the physical principles and mathematical model at the base of Near-Infrared Spectroscopy, followed by the instrumentation and different techniques implemented to collect optical signals.
- Chapter 2 characterizes from an instrumental (technological components) and methodological (signal processing) point of view the probe used in this study based on the novel Dual Slope (DS) method, followed by a careful analysis of the sensitivity performances through simulations.
- Chapter 3 reports *in vivo* measurements collected on skeletal muscles with the DS probe during a protocol based on venous and arterial occlusion tests, evaluating tissue oximetry and hemodynamic response through the recovery of physiological parameters.
- Chapter 4 shows *in vivo* application of the novel DS probe on brain tissue, focusing on the focal functional response on the human prefrontal cortex (PFC), during a neurocognitive task, defined Stroop Color and Word Test.

1. Near-Infrared Spectroscopy (NIRS)

1.1 Principles of NIRS

Since its first introduction by Jöbsis, who demonstrated the possibility to continuously and non-invasively monitor physiological quantities and tissue oxygenation with *in vivo* measurements, Near Infrared Spectroscopy (NIRS) has been widely used to analyze many types of tissue, especially brain and muscles [1].

The basic idea of optical spectroscopy is to investigate tissue physiology and function illuminating the target tissue, with a proper light source, and collecting the transmitted or reflected light few centimeters away from the emitter location, using an optical detector [2]. From the collected signal, based on the wavelength-dependent interaction of light with matter, it is possible to recognize and quantify different biological compounds, obtaining information of the probed sample non-invasively and in real-time. In this sense, it's important to select the correct range of wavelengths in which the light is weakly absorbed and can be detected, reducing the quantity of photons losses due to absorption. In fact, inside the visible-NIR range (650-900 nm), also called “optical window”, biological tissues behave like diffusive media when light interacts with them, allowing photons to cross the tissue and reach components relatively deeply (up to a few centimeters below the surface), since they undergo scattering events at a much greater rate than absorption events [3].

Depending on source-detector position, on the same or opposite side of tissue surface, the re-emerging light is considered reflected or transmitted respectively. In general, Diffuse Reflectance Spectroscopy (DRS) is the common configuration used for brain and muscle measurements, with the emitting and receiving components on the same side of the tissue, since the dimension of the investigated volume is too big to achieve a transmitted signal. From source-detector distance depends also the volume probed and the signal quality, in terms of amplitude and signal to noise ratio (SNR). Scattered light propagates inside heterogeneous tissues showing a banana-shaped path, with narrow edges at source-detector locations and the highest penetration depth in the middle of their distance (see Fig. 1). In general, the bigger the source-detector separation, the greater the volume investigated. Short source-detector distances

(~ 0.5 cm) have a low depth of penetration and recover physiological contributions (noise) from the superficial layers (scalp and skull, for brain, adipose tissue for muscle). However, too large distances result in the detected signal reduction, due to tissue properties, so a good compromise is around 3-4 cm separation. Another important factor to consider is the intensity of the incident light on the tissue surface, which should be high enough for a good signal quality, but at the same time kept within safety levels, avoiding surface overheating. All these limits are the main reasons why NIRS is not among the best imaging methods in terms of spatial resolution (~cm).

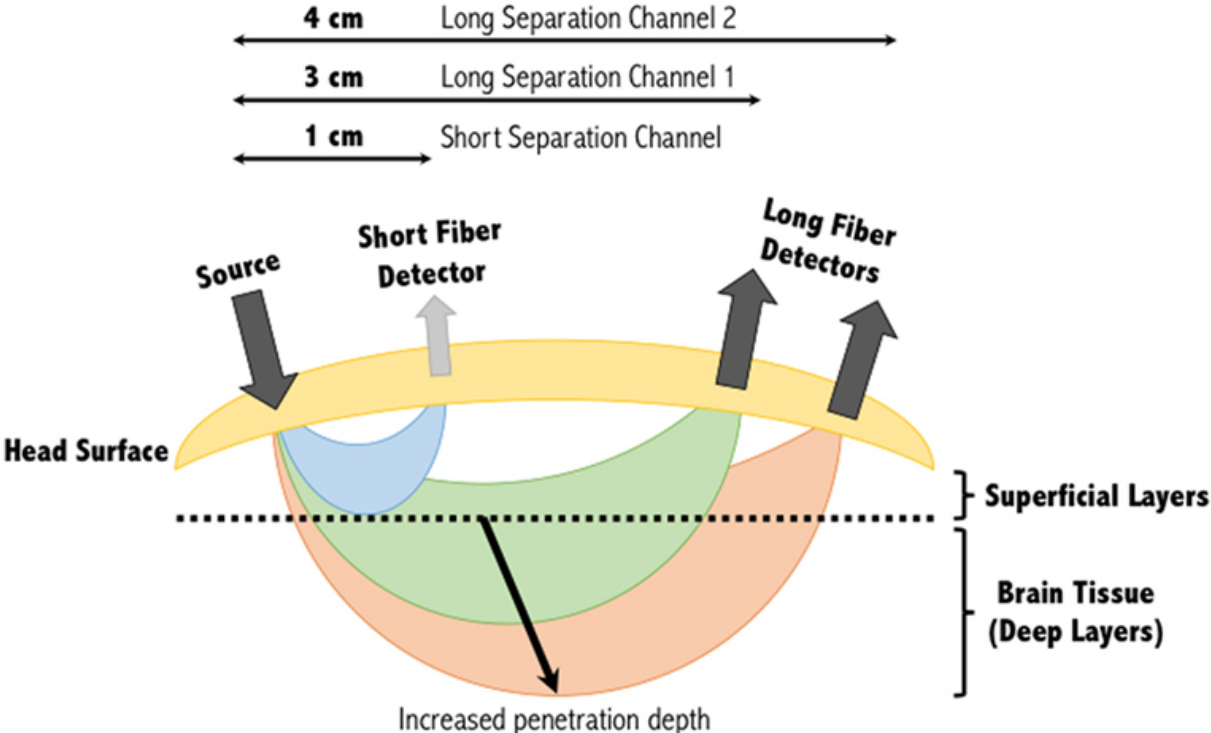


Figure 1: Banana shape pathlength NIRS signal at multiple source-detector separations: short distance in blue (1 cm) to recover superficial contributes and long distances in green and orange (3-4 cm) for deeper layer contributions [4].

1.2 Tissue optical properties

Once emitted by the source, photons travel through diffusive media undergoing different interactions with tissue components, that cause consecutive changes in their direction before being detected and appearing diffuse [5]. Depending on particles sizes, index of refraction and wavelengths beam of light, the general result is a total pathlength travelled by photons that exceeds the geometrical distance between source and detector. Some photons escape from the detection zone because of forward and backward scattering and cannot even be revealed, causing a loss of information. In fact, of the whole emitted NIR light that penetrates the tissue, only a part scattered several times results in a final backward trajectory, towards the surface where it can be captured. The random pathways and photons lost during photon migration can be described by two optical properties: the scattering (μ_s) and absorption (μ_a) coefficients (see Fig. 2). These two parameters, usually expressed in units of [cm^{-1}] for biological tissues, represent the probability per unit pathlength of a photon to be either scattered or absorbed respectively.

In particular, the scattering coefficient (μ_s) is related to discontinuities in the index of refraction within the tissue and it contains information about the size and density of the scattering centers. Usually, μ_s is corrected by the anisotropy factor into the so-called reduced scattering coefficient (μ'_s) since it takes into account not only the scattering probability but also the average direction of photons. Therefore, for biological tissues with particles size usually comparable or bigger than the wavelength of light, the reduced scattering coefficient follows a wavelength dependent power law, and according to Mie theory (see Eq. 1):

$$\mu'_s(\lambda) = \mu'_s(\lambda_0) \cdot \left(\frac{\lambda}{\lambda_0}\right)^{-b} \quad (1)$$

where b is the scattering power coefficient and $\mu'_s(\lambda_0)$ is the reduced scattering coefficient at a reference wavelength, λ_0 [4].

The absorption coefficient μ_a , instead, represents the loss of photons due to the presence of absorbing components, responsible of converting intensity of the emitted light into other form of energy (radiative or non-radiative). This parameter is strictly proportional to the molar

concentration C_i (M=mol/L) and molar extinction coefficient ε_i (cm^{-1}/M) of these biological compounds, through the wavelength dependent relation (see Eq. 2):

$$\mu_a(\lambda) = \sum_{i=1}^{nc} C_i \cdot \varepsilon_i(\lambda) \quad (2)$$

where nc is the total number of absorbers.

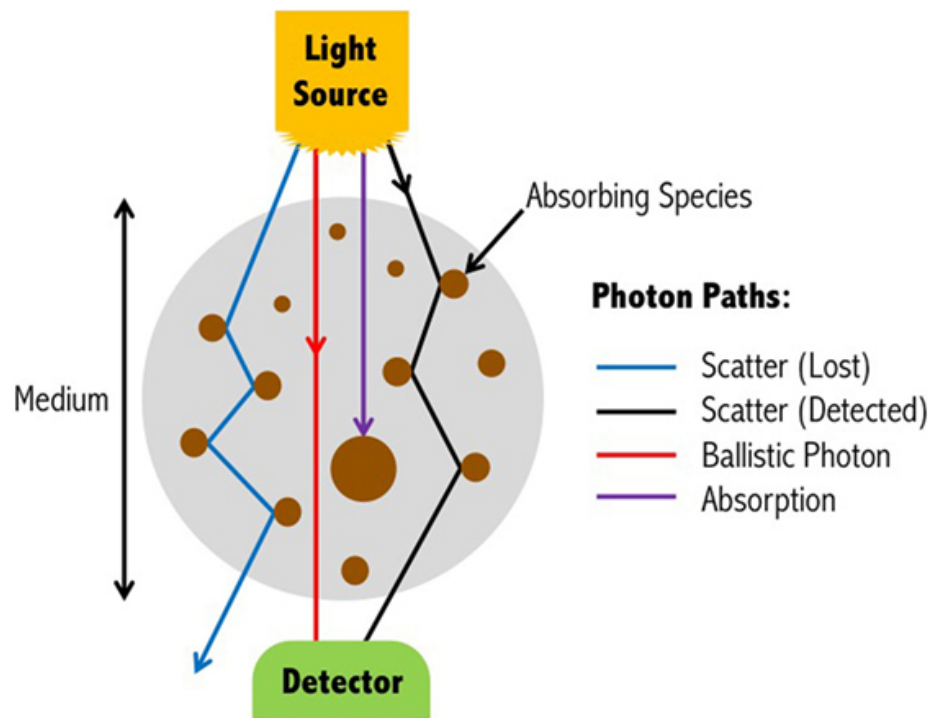


Figure 2: Light propagation paths through a medium: scattered photons undetected and collected (blue and black respectively) and absorbed photons (purple) [4].

Since each absorber contributes differently to the overall absorption process with its own spectral fingerprint, it is possible to separate their contribution and quantify their concentration, paying attention on the choice of the emitted spectral range of light. In the optical window, the absorption spectra mainly evaluated are the ones of chromophores (such as hemoglobin, melanin, cytochrome-c oxidase, CtOx) and non-chromophore compounds (like water and lipids). As concerns water, despite being the main constituent of biological tissues, its

absorption spectrum presents higher peaks outside the optical range (650-900 nm), for wavelengths in the UV and IR range (see Fig 3).

In the same window, other substances with higher absorption power are present, like collagen, fat and CtOx, but their concentration is relatively low. Therefore, together with water, for opposite reasons, they are not considered as the main absorbers and their contribution to absorption to a first approximation can be neglected. In fact, in the NIR range the bigger absorption contribute is given by the hemoglobin, a globular protein responsible for oxygen transport and present in biological tissue in two different states: oxidized (oxyhemoglobin, HbO₂) and reduced (deoxyhemoglobin, Hb). Except at the isosbestic point (around 800 nm), in which they have the same absorption coefficient, HbO₂ and Hb have a different spectral shape through which they can be discriminated.

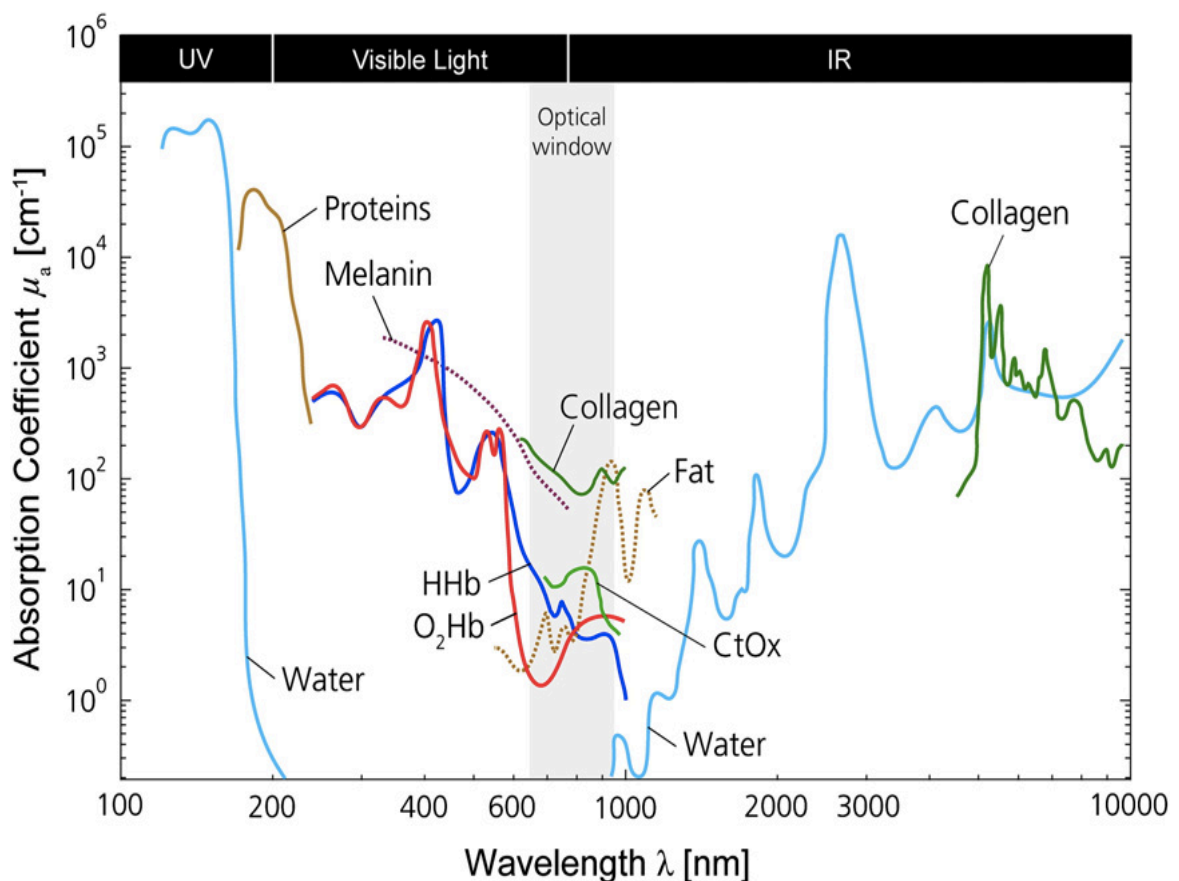


Figure 3: Absorption spectra with natural logarithmic base, for different chromophores present in human tissue. Concentrations expressed in mM in the range from 100 to 10000 nm [6]. Acronyms: oxyhemoglobin (O₂Hb), deoxyhemoglobin (Hb), cytochrome-c oxidase (CtOx).

By quantifying hemoglobin concentration in the target tissues, important hemodynamic and tissue oxygenation parameters are recovered, like the total content of hemoglobin (HbT, sum of the two species) and the oxygen saturation level (StO₂, ratio between oxyhemoglobin and total hemoglobin), that find application in many different fields [1]. Many studies have investigated the potential use of functional NIRS (fNIRS), for monitoring both the hemodynamic response and functional activation of the brain, trying to distinguish between healthy and unhealthy subjects, focusing on the analysis of psychiatric disorders, like Parkinson's and Alzheimer's disease [7]. Different research groups have also applied this technique to monitor skeletal muscle oxygenation and energy metabolism, comparing healthy and clinical population, during resting state or exercise conditions [8].

1.3 Comparison with other methods

The growing interest in NIRS devices has increased the number of its applications in the biomedical field and the development of sophisticated systems, moving from simple tools with single channels (one source, one detector) to multi-channel instruments. Over time researchers realized the importance not only to quantify signal variations but also to map through images where concentration changes occur, and to do so it was necessary to enhance the investigated tissue area by using imaging system with several source-detector separations. The new imaging NIRS technology, called near-infrared imaging (NIRI) is divided in two categories, based on the dimension of image reconstruction: near-infrared topography (2D) and tomography (3D) [2].

Although NIRI instruments are widely used as research tools for investigating groups of subjects, their application in clinical studies is still limited to their insufficient reliability in single person measurements. Possible reasons for this lack can be found in signals contamination due to superficial tissue layers or systemic physiological changes, that behave as confounding contributions. Another drawback of NIRS instruments is the relatively low spatial resolution, due to the properties of light transports in tissues, that limits the penetration depth reachable around few centimeters. However, different possibilities can be adopted to compensate these limits: on the instrumental level, it is important to select the correct wavelengths, sources, detectors and exploit special arrangements capable of reducing crosstalk contributions. On a methodological level instead, measurements can be improved by separating signal components, involving mathematical approaches (univariate or multivariate methods) [6].

Beyond these drawbacks, NIRI systems have different advantages with respect to other non-invasive imaging techniques widely used in the biomedical field (see Table 1), such as MRI (Magnetic Resonance Imaging) and EEG (Electroencephalography). NIRS technology is portable, not expensive, robust against motion artifacts and with relatively high temporal resolution (ms), compared to MRI (s) and it's also robust against environmental noise, that usually affects EEG measurements [9]. For all these strengths, Near Infrared Spectroscopy has seen great development over time and it is one of the most studied techniques in the biomedical imaging industry.

Table 1: Characteristics of different imaging techniques: Near-Infrared Imaging (NIRI), Magnetic Resonance Imaging (MRI), Electroencephalography (EEG).

Characteristics	Imaging techniques		
	NIRI	MRI	EEG
Spatial resolution	~ cm	mm	cm
Temporal resolution	ms	s	~ ms
Portability	Yes	No	Yes
Cost	Moderate	High	Low
Sensitive to	Hair, extra-cerebral hemodynamic	Motion artifacts	Environmental noise

1.4 Mathematical model

The typical photon pathlength inside biological media is controlled by absorption, strictly related to photons loss, and scattering interactions. The attenuation of light only due to absorption, in the absence of scattering, is represented by the absorbance (A) or optical density (OD) and it is described by the Beer-Lambert's law (BLL). It provides a wavelength and time dependent relationship between A and the chromophores concentrations (see Eq. 3):

$$A(t, \lambda) = -\log_{10} \left(\frac{I(t, \lambda)}{I_0(t, \lambda)} \right) = \sum_i \varepsilon_i(\lambda) \cdot c_i(t) \cdot d \quad (3)$$

where I and I_0 represent the intensity of reflected and emitted light, ε_i is the molar extinction coefficient ($\text{cm}^{-1}/\mu\text{M}$), c_i is the molar chromophores concentration (μM), both indexed by i for each chromophore, and d is the source-detector geometrical distance. The same equation can also be rewritten in terms of natural logarithm and a new molar extinction coefficient that differs from ε by a scaling factor (see Eq. 4-5):

$$A(t, \lambda) = -\ln \left(\frac{I(t, \lambda)}{I_0(t, \lambda)} \right) = \sum_i \alpha_i(\lambda) \cdot c_i(t) \cdot d \quad (4)$$

where:

$$\alpha(\lambda) = \frac{\varepsilon(\lambda)}{\ln 10} \quad (5)$$

However, since these equations do not include the scattering effect, they are not suitable for describing what happens inside biological tissues, where scattering occur more than

absorption events. The model that best describes both the effects is provided by the Modified Beer - Lambert Law (MBLL), an extension of the Beer-Lambert's Law, which introduces two unitless parameters: the differential pathlength factor (DPF), which encompass the extra pathlength of scattered photons and the G factor, that represents scattering dependent photons loss (see Eq. 6) [2].

$$A(t, \lambda) = -\log_{10} \left(\frac{I(t, \lambda)}{I_0(t, \lambda)} \right) = \sum_i \varepsilon_i(\lambda) \cdot c_i(t) \cdot d \cdot DPF(\lambda) + G(\lambda) \quad (6)$$

Since G varies according to the heterogeneous geometric conformation of target tissue and is not uniquely defined, it's not possible to evaluate absolute quantities from this equation. However, different assumptions allow relative measurements of chromophores concentrations: considering scattering change in time smaller than the absorption one, G can be assumed to be time invariant and canceled out when determining the optical density variation at two different time points (t_0 and t_1). In addition, the intensity of emitted light I_0 is assumed to be constant, ideally without temporal fluctuations and so it can be neglected too, when calculating the absorbance change at two different times (see Eq. 7).

$$\Delta A(\Delta t, \lambda) = -\log_{10} \left(\frac{I(t_1, \lambda)}{I(t_0, \lambda)} \right) = \sum_i \varepsilon_i(\lambda) \cdot \Delta c_i \cdot d \cdot DPF(\lambda) \quad (7)$$

where $\Delta c_i = c_i(t_1) - c_i(t_0)$ represents the concentration change for each chromophore.

Even though the spatial resolution is limited by scattering effect, according to the latter relation the recovered NIR signal contains rich contrast, since a small change in attenuation will result in a large intensity change. The model also assumes that changes in detected light are mainly due to homogeneous absorption changes due to tissue chromophores, especially oxyhemoglobin [HbO_2] and deoxyhemoglobin [Hb]. This approximation of homogeneity involves confounded contributions from superficial layers since it doesn't considerate that effective changes occur in cerebral tissue rather than in skin and bones.

Errors in quantification are even increased when considering the uncertainties linked to the knowledge of DPF value. In fact, this factor varies between subjects and tissues, introducing variability on the recovered concentrations Δc , given their inversely proportional relation. To reduce this error, time domain spectroscopy can be applied, since it's capable of recovering the DPF value [6]. However, this solution requires instruments more complicated, expensive and not always necessary, when considering that quantification of exact chromophores concentration is not a priority goal in functional studies and what really matter is signal changes discrimination between activity and resting states. Despite the fact that homogeneity assumptions and DPF value approximations lead to underestimated hemoglobin concentrations, the signal recovered during functional tasks still contains qualitative information about whether or where activation is present, and it is sufficient to discriminate it against recovery or resting states. Therefore, the goal of the study together with the amount of information required are the important parameters to take into account when choosing a method, reducing as much as possible costs and complexity.

By inverting Eq. 7 and considering it at different wavelengths (at least two), it is possible to recover relative changes of $[HbO_2]$ and $[Hb]$ separately (see Eq. 8).

$$\begin{bmatrix} \Delta[Hb] \\ \Delta[HbO_2] \end{bmatrix} = d^{-1} \cdot \begin{bmatrix} \varepsilon_{HHb\lambda_1} & \varepsilon_{HbO_2\lambda_1} \\ \varepsilon_{HHb\lambda_2} & \varepsilon_{HbO_2\lambda_2} \end{bmatrix}^{-1} \cdot \begin{bmatrix} \frac{\Delta A(\Delta t, \lambda_1)}{DPF(\lambda_1)} \\ \frac{\Delta A(\Delta t, \lambda_2)}{DPF(\lambda_2)} \end{bmatrix} \quad (8)$$

The choice and the number of wavelengths used to evaluate chromophore concentrations depend on different variables, among which the number and types of absorbers investigated, and the background model adopted (homogeneous vs heterogeneous tissue). To solve a linear problem with the number of wavelengths equal to the unknowns, two values are usually selected to recover hemoglobin concentration. In particular, considering the spectral fingerprint of HbO_2 and Hb far from their isosbestic point (800 nm), where their crosstalk is high and the recovery sensitivity lower, 690 and 830 nm proved to be a good pair of wavelengths to use [14].

Using a broadband spectrum, it is possible to escape the optimum wavelengths selection process and evaluate concentration of other absorbing compounds, such as lipids and water, avoiding also the hemoglobin content overestimation [10, 11]. However, when using multi-

spectral approaches, two drawbacks should be considered: higher computational complexity and incident light power increase, compared to a device using only few wavelengths.

To extend the use of NIRS technology in biological application as a tool for monitoring not only functional activation, but also baseline and resting state conditions, absolute optical measurements are required. But to be recovered, both instrumental contributions and tissue scattering must be accounted for. From an instrumental point of view, an important progress was achieved switching from single distance (SD) to multi-distance approaches (MD), which relies on measurements at several distances at the same time. Instead concerning the measure of tissue scattering, methods resolved in time domain were applied [6, 11].

There are two main types of MD methods: the Spatially Resolved Spectroscopy (SRS) and Self-Calibrating method (SC), which unlike the first method doesn't require a preliminary calibration on a phantom to recover absolute properties. However, compared to SD measurements, multi distance methods have two main advantages:

1. they provide absolute measurements more robust against motion artifacts and instrumental drifts, since a change in optical coupling has a similar effect on all distances and it cancels out,
2. they are more sensitive to deep tissues since they measure intensity changes at different distances, including the ones containing information of superficial layers, that can be removed with regression process.

Hence, providing absolute measurements within and among subjects and tissues, MD approaches can increase the amount of information introduced by relative measurements, and improve the accuracy, reliability, and reproducibility of NIRS [10].

1.5 Instrumentation

From a technological point of view the main components of NIRS devices are light sources, probes, to transport the emitted light to and from the target tissue, and detectors, to collect the diffuse reflectance light that re-emerge from the surface after passing through the media.

1.5.1 Sources

Regarding the light source emission, the relevant properties for optical tissue spectroscopy are [5]:

- the range and number of wavelengths used (finite or broadband),
- the temporal emission (constant, pulsed or intensity modulated),
- the maximum permissible exposure (MPE) of the skin to optical radiation.

In this sense, both LDs (Laser Diodes) and LEDs (Light Emitting Diodes) are suitable and can be used in NIR spectroscopy, with the advantage that the latter are cheaper, safer, and smaller compared to lasers [6].

1.5.2 Optical fibers

Although existing methods require sources to be in contact with the surface, like the structured illumination of the tissue, the most common approach of light delivery in NIR spectroscopy is through optical fibers. These components are responsible to transport light to the media, minimizing the losses, based on the total internal reflection phenomenon. The quality of the signal recovered is closely related with the choice of these optodes, which can be selected among two models (single mode vs multimode), depending on different variables: optical coupling with the tissue, sources and detectors, mechanical properties (flexibility) and the numerical aperture, which influences the amount of light collected from the tissue.

Usually, core diameters of detector optical fibers are larger than those of source optical fibers, to increase the amount of light collected. During an experimental setup, it is important to pay attention and prevent the direct detection of light from source and pressure changes between tissue and optical fibers contact, which may introduce artifacts.

1.5.3 Detectors

The basic idea of tissue spectroscopy detectors is to transform the optical signal (the tissue re-emerging light) into an electrical signal (electrons converted in photocurrent), through the photoelectric effect. Based on this phenomenon, two types of detectors can be distinguished: the photomultiplier tubes (PMTs), with electrons emitted by a photocathode (external photoelectric effect), and photodiodes (PDs), based on electrons excited into the conduction band of a semiconductor (internal photoelectric effect). The type of detector chosen depends on key parameters [5]:

- the spectral sensitivity, determined by the materials used,
- the linearity and dynamic range, over which the photocurrent is a linear function of the intensity detected,
- the temporal response, defined as the time from 10% to 90% of the final signal level in response to a step input signal.

In general, PMTs feature larger electron gain and faster speed, instead PDs have higher dynamic range, smaller sizes, and robustness against ambient light exposure [6].

1.6 Techniques

Depending on the type of emitters used, three different configurations can be distinguished: pulsed light in time domain (TD), amplitude modulated light in frequency domain (FD) and constant light in continuous wave domain (CW). Each method has its own strengths and drawbacks and requires a different apparatus that influences both the portability and instrumental cost (see Table 2). Moreover, since they provide different amount of information, the choice of the method is also based on the type of application and the study to carry out.

1.6.1 TD-NIRS

TD-NIRS technique detects single photons intensity and their time of flight, employing an ultra-short light impulse in the picoseconds range. The broadened and attenuated signal detected from the re-emitted photons after passing through the highly scattering medium, called temporal point spread function (TPSF), represents the distribution of photons time of flight, with a temporal resolution of nanoseconds (Fig. 4. a, b).

Analyzing the TPSF shape it is possible to obtain information about tissue optical properties. The arrival time distribution is strictly correlated with the penetration depth achieved by photons, so that the ones detected after a shorter period (ps) belong to superficial layers, instead the ones that spend more time (ns) within the media, with higher probability have reached deeper regions [1]. Absorption and reduced scattering contribution can be decoupled from the TPSF signal, since the first is related to the asymptotic slope of the curve and the second to its broadened shape and initial rise. Therefore, this approach allows to directly estimate absolute optical properties and chromophore concentrations, by fitting recovered data through a suitable theoretical model describing the photons diffusion propagation in a turbid media.

Since it contains information about the signal provenance and absolute hemoglobin levels, time-resolved method provides the highest level of information, managing to discriminate between systemic hemodynamic changes of superficial layers and the ones

occurring in deeper regions, such in brain cortex and muscle tissue. However, due to the high technological complexity and instrumental cost, time domain NIRS is not widely available in terms of clinical application, compared to the other methods.

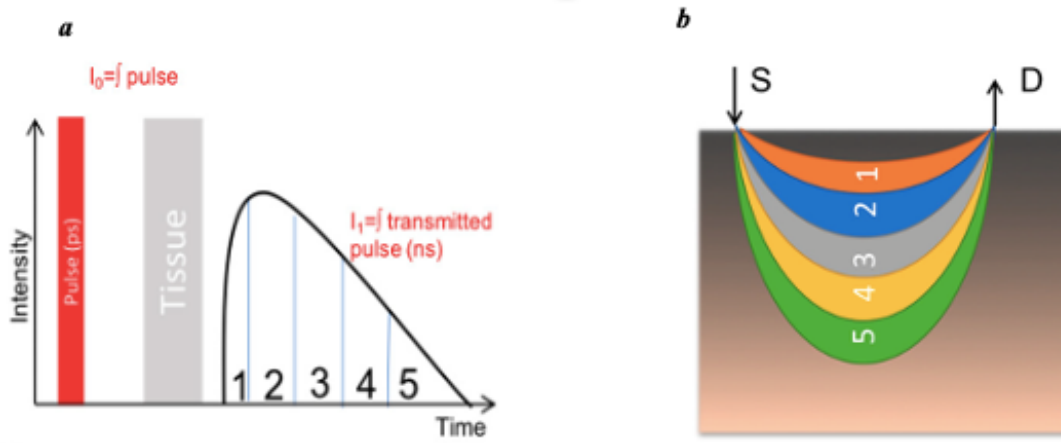


Figure 4: Representation of input and output intensity signals in time recovered with TD-NIRS using an ultra-short impulse light (ps), on the left (a); representation of photon pathlengths numbered according to the time of flight (increasing numbers for increasing time of flight and depth achieved) on the right (b). Acronyms: S for source and D for detector [2].

1.6.2 FD-NIRS

The basic idea of frequency domain NIRS is to use intensity-modulated sources at frequencies (f) in the MHz range and acquire output signals expressed by two terms, one in direct current (DC), and a phasor with amplitude, expressed in alternative current (AC), and phase (φ), (see Eq. 9):

$$FD_{signal} = DC + AC \cdot e^{i\varphi} \cdot e^{-i\omega t} \quad (9)$$

where ω is the angular frequency ($\omega = 2\pi f$).

The choice of the modulation frequency defines the temporal resolution, and its value is strictly connected to light propagation in biological tissues by the relationship $\varphi \approx \omega \langle t \rangle$, linking the signal phase to the photon mean time of flight. In particular, too low values would

provide a phase-shift under the limit of detectability, instead greater frequencies would result in AC amplitude equal or below the level of noise, according to the phasor attenuation [12].

The measured optical signal appears reduced in amplitude and shifted in phase (see Fig. 5.a) due to diffusive media properties, which affect both quantities in a different way: photon absorption influences the reduction of intensity in terms of amplitude, instead the phase-shift is mainly related to the photon pathlength (see Fig 5.b) through the scattering effect.

As in TD-NIRS, with frequency domain it is possible to recover absorbance and reduced scattering coefficients separately, obtaining absolute quantification of chromophores concentration. Another important advantage of FD-NIRS is that using intensity and phase signal with properly designed source-detector arrays, it's possible to control the region of sensitivity in the probed tissue, minimizing confounding contributions from superficial layers, such as scalp, for brain, and adipose tissue, for muscle measurements. Moreover, compared to continuous wave signals, based on DC intensity, AC data present reduced undesired contributes since they are less affected by room light [11]. However, both the complexity of acquisition electronics and the cost are relatively high with instruments less miniaturized compared to CW systems.

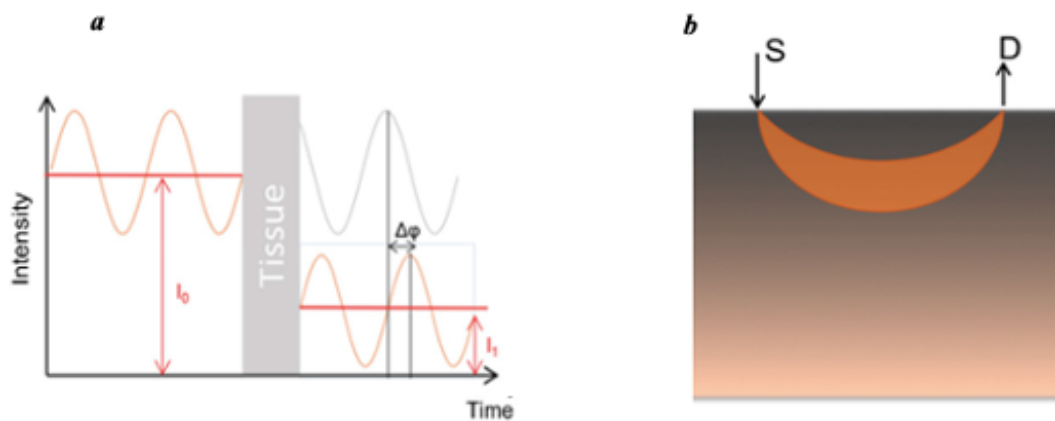


Figure 5: Representation of input and output intensity signals in time recovered with FD-NIRS using intensity modulated light (MHz), on the left (a); representation of photon pathlength on the right (b). Acronyms: S for source and D for detector [2].

1.6.3 CW-NIRS

In contrast to time resolved techniques, which can reach information based both on intensity and time of flight, CW systems employ constant-emission light sources and measure only intensity variations of the reflected light (Fig. 6.a). Measuring intensity attenuation changes between the collected and emitted light at several wavelengths, and assuming a constant scattering effect at different time intervals, CW domain can be used to extrapolate relative changes in chromophore concentration using the MBLL. In fact, since this method cannot distinguish between absorption and scattering coefficients, absolute concentrations and the DPF value cannot be evaluated. Indeed, the latter can be extrapolated from modelling approaches or tabulated values, but this decreases the accuracy of CW method making it not patient specific, because of the DPF high inter subject (heterogeneity of population) and intrasubject (tissue) variability.

In any case, different extensions of the CW method were proposed in order to overcome this important limit, one being spatially resolved spectroscopy, SRS (see Fig. 6.b). The SRS approach is based on the detection of optical signals at different source-detector separations, so that fitting the spatial dependence of the light intensity at several wavelengths with diffusion theory, one can evaluate absolute optical properties under specific conditions [2].

In some applications, especially during functional brain measurements, quantification of absolute values of the tissue optical properties is not essential, because it's more important to significantly and statistically detect changes during activation tasks. For this reason and thanks to their portability, relatively low cost and simpler instrumentation, CW NIRS systems are the most commonly used in both research and clinical applications [6].

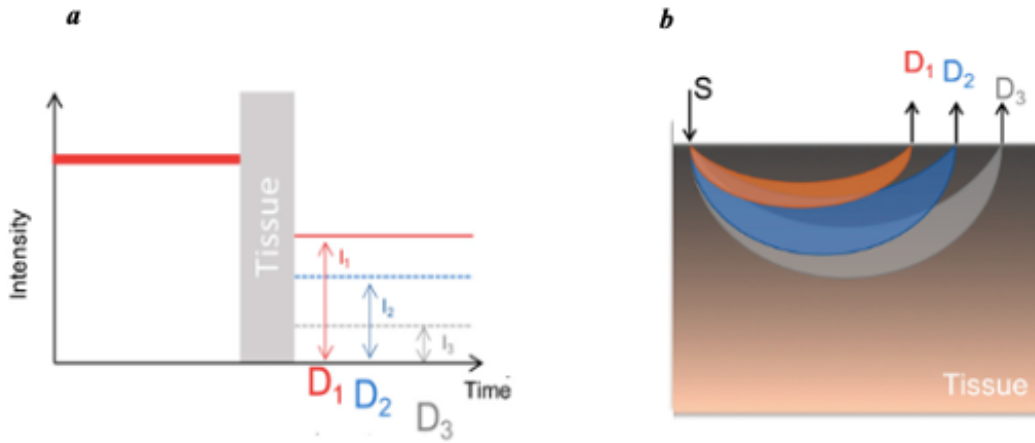


Figure 6: Representation of input and output intensity signals in time, considered at different detector positions, recovered with CW-NIRS using constant emitted intensity light, on the left (a); on the right, representation of photon pathlength. Acronyms: S for source and D1, D2, D3 for detector at different positions (b) [2].

Table 2: Characteristics of NIRS techniques: Time Domain (TD), Frequency domain (FD), Continuous Wave (CW).

Characteristics	Technique		
	TD	FD	CW
μ_a , μ_s' , DPF	Absolute	Absolute	Relative
[HbO ₂], [HB]	Absolute	Absolute	Relative
Commercial systems	Few companies	Few companies	Multiple companies
Cost	Very high	High	From low to high
Size	Depends on the number of channels, wearable systems available	Bulky but transportable	Bulky but transportable
Number of channels	High	High	Low
Source	Ultra-short impulse light	Modulated intensity light	Constant intensity light

2. Dual Slope technique

During *in vivo* measurements, one of the main issues shared by NIRS techniques is the strong sensitivity to hemodynamic changes occurring in superficial layers, close to sources and detectors. Over time, several solutions have been investigated with the aim of reducing these confounding contributions, in order to improve the accuracy and image resolution. From a methodological point of view, numerous approaches have been proposed to decouple systemic hemodynamic changes from the one of interest, including statistical analysis (principal component analysis, PCA) and signal processing (adaptive filtering, regression procedures). However, instead of using methodological approaches, usually more complicated, it would be better to have systems intrinsically more robust against noise artifacts.

From an instrumental point of view, particular attention has been paid to optodes arrangements and their influence on the recovered signals. Simulation studies showed how increasing optodes density and overlapping light paths affect positively the image resolution. From simpler single distance systems (SD), with one source-detector pair, more advanced multiple distances (MD) tools started to be produced. Hence, the need of a new analysis approach that, instead of measuring light attenuation at a single distance from the source, was based on light intensity decrease between different positions, by measuring its slope (as a function of source-detector distances) [14].

Early MD slope systems consisted of only one source and N detectors (or vice versa), so that each single slope (SS) was recovered by measuring light intensity attenuation between paired positions. Compared to SD systems, slope methods proved to be effectively less sensitive to superficial changes, thanks to the relationship that binds distances and penetration depths. However, in addition to being able to discriminate signals from different locations, a good method should also be robust enough against instrumental drifts associated with both sources and detectors. This is the case for the self-calibrating approach (SC), a MD configuration free from calibration, which can increase the sensitivity to deep tissues and compensate time variations in optical coupling between probes and tissue, through a specific arrangement based on two source-detector symmetric pairs.

In general, analytical solutions of the diffusion theory for MD systems show that, regardless of the domain used to collect data, functions of the measured signals (F) are linearly dependent on inter-optodes distance (ρ), through the slope (S), with the addition of source (K_{source}) and detector ($K_{detector}$) contributions that affect actual values recovery, according to Eq. 10 [12]:

$$F(\rho, \mu_a, \mu'_s) = S(\mu_a, \mu'_s) \cdot \rho + K_{source} + K_{detector} \quad (10)$$

However, when using the SC approach that is based on the average of two paired single slopes, these K terms give opposite contributions to the paired single slopes so that they cancel out in their average. This is the reason why SC systems do not require any preliminary calibration, since contributions such as motion artifacts, light fluctuations (at source and detector sides) and variable optical coupling, all contained in K terms, can be canceled out when measuring the attenuation slopes. Moreover, by using different source-detector separations, the SC approach can discriminate between superficial layers contributions, detected at short distances, and deep layers measurements, mainly collected at larger separations. From these considerations, a new probe with linear SC arrangement was developed, based on the measurement of two source-detector paired averaged slopes, hence the name of dual slope (DS) [14].

First, multi distance approaches were applied to continuous wave instruments, because of their simplicity, but since CW systems are not capable of measuring absolute optical properties directly, the absolute recovery of [Hb] and [HbO₂] is only possible with reasonable assumptions of μ_s' , treating the tissue and concentration changes as homogeneous. To overcome the limit introduced by homogeneity approximation and quantitatively determine spatio-temporal absorption changes, extensions of the approach were proposed by performing forward and inverse models with two or more layers, based on numerical (Finite Element Method, FEM and Monte Carlo, MC) or analytical solutions of the diffusion equation [18].

The use of slope approach was then extended to time resolved methods in order to achieve absolute measurements with improved resolution. In fact, a study based on *in vivo* measurements on brain with FD, considering intensity and phase signals separately, confirms the strengths of using multi-distance slope methods to improve image resolution, by comparing

region of sensitivities achieved by SD, SS and DS [13]. Sensitivity was assessed as the relative ratio between the recovered absorption coefficient and a localized actual absorption perturbation (see Fig. 7). While SD sensitivity map has the typical banana shape with higher values close to the surface, slope methods result less affected by undesired hemodynamic components, with negative sensitivity close to superficial layers. In particular, DS method has small positive contributions from superficial layers and reaches the deepest maximal sensitivity. Among all, dual slope phase data (DS ϕ) have the highest penetration depth, albeit with a lower signal to noise ratio (SNR) compared to DS intensity data (DSI) [51].

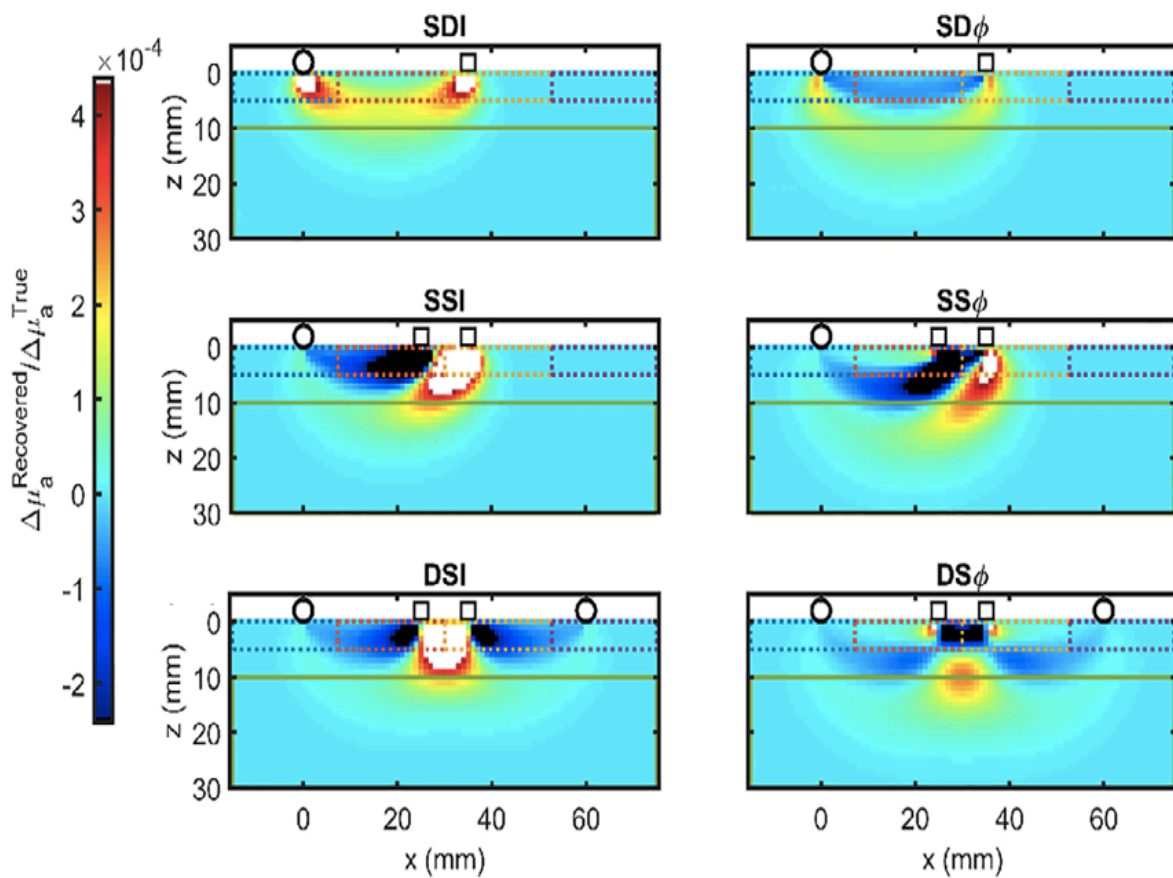


Figure 7: Sensitivity maps to a localized absorption perturbation for each method, SD, SS and DS (top, center, bottom row respectively) and each datatype, intensity (left column) and phase (right column). Sources (circles) and detectors (squares) are positioned on the boundary surface [13].

To exploit the strengths of continuous wave and frequency domain systems, the new probe proposed in this study combined the two most used NIRS techniques together, to decouple absorption and scattering contributions and achieve absolute chromophores measurements [3]. On one hand, a frequency domain component (FD-NIRS), used to retrieve absolute optical properties at two wavelengths, on the other hand, diffuse reflectance spectroscopy with a continuous-wave broadband source (CW-bDRS), applied to recover quantitative absorption spectra for a range of wavelengths (between 650 and 1064 nm). The frequency domain is typically not implemented in broadband spectroscopy, because of its high instrumental complexity and cost, instead CW alone is not capable of measuring absolute quantities.

2.1 The probe

The probe configuration used in this study employs the symmetric geometry typical of the self-calibrating approach, thus resulting in measurements more robust against instrumental drifts, coupling factors, motion artifacts and free from a need for any calibration. Each side of the probe (with different domain) is made of two sources and two detectors, positioned at the ends and center of the linear configuration, respectively (see Fig. 8). It is defined Dual-Slope (DS) or Self-Calibrating (SC), depending on whether it refers to a single data type (intensity or phase) or the combination of intensity and phase data in the frequency domain. The optodes arrangement was obtained by inserting the source and detector optical fibers into a black silicon mold, flexible enough to be modelled according to the shape of the investigated tissues.

Regarding the time-resolved component, data were collected using a multichannel dual wavelengths (690 and 830 nm) FD instrument (Imagent V2, ISS, Champaign IL, USA), with a modulation frequency of 140.625 MHz. The symmetric arrangement was obtained by using two source fibers (\varnothing 400 μ m) and two detector fiber bundles (\varnothing 3 mm) paired at four fixed distances, short (25 mm) and long (35 mm). Frequency-domain measurements return, as elaborated output, complex reflectance signals against source-detector distance (i.e., the net optical flux exiting the tissue per unit source power) in two datatypes (intensity and phase), from which one can derive absolute optical properties of the diffuse medium [3].

The continuous wave probe component was realized with the same arrangement, based on two sources (shuttered tungsten halogen lamps AvaLight-HAL-S-Mini, Avantes) and two detectors (multi-mode broadband fiber switch LightBend 1x2 Mini, Photonwares, Woburn MA, USA) located at symmetric paired distances each other (the same used for the frequency domain side) [11]. The broadband emitted light was delivered using two fiber bundles (\varnothing 2 mm) and the shuttered state of light was controlled through a Transistor-Transistor Logic (TTL) signal from a micro-controller (Uno R3, Arduino, Ivrea, IT), connected to a control computer (see Fig. 9). The diffuse light instead, was collected by two detector fibers (\varnothing 600 μ m), connected to a spectrometer (AvaSpec-HERO, Avantes), through a fiber switch (LBMB, Photonwares, Woburn MA, USA). The latter was employed to acquire reflectance signals (real in CW domain) with a multiplexed system, sequentially switching all the possible source-detector combinations at different time interval.

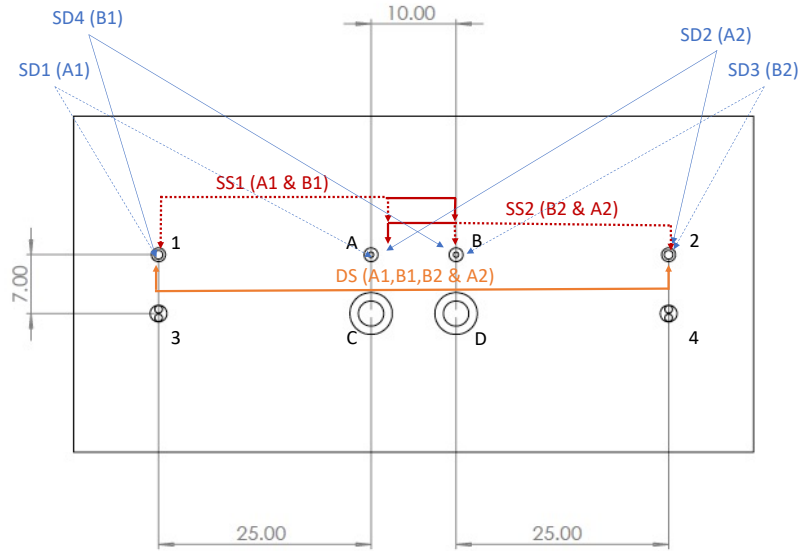


Figure 8: Scheme of the dual slope probe geometry combining CW and FD spectroscopy, each side containing two sources (1-2 for CW and 3-4 for FD) and two detectors (A-B for CW and C-D for FD). Source and detector distance is either 25 mm (short) or 35 mm (long). For each domain the possible configurations are: four single distance measurements in blue (SD), two shorts (dot arrows) and two long (solid arrows), two single slopes in red (SS), each one with short and long distances, one dual slope in orange (DS), with all the distances combined.

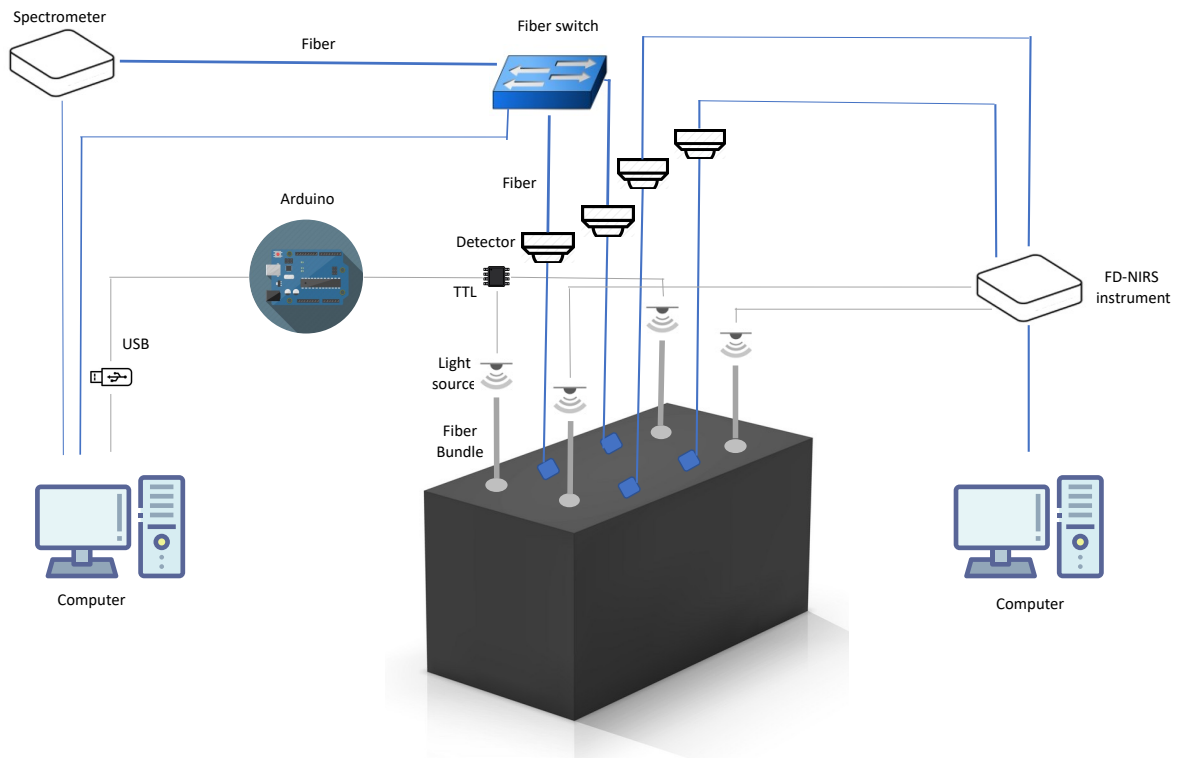


Figure 9: Device and instrumentation scheme to achieve absolute absorption spectra combining CW and FD spectroscopy. Acronyms: Transistor-Transistor Logic (TTL) and Universal Serial Bus (USB).

The multiplexing time required for a complete DS acquisition achieves sampling rates between 0.1 and 2.5 Hz, depending on whether higher SNR or speed is required, respectively [11]. This sampling value is too low to conduct functional measurements on the brain, since it's not fast enough to follow physiological signal changes, nevertheless it is sufficient for measuring skeletal muscle oxygenation, especially during arterial occlusion test. This drawback can be solved by introducing detectors with larger diameters, allowing for faster sampling rates suitable for brain measurements too. Another way adopted to increase the sampling rate is the optimization of all source and detector combinations, within each DS acquisition, by working on the fiber switch to reduce the switching number on the detector side, which takes the longest commutation time. An example of a full acquisition set using the DS-bDRS probe, with all sources (named with numbers, 1 and 2) and all detectors (named with letters, A and B) is given by:

$$\dots 1A] \rightarrow [1A \Rightarrow 2A \blacktriangleright 2B \Rightarrow 1B] \rightarrow [1B \Rightarrow 2B \blacktriangleright 2A \Rightarrow 1A] \rightarrow [1A\dots$$

where “ \Rightarrow ” and “ \blacktriangleright ” correspond to the source and detector fiber switch respectively. For each cycle acquisition, enclosed in squared brackets and separated by “ \rightarrow ”, only one detector switch appears.

Before being used for *in vivo* applications, the new instrument combining SC FD-NIRS with DS CW-bDRS was first validated using liquid phantoms, made with water and milk, with the addition of three-color dyes to achieve turbid media properties. The validation process confirmed the feasibility and capability of the system to measure absolute optical properties and distinguish spectral fingerprints of different dyes [3].

2.2 Mathematical model

2.2.1 Absolute optical properties

Absolute measurements are particularly important for monitoring tissues perfusion during resting states and improving relative measurements, adding information to assess intra and inter subject variability. The basic idea of the new probe is to obtain quantitative measurements of the absorbance spectra, by decoupling absorption and scattering contributions from the combination of CW with FD domain techniques. Even though they provide different information (complex signals in AC and phase for FD, and real signals in DC for CW), the same basic analysis was applied to DS intensity and phase measurements (DSI, DS ϕ), with an iterative method repeated for each separate wavelength.

Data were collected in a reflectance mode, with source and detector on the same side of tissue boundary and analyzed through analytical solutions provided by diffusion theory, considering the tissue as a semi-infinite medium. According to these expressions rearranged, the modified reflectance (\tilde{R}_{mod}), measured at different source-detector distances (ρ), results to have a quasi-linear relationship with ρ through the effective attenuation coefficient ($\tilde{\mu}_{\text{eff}}$) (see Eq. 11):

$$\ln(\tilde{R}_{\text{mod}}) = -\tilde{\mu}_{\text{eff}} \cdot \rho \quad (11)$$

where μ_{eff} is particularly significant in biomedical optics since its inverse provides a measure of the penetration depth achievable and it is strictly related to the tissue optical properties through the relationship (see Eq. 12) [5]:

$$\mu_{\text{eff}} = \sqrt{3 \cdot \mu_a \cdot (\mu'_s + \mu_a)} \quad (12)$$

Intensity and phase signals were first analyzed in the frequency domain, to convert and decouple complex μ_{eff} , into absorption ($\mu a_{\lambda_{1,2}}$) and reduced scattering coefficients ($\mu s'_{\lambda_{1,2}}$) at two wavelengths ($\lambda_1 = 690 \text{ nm}$ and $\lambda_2 = 830 \text{ nm}$). Then, with the same iterative method applied to CW data, absolute absorption spectrum was achieved by separating real μ_{eff} from a broadband $\mu s'_{\lambda_{CW}}$ [3, 11]. The latter was extrapolated for the CW spectrum of wavelengths (λ_{CW}), from $\mu s'_{\lambda_{1,2}}$ at discrete wavelengths (obtained from FD) and the power law decay expressed by Eq. (1), valid for turbid media (see Fig. 10).

Temporal variations in the absorption spectra were collected with the multiplexing approach, switching sources and detectors combinations. Since data recovered for each pair happened at different time points, reflectance measurements were linearly interpolated to the average time of the corresponding complete acquisition set. Thanks to this synchronization, dynamic data were recovered preventing potential temporal artifacts.

Once the absolute spectrum is retrieved across a full range of wavelengths, effective homogeneous concentration time traces of oxyhemoglobin and deoxyhemoglobin are calculated, by inverting Eq. 2. Moreover, through the same relationship, using the broadband spectrum it is also possible to recover concentration of other compounds, such as water and lipids, by using their known molar or specific extinction coefficients.

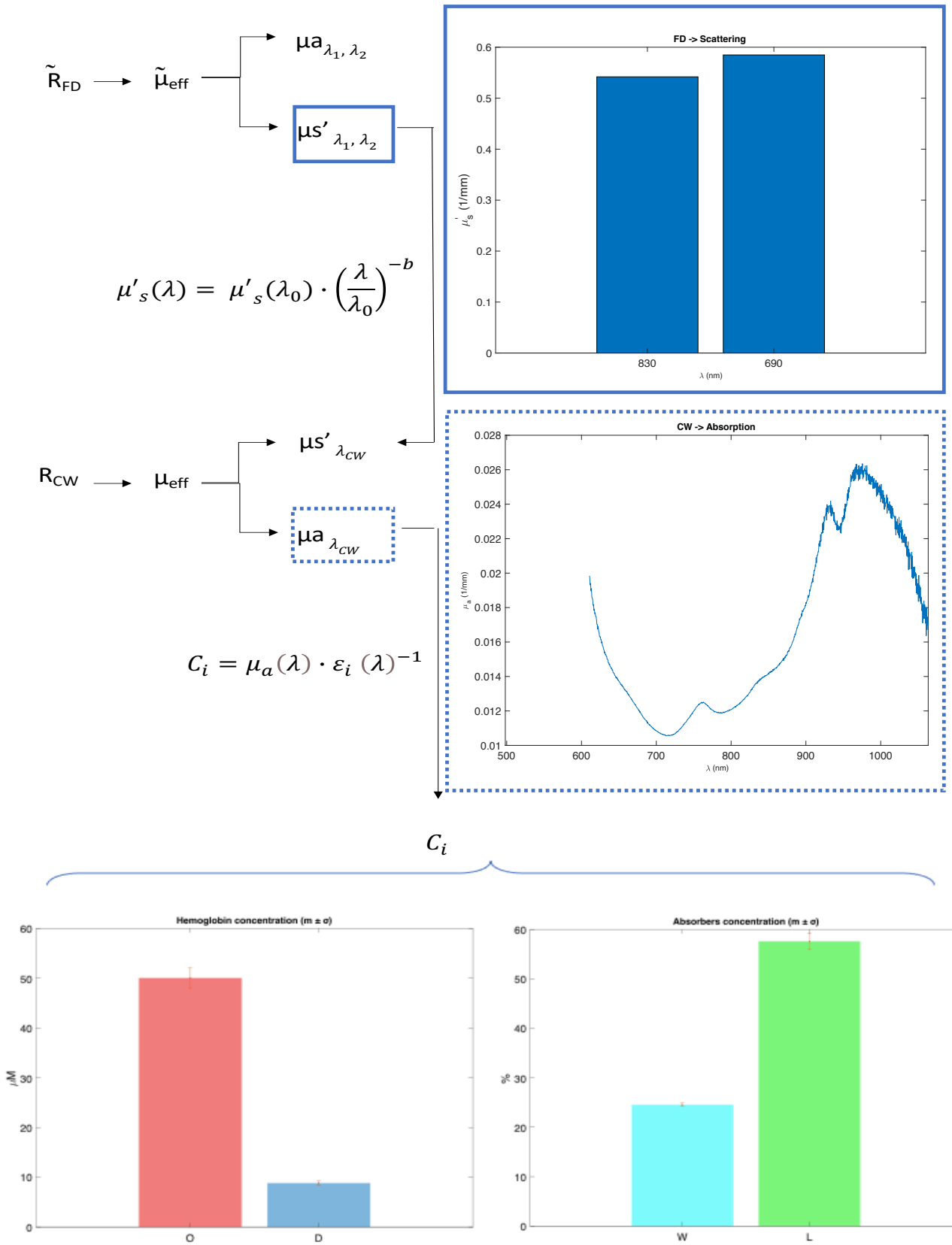


Figure 10: Flow-chart to achieve absolute absorption spectra and absorbers concentrations combining FD and CW spectroscopy with the DS probe. Representative plots are based on muscle in vivo measurements (gastrocnemius): first plot (on top) shows μ'_s recovered at two wavelengths (690-830 nm) from FD data. The second one represents broadband absorption spectra μ_a from CW data. Bottom plots show concentrations (C_i) recovery of oxy- (HbO₂) and deoxyhemoglobin (Hb) (on the left), expressed in μM and water and lipid (on the right), expressed in % v/v.

2.2.2 Relative optical properties

During functional NIRS protocols, information provided by absolute measurements is not essentials since what really matters is the capacity to discriminate between two conditions: activation during tasks and baseline at rest. To evaluate hemodynamic response and tissue oxygenation, it is therefore sufficient to measure relative changes in absorption coefficient, which in turn can be translated into relative chromophores concentrations.

In this study, relative absorption changes for all the methods (SD, SS, and DS) were collected in frequency domain at two wavelengths (λ_1, λ_2), evaluating intensity (I) and phase (ϕ) data separately, with the goal to achieve localized and deeper sensitivity of the investigated tissue [14]. To recover these absorption variations, first it is necessary to calculate the differential pathlength factor DPF, for SD measurements (or the differential slope factor DSP, analogous for slope methods, SS and DS), which depends on the ratio between the total optical pathlength $\langle L \rangle$, travelled by photons, and source detector distance (ρ) (see Eq. 13):

$$DPF = \frac{\langle L \rangle}{\rho} \quad (13)$$

Through this relationship, DPF is related to absolute values of absorption (μ_{a0}) and reduced scattering coefficients (μ'_{s0}), both recovered and averaged during a baseline period, in which they are considered constant (see Eq. 14, 15):

$$\mu_{a0} = \frac{wn}{2c} \cdot \left(\frac{DS\phi_0}{DSI_0} - \frac{DSI_0}{DS\phi_0} \right) \quad (14)$$

$$\mu'_{s0} = \frac{DSI_0^2 - DS\phi_0^2}{3\mu_{a0}} - \mu_{a0} \quad (15)$$

where w is the angular modulation frequency ($w=2\pi f$ with $f = 140.625 \text{ MHz}$), n is the index of refraction of the medium ($n = 1.4$) and c is the speed of light ($c = 2.99810 \cdot 10^8 \text{ m/s}$). Absolute properties are used exclusively for the calculation of $DPF_{I,\emptyset}$ or $DSF_{I,\emptyset}$, and are obtained by evaluating together intensity and phase data, collected with the dual slope probe in frequency domain[13].

Therefore, time traces of effective absorption changes can be recovered for each method (SD, SS, DS) and datatype (I, \emptyset). In particular, single distance intensity (SDI) data can be converted into $\Delta\mu_{a,SDI}$ using the modified Beer-Lambert Law and the DPF_I (see Eq. 16):

$$\Delta\mu_{a,SDI}(t) = -\frac{\frac{\Delta SDI(t)}{SDI_0}}{\rho \cdot DPF_I} \quad (16)$$

and a similar relation can be obtained for $SD\emptyset$ data (see Eq. 17):

$$\Delta\mu_{a,SD\emptyset}(t) = -\frac{\frac{\Delta SD\emptyset(t)}{SD\emptyset_0}}{\rho \cdot DPF_\emptyset} \quad (17)$$

Relative single slope changes can be converted as well into apparent (homogeneous) absorption changes by using the $DSF_{I,\emptyset}$, through the relationship expressed by Eq. 18, 19 (for single slope intensity, SSI , and phase, $SS\emptyset$, respectively).

$$\Delta\mu_{a,SSI}(t) = -\frac{\frac{\Delta SSI(t)}{SSI_0}}{DSF_I} \quad (18)$$

$$\Delta\mu_{a,SS\emptyset}(t) = -\frac{\frac{\Delta SS\emptyset(t)}{SS\emptyset_0}}{DSF_\emptyset} \quad (19)$$

Dual slope data are obtained by averaging two single slopes measurements and use the same $DSF_{I,\emptyset}$ (see Eq. 20, 21):

$$\Delta\mu_{\alpha,DSI}(t) = -\frac{\Delta SSI_1(t) + \Delta SSI_2(t)}{2 \cdot DSF_I} \quad (20)$$

$$\Delta\mu_{\alpha,DS\emptyset}(t) = -\frac{\Delta SS\emptyset_1(t) + \Delta SS\emptyset_2(t)}{2 \cdot DSF_{\emptyset}} \quad (21)$$

Hence, each time trace of the absorption effective changes, recovered with different methods, can be converted into time traces of oxyhemoglobin (ΔHbO_2) and deoxyhemoglobin (ΔHb) concentration changes through their known extinction coefficient, by inverting Eq. 2.

2.3 Simulations

A further characterization of the method was achieved through a parametrical simulation study based on diffusion theory, performed to evaluate the sensitivity region of the DS data in two-layer media. In fact, compared to the commonly used hypothesis of homogeneous medium, two-layer models allow to better represent heterogeneous properties that characterize biological tissues. Previous studies have shown the optical characterization of turbid media comparing homogeneous and two-layer model analytical solutions of the diffusion equation using time-resolved spectroscopy [15, 16, 17, 18].

In this study, a forward model, based on the simulated instrument comprising FD and CW domain portion at two source-detector distances of 25 and 35 mm, has been used to model a two-layer medium [11]. The model took 13 parameters as input, parametrized within physiological ranges (featuring adipose tissue on top layer and skeletal muscle on bottom), and returned as output the complex reflectance in FD at two wavelengths (690 and 830 nm) and the real CW reflectance for a broadband spectrum of wavelengths ($\sim 650\text{-}1000$ nm). The parameters described the chromophores concentration and scattering optical properties wavelength-dependent in the two layers and they were represented by total hemoglobin content, oxygen saturation, water and lipid content, reduced scattering coefficient $\mu_s'(\lambda)$ at 830 nm, the power law exponent (b) and the top layer thickness.

From the linear combination of extinction coefficients weighted by chromophores concentration, the absorption coefficient was recovered for each layer and used with the broadband $\mu_s'(\lambda)$ to retrieve the complex and real reflectance, for FD and CW domain respectively. By inverting this model with mathematical formula exposed in Section 2.2, the simulated reflectance was now used as input to recover the absolute chromophores concentrations. These recovered concentrations are defined apparent, since with the inversion model only a single value is recovered, comprised in the input range of values characterizing the two-layer model (see Table 3).

Table 3: Two layers model actual parameters (forward model) and recovered parameters (inverse model). Acronyms: total hemoglobin (T), oxygen saturation (S), water (W) and lipid (L).

Simulation parameters						
	T (μM)	S (%)	W (%)	L (%)	$\mu\text{s}'(830\text{nm})$ (1/mm)	b
1st layer	12	83	5	70	0.6	0.1
2nd layer	120	67	90	20	0.4	1.5
Recovered	94	69	48	30	0.5	0.9

By changing one parameter at a time, it was evaluated its influence on the recovery of the others, as resume by Figure 11 and 12. For simplicity there are shown only parameters changed in the first layer (top), but the following consideration can be applied also if the changing values were in the bottom layer. Solid lines represent the recovered values whereas dashed and dotted lines refer to top and bottom layer actual values. Colors indicate in order total hemoglobin (T), oxygen saturation (S), water (W) and lipid (L). Regarding the tissue absorbers, apart from total hemoglobin (sum of oxy- and deoxyhemoglobin), which also affects water and lipid content recovered values, probably because of their crosstalk spectra with oxyhemoglobin, each other parameter influences mainly its corresponding recovered value.

By changing optical properties such as reduced scattering coefficient at 830 nm all the recovered values are slightly affected, pointing out how this property plays a role and affects results during *in vivo* measurements (see Fig. 12). In particular, as the reduced scattering coefficient increases, water and lipid recovered increase whereas total hemoglobin slightly decreases. As concerns the power value (b), it affects mostly water and lipid content without changing hemoglobin parameters. Finally, it has been evaluated how changing the first layer thickness (expressed as z_{top}) could affect results: as this value increases, the recovered values get closer to actual values of the top layer.

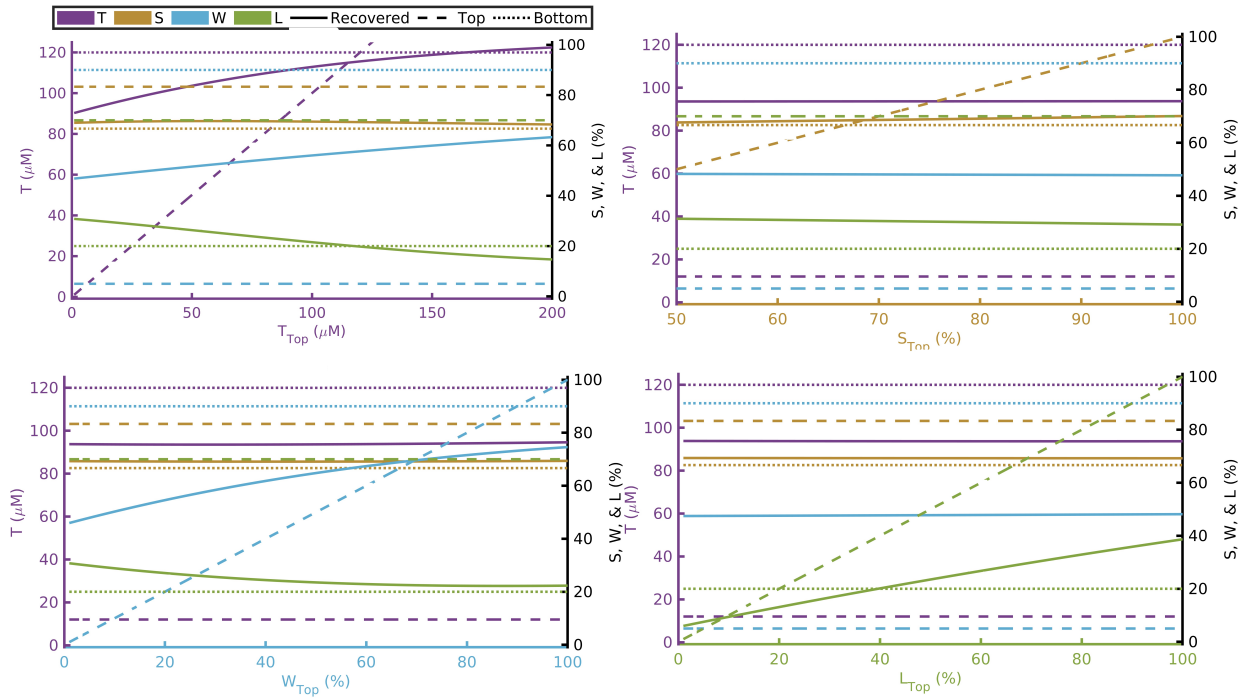


Figure 11: Parametric simulation obtained by changing one parameter at a time, to study how it affects the other recovered values. The figure shows the effect of changing total hemoglobin (top left), oxygen saturation (top right), water (bottom left) and lipid content (bottom right) in the top layer.

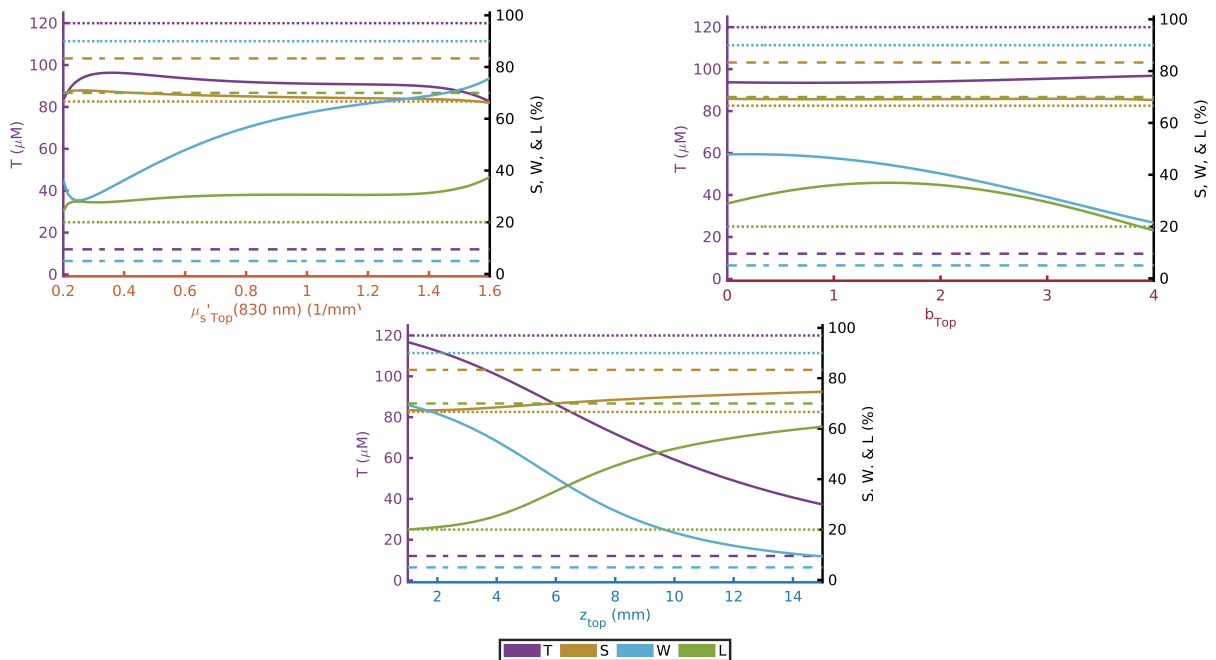


Figure 12: Parametric simulation obtained by changing one parameter at a time, to study how it affects the other recovered values. The figure shows the effect of changing reduced scattering coefficient at 830 nm (top left), power law exponent, b (top right), and first layer thickness (bottom right) in the top layer.

The aim of this simulation study, based on a two layer-model, was to investigate the relationship between actual values, on top and bottom layers, with the recovered effective ones, highlighting how each parameter could affect differently the others. These results should be taken into account when considering a real tissue, being more representative of the heterogeneity that characterized it.

3. Measurements on skeletal muscles

3.1 Introduction

The capacity of monitoring in real-time oxygenation levels and metabolism parameters of biological tissues, such as skeletal muscles and brain, is of great importance in order to assess their functional capacity and pathophysiological mechanisms underlying some disease conditions [20, 21, 22]. However, the measurement of these quantities often requires expensive instruments or employs invasive and not portable techniques, not suitable in dynamic environments and in patients where testing opportunities are restricted. In this context, near-infrared spectroscopy has been proposed over time as an alternative, non-invasive, portable, and cost-effective method capable of evaluating oxygen supply and consumption, as indicators of tissues oxidative capacity, by measuring local hemoglobin concentrations [23].

As concerning studies on skeletal muscles, the main absorbing compounds in the window (~ 650 -1000 nm) are hemoglobin and myoglobin (Mb), defined as the oxygen-carrier proteins in blood and in muscle cells respectively, followed by water and lipid for the upper limit of wavelengths. Unfortunately, the spectral absorbance of the two protein chromophores is superimposed and their indistinguishable contributions to the signal should be taken into account when considering absolute measurements. However, Mb contribution can be assumed negligible in studies that involve relative measurements resulting from hemodynamic perturbations, due to its lower molar extinction coefficient and limited spatial distribution compared to hemoglobin. In fact, Mb is localized in muscle cells and unlike hemoglobin, Mb is not present in neighboring tissues investigated by optical measurements [24]. In particular, the contribution provided by hemoglobin to NIRS signal mainly originates in microvascular circulation, with blood vessels < 1 mm of diameter, since light is almost completely absorbed in larger ones [23].

From hemoglobin concentrations, two relevant physiological parameters can be recovered for skeletal muscles response: muscle blood flow (mBF), defined as the amount of blood flowing per unit volume of tissue per unit time (expressed in $\text{mL}_{\text{blood}}/100 \cdot \text{mL}_{\text{tissue}}/\text{min}$) and oxygen consumption ($\text{m}\dot{\text{V}}\text{O}_2$), defined as the amount of oxygen consumed per unit volume of tissue per unit time (expressed in $\mu\text{molO}_2/100 \cdot \text{mL}_{\text{tissue}}/\text{min}$) [5]. To evaluate their hemodynamic response following blood circulation perturbations, commonly used NIRS

protocols involve venous and arterial occlusions, either at rest or during exercise conditions [19, 20, 27, 28]. By controlling the inflation pressure of a cuff placed around a subject's limb, occlusion experiments affect the blood circulation in distal tissues. Pressures were selected below and above the reference systolic (120 mmHg) and diastolic (80 mmHg) arterial pressures, depending on the blood perturbation desired. In particular, a pressure of 60 mmHg, below arterial pressure range and higher than venous one, blocked only the venous return, featuring a blood accumulation and local changes of mBF. Instead, a pressure of 230 mmHg, out of both pressure intervals, also occludes the arterial compartment and interrupts all blood flow to and from distal tissues. Under this condition, part of oxyhemoglobin is converted into deoxyhemoglobin, in agreement with tissues oxygen demand from plasma, and the rate of this desaturation process provides a direct measure of $m\dot{V}O_2$.

In general, NIRS measurements are commonly affected by confounding contributions from skin vascularization, closely connected with different adipose tissue thicknesses. Trying to reduce these noisy effects, different studies evaluated the site and probe-spacing dependence on deep layer sensitivity, finding a potential solution in the use of multi-distance approaches, given their greater ability to discriminate space-dependent signals [29]. In this work, *in vivo* measurements of the muscle blood flow and oxygen consumption of the calf muscle are presented, involving a protocol based on two occlusions performed at rest. Data have been collected with the Dual Slope probe, combining Frequency Domain and broadband Continuous Wave spectroscopy, to achieve absolute concentrations of oxyhemoglobin [HbO_2], deoxyhemoglobin [Hb], water and lipid, by employing light sources in the wavelengths range between 650 and 1000 nm. Moreover, it has been investigated the deep layer sensitivity and potential use of the novel multi distance approach, by comparing it with mBF and $m\dot{V}O_2$ values recovered using the more traditional method based on single distances.

3.2 Materials and Methods

3.2.1 Protocol

The protocol of this study evaluates the hemodynamic response and tissue oxygenation levels in human calf muscle, specifically gastrocnemius, during a venous occlusion (VO) and arterial occlusion (AO) test. Three healthy subjects participated, giving their written informed consent according to a protocol approved by the Tufts Institutional Review Board. Measurements were taken five times over different days for each volunteer. Characteristics of the subjects and skinfold thicknesses are shown in Table 4. Adipose tissue thickness above the muscle, composed by skin layer and fat, was measured using a skinfold caliper and divided by 2. The experiment was conducted with subjects lying on a bed, with the involved leg slightly raised to avoid venous pooling of the blood [26].

Table 4: Subjects' demographic information and thickness of forearm and calf tissues.

Subjects' information						
Sub	Age	Sex	Height (m)	Mass (Kg)	Tissue	Thickness (mm)
1	25	Female	1,63	50,5	Forearm	$2.1 \pm 0,3$
					Calf	$4.6 \pm 0,6$
2	28	Male	1,96	99,8	Forearm	$5,8 \pm 0,2$
					Calf	$6,4 \pm 0,2$
3	25	Female	1,47	57,4	Forearm	$4,8 \pm 0,2$
					Calf	$9,4 \pm 0,5$

The probe was positioned on the calf muscle using a sport tape and covered by a black tool to achieve a good contact between the probe and the tissue and avoid environmental light effects (see Fig. 13). The pneumatic cuff used for the occlusions was placed around the thigh of the subject and tightened with a belt to avoid outward expansion, when turned on.

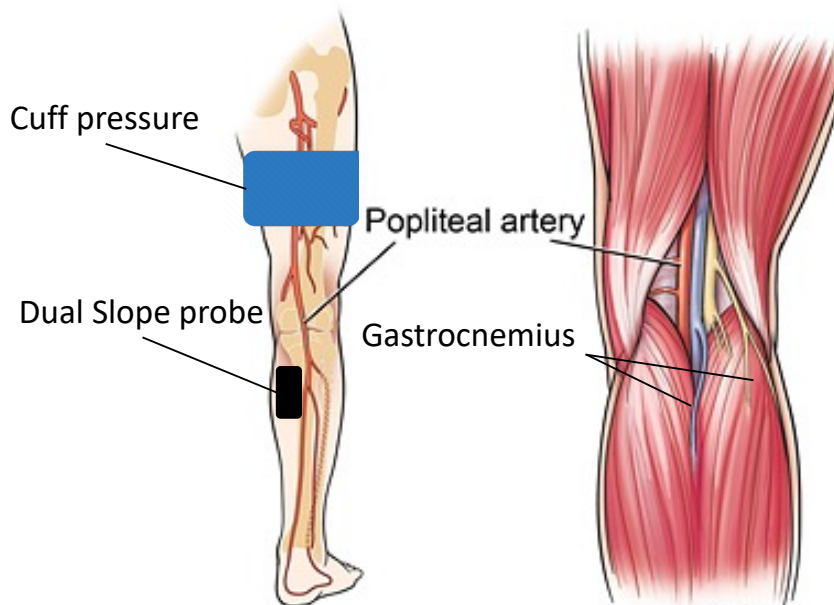


Figure 13: Scheme of the probe and cuff pressure placement, on the calf muscle (gastrocnemius) level.

The entire protocol can be divided in two sections, according to the information content desired (absolute optical properties or chromophores concentration) and the techniques used to achieve it. In particular, frequency domain NIRS was used before and after the occlusion protocol, to recover absolute optical properties during baseline periods of 1 min. Then, measurements of the hemodynamic response and chromophores times traces during the occlusion test were recovered using the broadband CW domain probe (see Fig 14). The experiment started with a baseline period of five minutes, followed in order by 1 min of venous occlusion (VO), 1 min of recovery, 2 min of arterial occlusion (AO) and 2 min of final recovery (lasting 11 min total). During the occlusions, cuff was inflated and the pressures (60 mmHg for venous occlusion and 230 mmHg for arterial occlusion) were maintained constant until the end of the perturbation period, releasing the pressure band through a deflation valve.

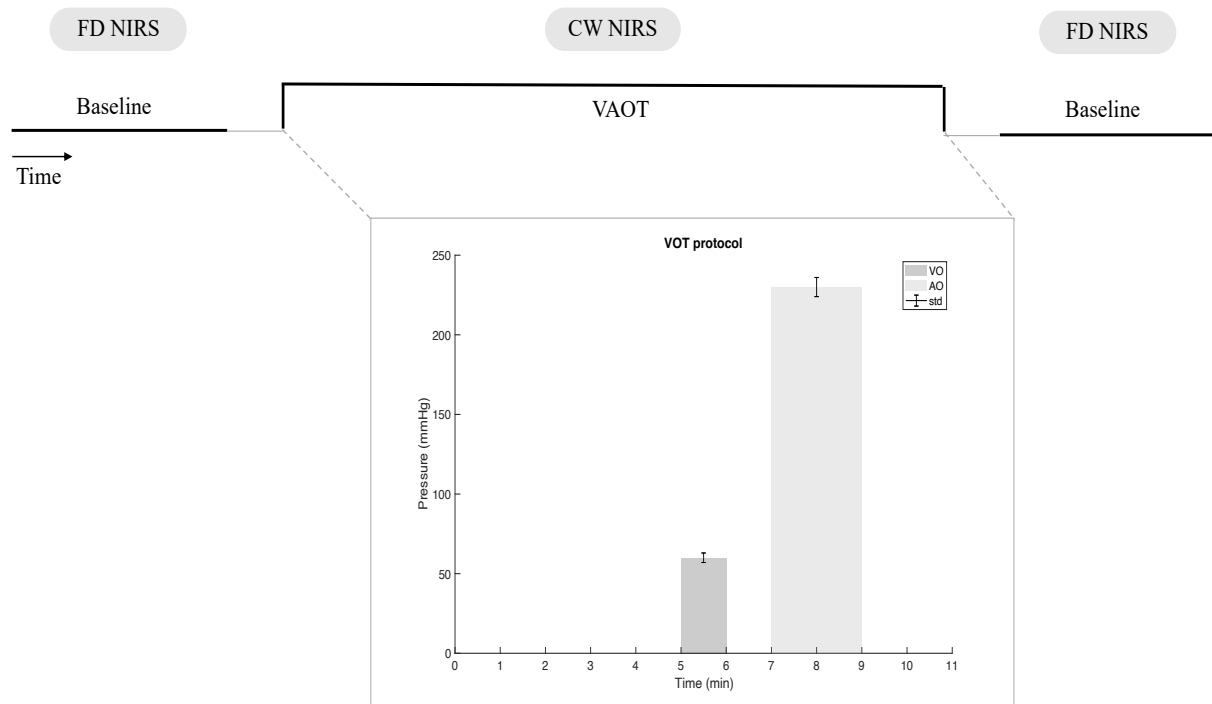


Figure 14: Venous and arterial occlusion test (VAOT) protocol scheme, combining Frequency Domain Near Infrared Spectroscopy (FD-NIRS) and Continuous Wave broadband Diffuse Reflectance Spectroscopy (CW-bDRS), using the Dual Slope (DS) probe on the calf muscle: two baseline measurements of 1 min each were collected before and after the occlusion test with FD, to achieve absolute $\mu s'0$. VAOT data were recovered with CW domain as following: 5 minutes of baseline, 1 min of VO, 1 min rest, 2 min of AO, 2 min rest (11 minutes total). Cuff was activated manually with a pressure of 60 mmHg and 230 mmHg, during VO and AO respectively.

3.2.2 Instrument

The measurements on skeletal muscles were performed using the Dual Slope probe, which combines FD and broadband CW domain NIRS. The experimental arrangement is depicted in Fig. 9 (Chapter 2.1). As concerns the frequency domain probe, data were collected at two wavelengths (690 and 830 nm) using an intensity modulated light at a frequency of 140.625 MHz. Each data point was achieved every 0.1 s with a sample rate of 10 Hz. CW data were recovered through a multiplexed system, which could afford a mean sample rate of 0,08 Hz, mean since each single acquisition took different times. This low value was considered suboptimal but acceptable to evaluate tissue oxygenation in skeletal muscles, but not suitable for studies involving the hemodynamic response of the brain. This is the reason why in the brain protocol of this work, data were collected only in frequency domain. In the future this problem could be solved by introducing detectors with larger apertures, achieving higher sample rates to follow faster signals.

Recovered diffuse optical signals were analyzed in two different ways depending on whether the goal was to evaluate absolute time traces of chromophores concentration or relative changes of hemoglobin, comparing Single Distance and Dual Slope methods (see Section 2). In both cases data were first collected in FD in order to achieve absolute optical properties during baseline periods (before and after the occlusion protocol). Hence, using the CW domain probe with a broadband spectrum of light between 650 and 1000 nm, the achieved values of μ_s' at two wavelengths were averaged and used, under the assumption of constant scattering, to quantify absolute absorbance spectra. From the latter, the concentration of four different absorbers was evaluated: oxyhemoglobin, deoxyhemoglobin, water and lipid. This is the reason why the range of wavelengths involved in this study has an upper limit (~ 1000 nm) higher than the commonly used one in NIRS studies (~ 900 nm), to include the absorbing effect of other compounds, like water and lipid, particularly present in muscle and adipose tissue, respectively.

As concerning relative measurements, baseline optical properties were used only to achieve the DPF and DSF specific for each subject (for single distance and dual slope methods, respectively) and measure changes of the absorption coefficient. In this case, only oxy- and deoxyhemoglobin were considered, in accordance with the assumption that water and lipid variations should be considered negligible during occlusions protocol performed at rest.

3.2.3 Total hemoglobin concentration and tissue oxygen saturation

The total content of hemoglobin can be calculated from the sum of absolute oxy- and deoxyhemoglobin concentrations, expressed in μM , as a measure of the blood volume in the investigated tissue (see Eq. 22):

$$[HbT] = [HbO_2] + [Hb] \quad (22)$$

Instead, the ratio of oxy- and total hemoglobin content provided a measure of tissue oxygen saturation (StO_2), expressed in % according to (see Eq. 23):

$$StO_2 = \frac{[HbO_2]}{[HbT]} \quad (23)$$

Tissue oxygen saturation is a result of the weighted average between the oxygenated levels of arterioles and deoxygenated blood of small veins. Typical values in muscle tissues during baseline periods are in the range of 60-100 μM for $[HbT]$ and 70-80% for StO_2 [5].

3.2.4 Muscle blood flow and oxygen consumption

During venous occlusion, the venous outflow is blocked, whereas the arterial inflow is not affected. This results in blood volume accumulation, due to the increase of oxy- and deoxyhemoglobin concentrations, hence of the total hemoglobin content $[HbT]$. StO_2 instead shows a slight decrease due to the accumulation of venous blood. A measure of the muscle blood flow (mBF) can be retrieved from the initial rate of increase of total hemoglobin, following the occlusion, through the relationship (see Eq. 24):

$$mBF = \frac{1}{C} \left. \frac{d[HbT]}{dt} \right|_{max} \quad (24)$$

where C is the hemoglobin concentration in blood (typically 2,3 mM) and the subscript *max* indicates the highest value of the time derivative of total hemoglobin concentration, after the cuff inflection. Typical values of $m\overline{BF}$ in skeletal muscle at rest are in the range 0,1-5,3 mL_{blood}/100·mL_{tissue}/min [25].

During arterial occlusion, both flow compartments are interrupted, and a portion of oxyhemoglobin is converted into deoxyhemoglobin, in accordance with oxygen demand which instead continues. Muscle oxygen consumption ($m\dot{V}O_2$) can be quantified from this rate of desaturation, according to Eq. 25:

$$m\dot{V}O_2 = 4 \cdot \frac{d}{dt} \left(\frac{[HbO_2] - [Hb]}{2} \right) \quad (25)$$

where the factor 4 considers the four oxygen binding sites in the hemoglobin molecule. In theory, the rate of changes of the two species of hemoglobin should be the same, as a result of constant blood volume (or [HbT]), but in practice a slightly local change can occur, due to blood redistribution within the limb. Consequently, StO_2 decreases as a result of the different balance between oxygen supply and utilization. Typical values of $m\dot{V}O_2$ in skeletal muscles at rest are in the range 1,5-12,3 $\mu\text{molO}_2/100 \cdot \text{mL}_{\text{tissue}}/\text{min}$ [25].

3.3 Results

3.3.1 Absolute measurements

Time traces of absolute concentrations of oxy- [HbO₂] and deoxyhemoglobin [Hb], expressed in μM , with water [W] and lipid [L], expressed in % v/v, are shown in Fig. 15, for each subject (one out of five representative trial). Values recovered during 5 minutes of baseline are in line with the ones found in a previous work for the calf muscle of subjects 2 and 3 [15]. Looking at each time trace, water and lipid almost remain constant during the experiment, as expected for protocol performed at rest, even though the latter shows a trend similar to oxyhemoglobin during the AO. This is probably due to crosstalk of their absorbance spectrum since the peak of lipid (around 930 nm) is overlapped to the oxyhemoglobin absorbance spectrum in this range (see Fig. 16).

Venous and arterial occlusion intervals are represented by grey windows, chosen visually considering time variability due to manual activation of the cuff. During venous occlusion oxy- and deoxyhemoglobin don't show the expected rate of increase and muscle blood flow values. This is probably due to the slow sample rate achieved by the multiplexed system, highlighted in this figure by using the dot line, where each dot represents a single data point. As concerns arterial occlusion instead, the decrease of HbO₂ and increase of Hb are visible and provide values of muscle oxygen consumption in agreement with the literature (see Fig. 17) [25].

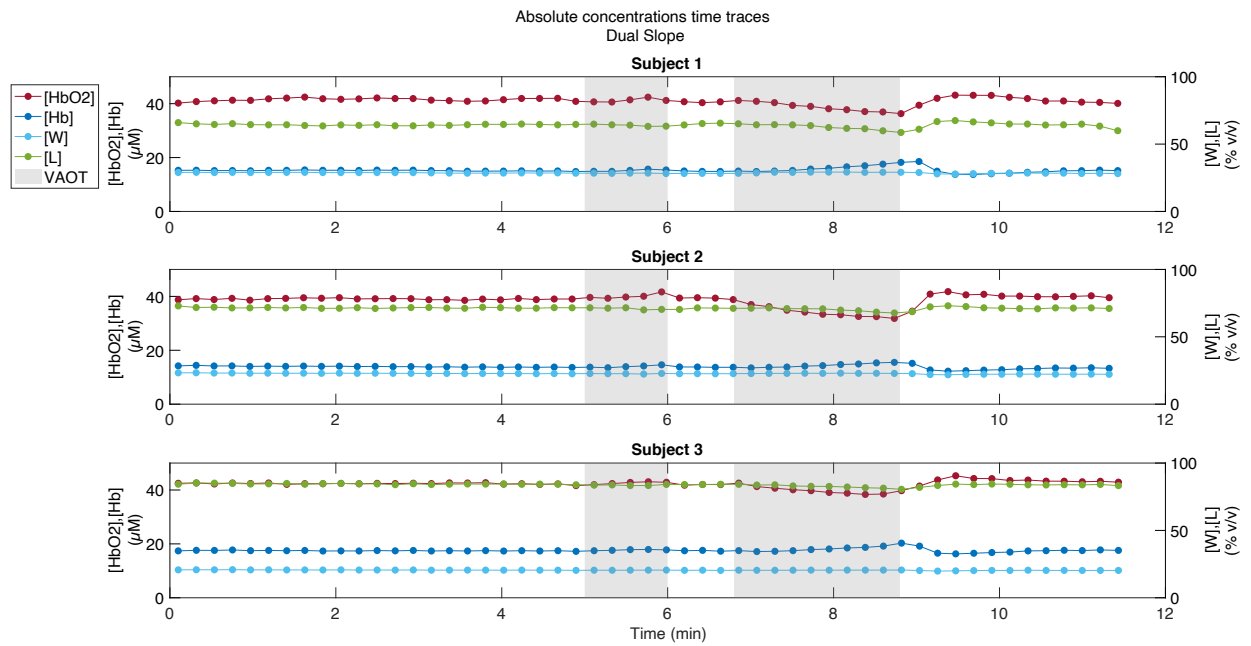


Figure 15: Representative absolute concentration time traces for each subject recovered during VAOT on calf muscle with CW domain probe. Oxyhemoglobin (red) and deoxyhemoglobin (blue) are expressed in μM , whereas water (light blue) and lipid (green) are expressed in units of % v/v. Grey windows represent time intervals with cuff pressure turned on for venous (60 mmHg) and arterial occlusion (230 mmHg).

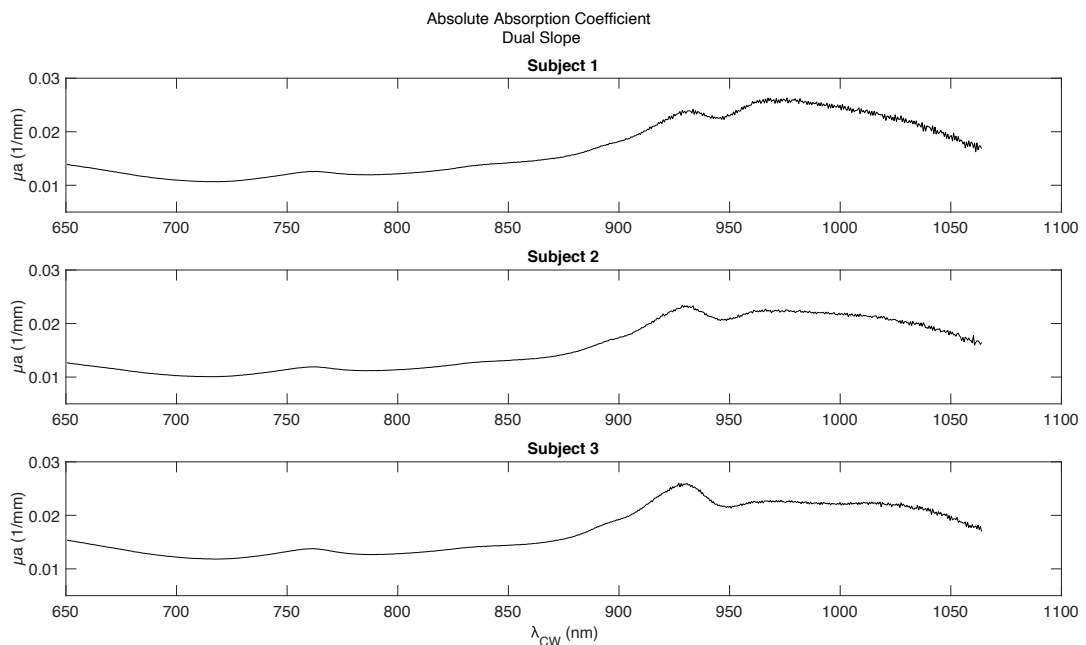


Figure 16: Absolute absorption coefficient (μ_a) recovered on each subject calf, averaged during baseline for each wavelength (range 650-1064 nm) and expressed in units of 1/mm. Peaks around 930 and above 950 are mainly due to lipid and water, respectively.

From oxy- and deoxyhemoglobin concentrations were calculated the values of the total hemoglobin content [HbT], expressed in μM , and tissue oxygen saturation (StO_2), expressed in %. During venous occlusion, as a result of blood accumulation, [HbT] shows only a slightly increase, confoundable with the baseline “noise”. This probably depends on the slow sample rate, the adipose tissue thickness covering the muscle or a high-pressure contact between the probe and the tissue, against which previous study have shown its effect on mBF during venous occlusion. StO_2 remains almost constant, whereas a linear decrease it’s evident during arterial occlusion, as expected by the imbalance between oxygen consumption and supply. The small decrease of HbT during AO is probably due to blood redistribution within the limb. After cuff release, StO_2 shows an overshoot related to the hyperemic response following blood flow interruption. The tissue oxygenation values recovered are coherent with what found in literature, whereas [HbT] measurements are slightly smaller. This is probably due to the broadband range of wavelengths used to include absorption effect of water and lipid, that underestimates oxy- and deoxyhemoglobin, compared to studies with more limited range of wavelengths.

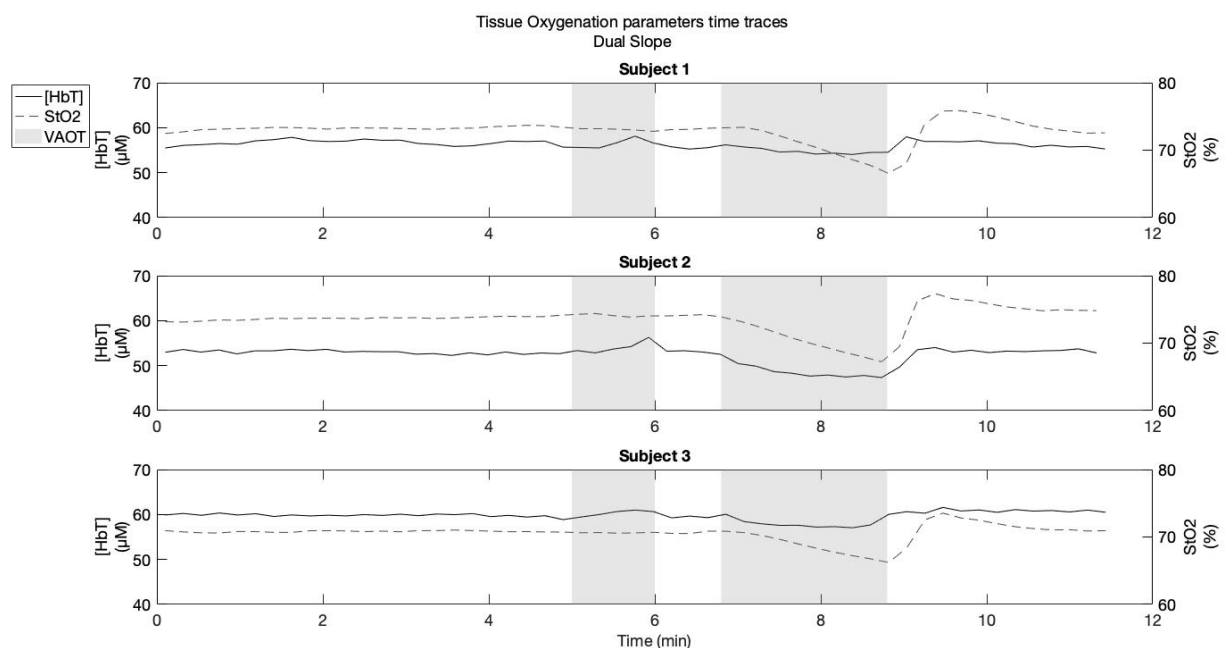


Figure 17: Representative tissue oxygenation parameters time traces recovered on each subject calf muscle during VAOT with CW domain probe. Total hemoglobin concentration [HbT] (solid black line), expressed in units of μM , and Oxygen Saturation Level StO_2 (dashed grey line), expressed in %. Grey windows represent time intervals with cuff pressure turned on for venous (60 mmHg) and arterial occlusion (230 mmHg).

Figure 18 shows time traces concentrations of oxy-, deoxy- and their half difference ($Hb_{diff} = (HbO_2 - Hb)/2$) for each subject, zoomed only during arterial occlusion since it gave a better hemodynamic response. The muscle oxygen consumption is evaluated by taking the minimum value of time derivative decrease of Hb_{diff} during the AO, close to cuff inflection. The different rate of oxy decrease and deoxyhemoglobin increase is visible and probably due to blood redistribution, following the occlusion.

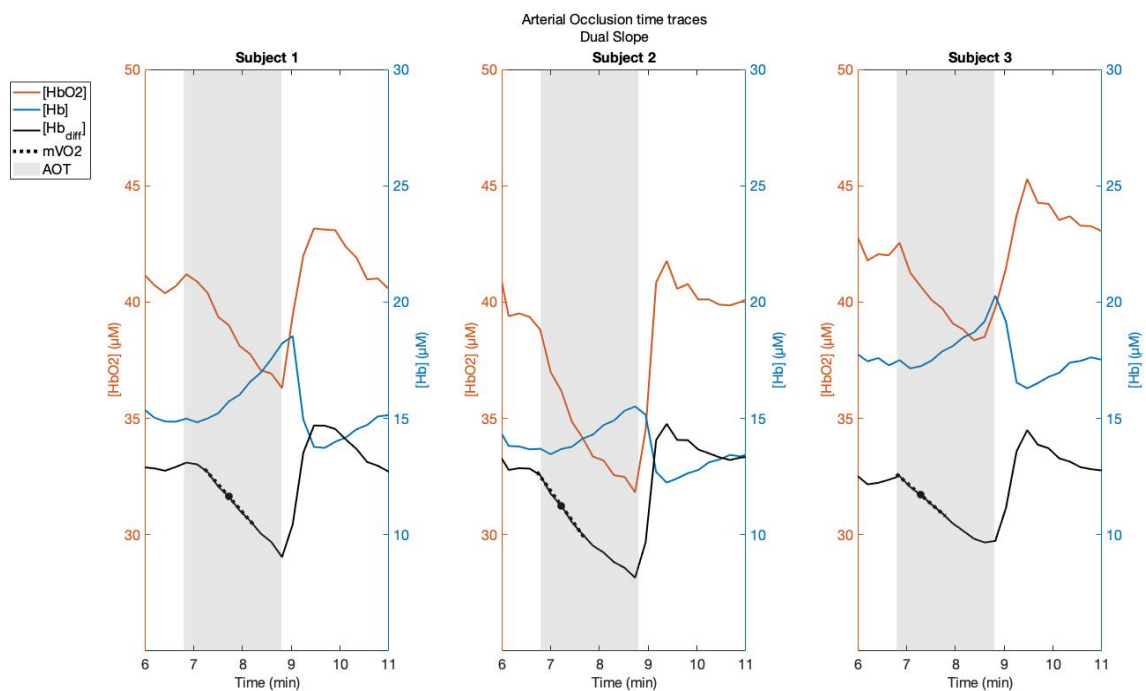


Figure 18: Representative absolute hemoglobin concentration time traces zoom during AO, recovered on each subject calf muscle with CW domain probe. Oxyhemoglobin $[HbO_2]$ (red), deoxyhemoglobin $[Hb]$ (blue) and their half difference $[Hb_{diff}]$ (black solid line) concentrations are expressed in units of μM . Dot line slope (black) represents Hb_{diff} decrease due to oxygen consumption during AO. Grey windows represent time interval with cuff pressure turned on (230 mmHg) during arterial occlusion.

3.3.2 Relative measurements

Figure 19 shows relative changes of oxy- and deoxyhemoglobin recovered with single distance (SD1, SD2, SD3 and SD4), single slope (SS1, SS2), and dual slope (DS) methods for subject 1 (considered as a representative case), assuming negligible changes for water and lipid. During arterial occlusion, long single distances and slope methods, that match deeper penetration depth (muscle tissue), measure higher hemoglobin concentration changes, compared to short single distances, more sensitive to superficial layers (adipose tissue). Whereas during venous occlusion this behavior is inverted, with higher values recovered by short single distances. These results affect in the same way muscle blood flow and oxygen consumption measured during VO and AO respectively, and they can find a possible explanation in previous studies, which demonstrated that muscle blood flow in adipose tissue appeared higher than in muscles [30], due to the little oxygen extraction by cutaneous tissues, that increases oxyhemoglobin signal in superficial layers [23]. Since the skin vascularization can contribute as a confounding effect on NIRS signals, whose goal is to achieve the hemodynamic response in deeper tissues (muscles), the fact that dual slope recovers smaller mBF values during venous occlusion and higher oxygen consumption during arterial occlusion, demonstrates its greater sensitivity to deeper layers.

Negative change in hemoglobin concentrations recovered with one single slope during VO is probably related to the negative region of sensitivity towards superficial layers, typical of this method. Dual slope can compensate this effect since data are recovered as the average of two symmetric single slopes and show more stable time traces.

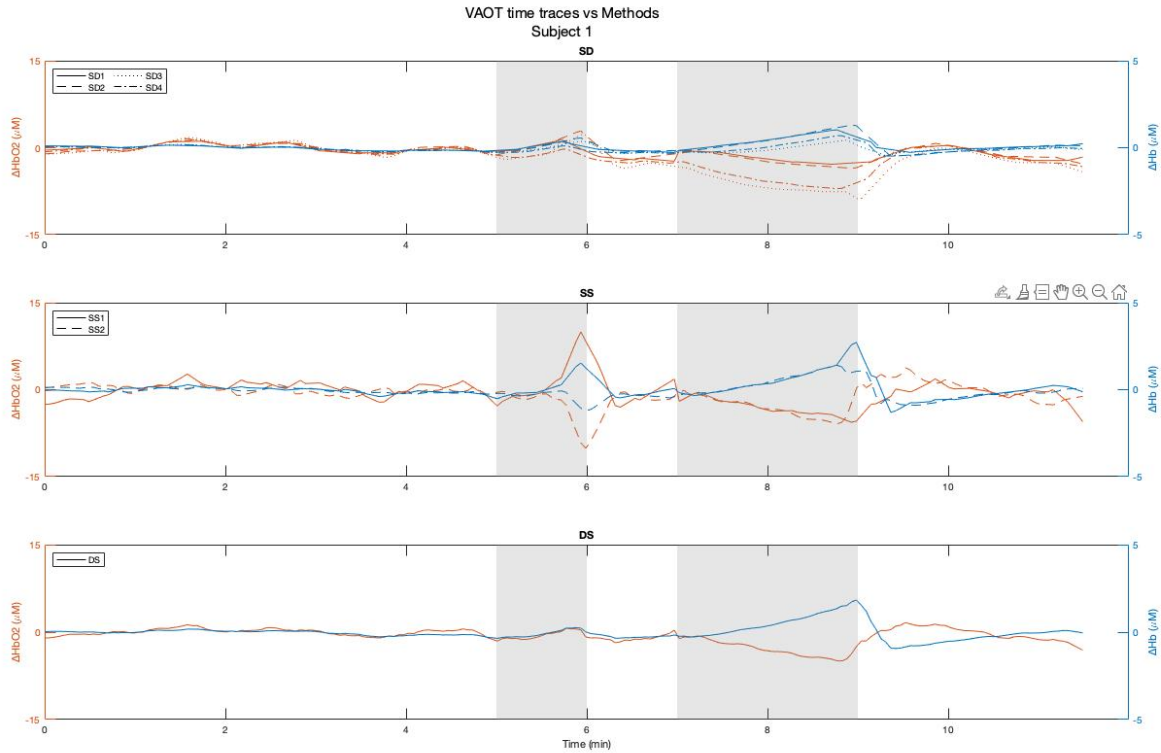


Figure 19: Representative time traces for subject 1 of relative hemoglobin concentrations, recovered on gastrocnemius with CW domain probe. Each subplot represents data recovered with a different method: Single Distance, SD (on top), Single Slope, SS (center) and Dual Slope, DS (bottom). Oxyhemoglobin [ΔHbO_2] (red) and deoxyhemoglobin [ΔHb] (blue) concentration changes are expressed in units of μM . Grey windows represent time intervals with cuff pressure turned on during venous and arterial occlusion. In the legend: SD_{1,3} and SD_{2,4} are short (25 mm) and long (35 mm) distances respectively, instead SS₁ and SS₂ are the two single slopes composed by short and long distance each.

Figure 20 shows the mean and standard deviation values of muscle oxygen consumption calculated during the arterial occlusion, from the time derivative of Hb_{diff} (see Eq. 25). Values are reported for each method, averaged across 5 trials for each subject. In general, long single distances (SD_{2,4}) show higher values than short ones (SD_{1,3}), due to their bigger penetration depth through deep layers (muscle). However, slope methods measurements have higher values than single distances, as a result of their enhanced sensitivity towards muscle tissue. In particular, one of the two single slopes shows always a higher value, and this is probably related with the specific orientation of the probe for each trial, which investigated volumes with different adipose tissue thicknesses covering the muscle. Dual slope values are around the middle of the two single slopes range, in agreement with what expected from the Eq. 20. In general, muscle oxygen consumption measurements in this study are coherent with the lower

limit range found in literature, probably due to the extension of the broadband range to include the contribution of lipid, resulting in the underestimation of the oxyhemoglobin concentration.

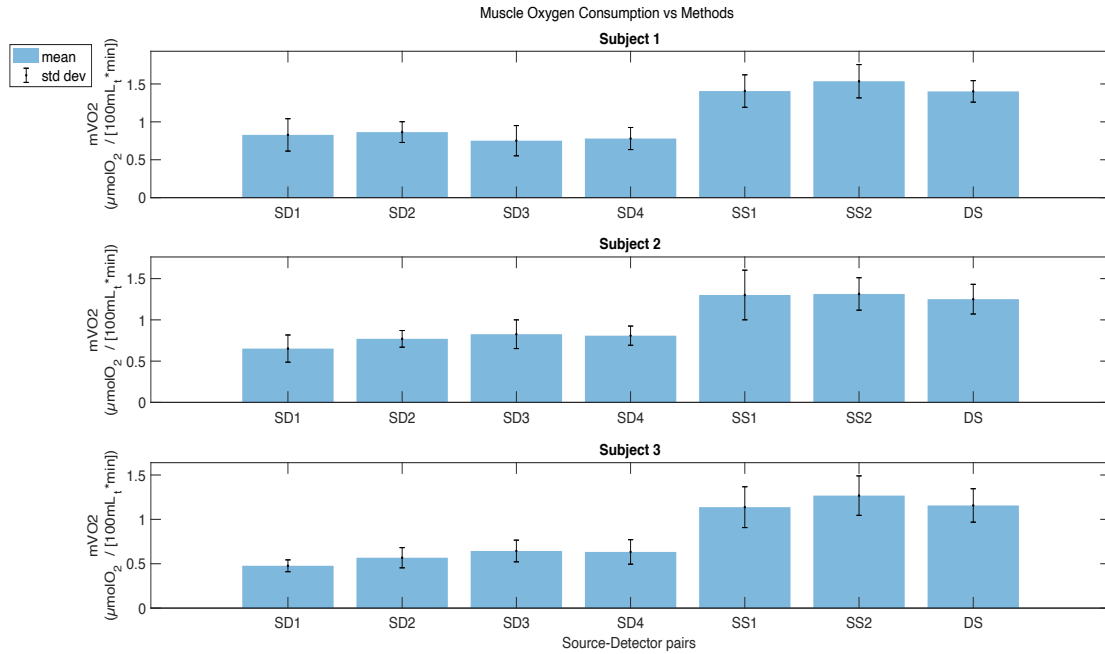


Figure 20: Histogram showing muscle oxygen consumption (mVO_2) expressed in $\mu\text{molO}_2/100\text{mL}_{\text{tissue}}/\text{min}$, recovered during arterial occlusion (AO) for each subject calf muscle with CW domain probe. Bars represent mean values with standard deviation across days (5 days-trials) for each subject. Acronyms: Single Distance (SD), Single Slope (SS) and Dual Slope (DS).

Since time derivative traces recovered for HbT with broadband multiplexed CW spectroscopy were too small, due to the slow sample rate achieved by the fiber switch (0.08 Hz), they were not shown and included in this study. However, in order to evaluate the effectiveness of the Dual Slope probe configuration regardless of the NIRS domain involved, a parallel study conducted in Frequency Domain featuring a faster sample rate (10 Hz) was taken as a reference for further considerations. Data were collected on two subjects involving a smaller muscle in the forearm (brachioradialis), covered with a thinner thickness layer of adipose tissue, compared to the gastrocnemius (see Table 4 for subjects' information). Moreover, unlike the first protocol, for this parallel study venous occlusion lasted 3 minutes in order to achieve the full filling of blood vessels (saturation level), before releasing the cuff.

Figure 21 shows the mean values and standard deviation of intensity and phase data, recovered separately from the FD signal. Each plot represents the relative changes of [HbT] for each subject during venous occlusion, using the DS approach. Time zero corresponds to the beginning of the occlusion and the square wave represents the interval with the cuff turned on (180 s). In general, intensity data have smaller variability due to the enhanced SNR compared to phase data. Moreover, muscle blood flow values recovered from intensity signals are higher than phase ones, as can be seen from the rate of increase (slope) of the total hemoglobin concentration, with the biggest rate of increase occurring within the first minute from the occlusion.

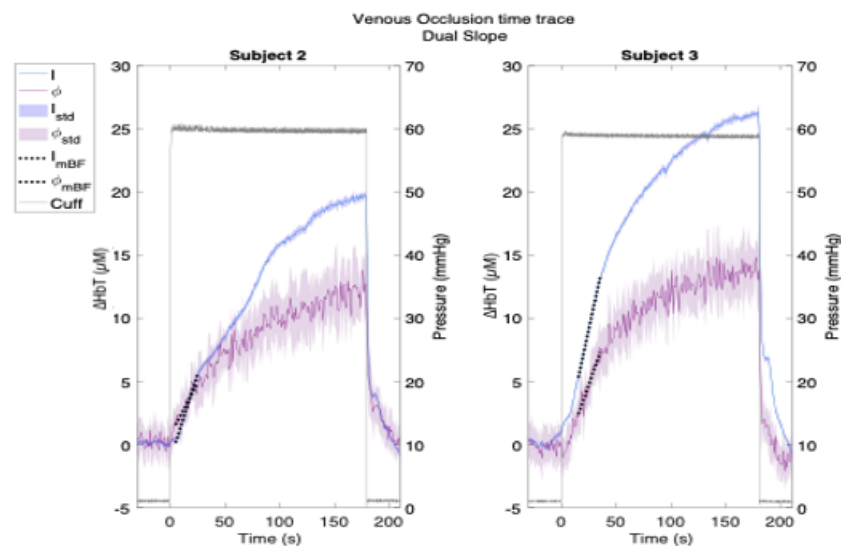


Figure 21: Representative time traces of total hemoglobin concentration change, expressed in units of μM , during 3 minutes of venous occlusion (VO) test, recovered on each subject forearm muscle (brachioradialis) with FD probe. Mean values and standard deviation of intensity (I) and phase (ϕ) data types, plotted in blue and violet respectively, are analyzed separately. Dot line slopes (black) represent ΔHbT increase during venous occlusion, as a result of blood accumulation. Square waves correspond to time intervals (expressed in seconds) with cuff pressure turned on (60 mmHg) during VO.

Figure 22 shows mean values and standard deviation of muscle blood flow for each subject brachioradialis muscle. Each plot compares intensity and phase data mBF, recovered with different methods using FD. In general, the values of muscle food flow measured in this parallel work are higher than the ones obtained in the previous protocol and closer to the literature range, with intensity mBF bigger than the ones measured with phase data. Single distances recovered the highest values compared to the slope methods. In particular, short single

distances, that are sensitive to more superficial layers (skin and adipose tissue), recovered bigger values compared to long distances, mainly sensitive to deeper tissues (muscle). This is explainable by the influence of the venous compartments perturbation which mainly affects superficial layers [30]. Different values between the two single slopes, recovered for each subject, can be explained by different adipose tissue thicknesses that cover the volume investigated by the probe. Dual slope values are within the range of single slopes, as expected by theory formulas.

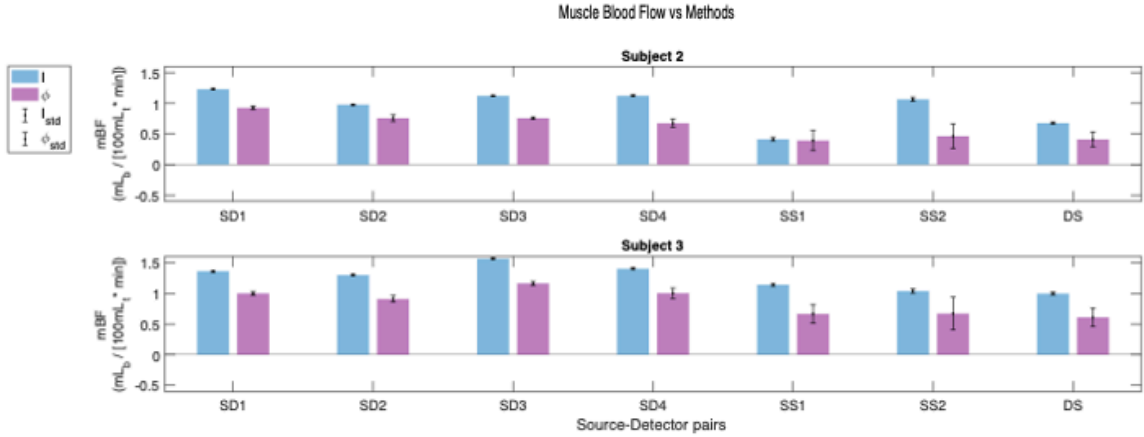


Figure 22: Histogram showing muscle blood flow (mBF), expressed in mL_{blood}/100mL_{tissue}/min, recovered during venous occlusion (VO) for each subject forearm muscle with FD probe. Bars represent mean values and standard deviation of mBF. Acronyms: Single Distance (SD), Single Slope (SS) and Dual Slope (DS).

3.4 Discussion

Absolute measurements obtained with dual slope using the broadband spectrum in CW domain recovered concentrations values coherent with what is found in literature [15]. In particular, oxyhemoglobin levels were slightly underestimated, as a result of the introduction of high wavelengths to include the contribution of water and lipid, whose absorption spectra is superimposed to oxyhemoglobin one. Water remains approximately constant during all the experiments for each subject as expected since no water change should be recovered in this kind of protocol performed at rest. Lipid instead shows a similar trend to oxyhemoglobin time trace during arterial occlusion, probably due to its absorbing peak (around 930 nm) overlapped with the absorbance spectra of oxyhemoglobin. However, this system has a drawback, related to the low sample rate achieved by the fiber switch, that provided not satisfactory results during venous occlusion. Future studies should take into account the possibility to include detectors with larger apertures to increase the sample rate and follow faster signals.

Relative measurements allow comparisons between different methods like single distance, single slopes and dual slopes. In general, results obtained using continuous wave and frequency domain confirm the enhanced sensitivity to deep layers achieved by slope methods. In fact, where the perturbation effect was shallower (during venous occlusion), higher values of muscle blood flow were recovered by single distance method, that features more superficial sensitivity, whereas where the perturbation mainly involved deeper tissues (arterial occlusion), bigger results of muscle oxygen consumption were achieved by methods with higher depth of penetration, i.e., single slopes and dual slopes. Future studies should take into account a higher number of subjects and tissues, to evaluate intra and inter subject variability, focusing on the effect of different muscles and adipose tissue layers. Moreover, the development of an array with dual slope channels would help to better assess the tissue heterogeneity and the origin of signals contributions, investigating at the same time a larger volume of tissue.

4. Measurements on brain

4.1 Introduction

Oxygen availability is crucial not only for studying the hemodynamic response of skeletal muscles but also for investigating the cognitive performance of the brain. An increase of neural activity leads to two physiological reactions: a neurometabolic coupling and a neurovascular coupling (see Fig 23) [6]. The first one is characterized by an increase in the rate of oxygen metabolism (or consumption), defined cerebral metabolic rate of oxygen (CMRO₂), due to energetic demands by the neuronal tissue, which reduce oxyhemoglobin levels and increase deoxyhemoglobin ones. In contrast, the neurovascular coupling is characterized by local changes of the hemodynamic response featuring a cerebral blood flow (CBF) and cerebral blood volume (CBV) increase in the activated area. This vascular response leads to enhanced levels of oxyhemoglobin concentrations and since the oxygen supply is bigger than its metabolic consumption, the resulting effect is represented by an increase of oxyhemoglobin levels [HbO₂], and a smaller decrease of deoxyhemoglobin [Hb] concentration during a functional activation [9].

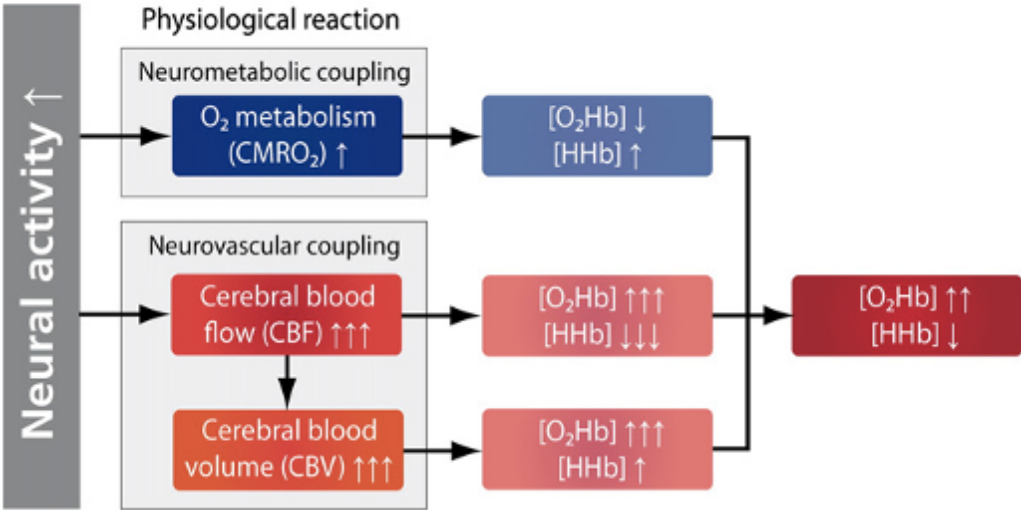


Figure 23: Scheme of cerebral hemodynamic response during neural activity, with neurometabolic and neurovascular coupling contributions [6].

Based on this physiological response, Near Infrared Spectroscopy has been considered over time as a suitable and promising neuroimaging tool to investigate non-invasively the human brain function, being able to quantify hemoglobin concentration changes in biological tissues. The past few decades have seen a rapid increase of its application in the biomedical field, involving many kinds of populations from newborns to elderly subjects, both in healthy as well as impaired conditions, such as dementia (like Parkinson's and Alzheimer's) or neuropsychiatric disorders (like schizophrenia, depression, autism spectrum) [31]. Thanks to its portability, cost-effectiveness, and robustness against motion artifacts, Near Infrared Spectroscopy has become over time an attractive alternative to the magnetic resonance imaging (MRI), commonly and likewise used in the neurocognitive field [32].

However, as already seen for skeletal muscles measurements, one of the main issues of NIRS signals acquisition is related to the presence of contaminating contributions that can be derived from superficial extracerebral compartments, like the scalp and skull. Moreover, functional signals can also be affected by physiological and systemic activities, which affect the task-related hemodynamic response, making it indistinguishable from spontaneous oscillations or systemic responses not related with the functional one itself. Over time, two common approaches have been followed to reduce these contaminating signal components. From an instrumental point of view, the introduction of multi distance arrangements demonstrated to be more sensitive to the cerebral compartments, compared to the commonly used single distances methods, sensitive to more superficial extracerebral tissues (scalp, skull and cerebrospinal fluid) (see Fig. 24). From a methodological point of view univariate methods based on signal processing, have been developed to reduce physiological confounding contributions by separating different signal components [6].

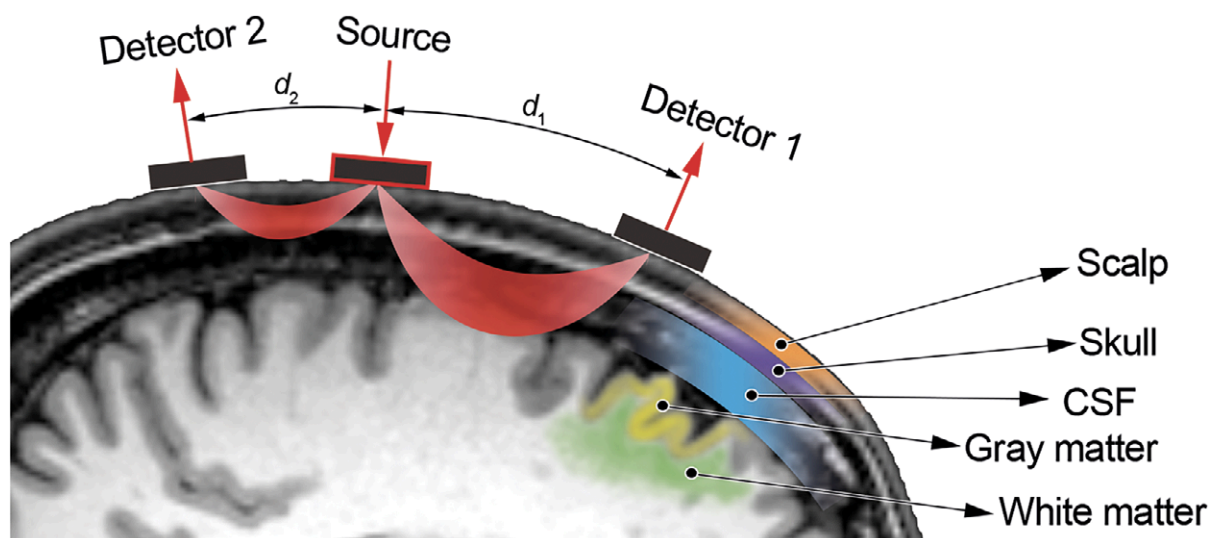


Figure 24: Illustration of the pathlength (in red) and penetration depth achieved by photons across different source detector distances, through the different layers of the head [32].

Several studies on cognitive processes have been investigated, and different paradigms have been applied according to the research field, from auditory to visual stimulations, from motor to cognitive tasks [33, 34, 35, 36]. Regarding the latter, studies involving functional MRI revealed how prefrontal cortex (PFC) is particularly involved in the hemodynamic response of the brain, playing a big role in functional activation during neurocognitive tasks [37]. In particular, a widely used cognitive task to evaluate the selective attention and assess the functional response in the frontal lobe is the Stroop Color and Word test [38, 39, 40, 41, 42]. In this task, the subject is asked to name the color of the word shown for example on a monitor. The word, whose meaning indicates itself the name of a color, can be represented with a color matching or not matching the meaning of the word (congruent and incongruent condition, respectively). Since reading a word is a more automatic process than naming the color, the subject is exposed to a competition process, defined interference effect, containing two contradictory information: goal maintenance and interference resistance. They are two interdependent components at the base of executive-cognitive function, working as a proactive control focusing on the goal (the first) and as a reactive control suppressing interference (the second). During incongruent task, the subject is asked to resist to the interference effect and maintain at the same time the task-specific goal, by inhibiting the incorrect response (reading the word) to give the correct answer (naming the color) [43].

The cognitive competition commonly results in behavioral responses which are characterized by higher reaction times (ms) and lower accuracy levels (% of correct responses) during incongruent rather than congruent tasks. Regarding the hemodynamic response, several studies have revealed how the cortical activation of PFC measured with fNIRS, with the typical variations in concentration of oxy- (increase) and deoxyhemoglobin (decrease), is strictly associated with the interference effect, featuring greater hemoglobin concentration changes during incongruent condition, being the more cognitively demanding task [39, 44].

In this study, a typical clinical version of Stroop Color and Word test has been proposed to evaluate the behavioral and hemodynamic response of two subjects during a cognitive task. Moreover, in order to assess the strengths of multi distance approaches, with enhanced deep layers sensitivity (brain), compared to single distance methods, more affected by superficial contributions (skull and scalp), data were collected using the Dual Slope probe. In this case, since CW spectrometer achieved a low sample rate, not suitable for functional brain signals, measurements were recovered in Frequency Domain with a sample rate of 10 Hz and signals were analyzed separating intensity and phase data to evaluate hemoglobin concentrations changes achieved by the two datatypes.

4.2 Materials and Methods

4.2.1 Protocol

Two healthy subjects participated to the Stroop Color and Word test, giving their written informed consent for the Tufts Institutional Review Board. Measurements were taken three times over different days for each volunteer. Data were collected in Frequency Domain with two Dual Slope probes, bilaterally placed on the left and right side of prefrontal cortex (PFC) of each subject, specifically in positions FP1 and FP2 according to the International 10-20 system (see Fig 25). The probe was placed using a sport band to maintain a good and stable contact with the subjects' scalp, avoiding movement of the probe itself. To evaluate the effect of other systemic contributions usually affecting the specific hemodynamic response of the brain during the cognitive task, three physiological signals were constantly monitored till the end of the experiment using a commercial plethysmograph (CNSystems CNAP Monitor 500, Graz, Austria): respiration, heart rate and blood pressure.

Each subject was seated in a comfortable armchair and was asked to relax and avoid as much as possible movements during the protocol, in order to minimize motion artifacts. Moreover, they were instructed not to overthink during resting states periods between sections, focusing all the attention during trials, since the functional hemodynamic response recovered with NIRS is sensitive to mind wondering. Words were visually presented on a TV monitor positioned at 1 m of distance from each subject, whereas answers were given through a keyboard near them. In particular, participants responded with three fingers positioned on three keyboard arrows configured as following: left for red, down for green and right for blue (see Fig. 25). The protocol code was written in Matlab exploiting the Psychophysics Toolbox, a free set of functions widely used for neuroscience research. Accuracy, trials and response times were recovered using two Arduino pins configured as output and saved in a subject specific folder. After explaining the protocol to the volunteers, a shorter training session was proposed to ensure that everything was clear.

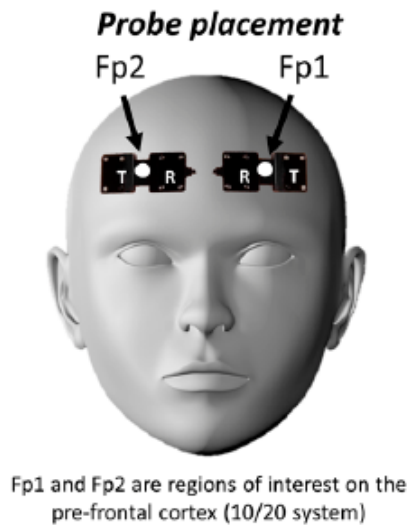


Figure 25: Scheme of the probe placement (top) and keyboard configuration responses (bottom) used in this study [40].

The experiment started with 30 s of baseline, followed by 20 sections of stimuli alternated with recovery periods, each one lasting 20 s. Sections were divided in two categories, according to the type of task, for a total of 10 congruent (word meaning matching the color) and 10 incongruent (word meaning not matching the color) sections [40, 45, 46]. Each of them encompassed a different number N of stimuli (words), depending on the time response (TR) taken by the subject to answer to each trial. Task sections and their corresponding trials were randomized with a permutation order. Each trial started with a fixation cross for 500 ms (interstimulus interval, ISI) to separate a given answer from the following stimulus. Both words and marks appeared in the center of the screen. At the end of the functional sections, another baseline period of 30 s was recovered, hence the experiment lasted in total ~15 minutes. The block design protocol and a clarifying example of each task section are shown in Fig. 26.

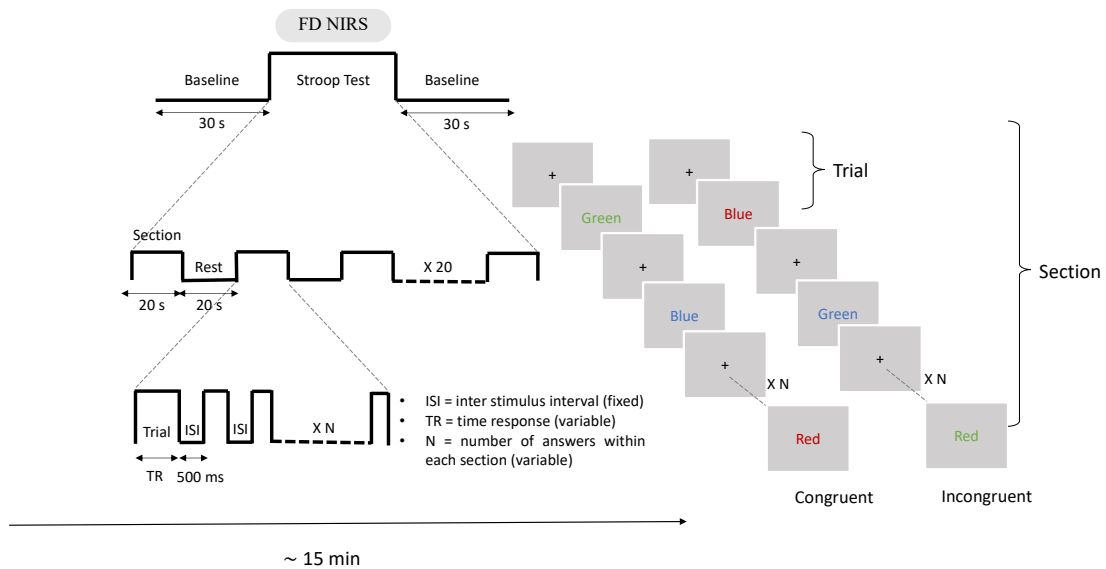


Figure 26: fNIRS block design protocol using FD. Functional protocol starts with 30 s of baseline, followed by 20 sections alternated with recovery periods, both of 20 s, and finishes with another 30 s baseline period, lasting almost 15 minutes in total. According to the type of task, there are 10 congruent and 10 incongruent sections in randomized order. Each section is composed by a number N of randomized trials (color-word stimuli), variable according to the time response (TR) required by the subject to answer within each 20 s section. An inter-stimulus interval (ISI) of 0,5 s separates each response from the following stimulus, by showing a cross mark. An example of congruent and incongruent tasks is shown on the right.

4.2.2 Instrument

The measurements on brain were performed with two Dual Slope probes in Frequency Domain, featuring a sample rate of 10 Hz. Data were collected at two wavelengths (690 and 830 nm) using an intensity modulated light at a frequency of 140.625 MHz. The diffuse optical signals recovered were analyzed by separating intensity and phase contributions, to assess the sensitivity achieved by each datatype, measuring changes and not absolute values of hemoglobin concentrations (see Chapter 2.2). Moreover, to evaluate the sensitivity towards deep layer tissues recovered by single distance and multi distance approaches, *in vivo* measurements achieved with both methods have been compared. Short and long single distances are 25 and 35 mm, respectively.

In agreement with the mathematical model exposed in Section 2.2, absolute optical properties (μ_s' and μ_a) measured during baseline were used only to calculate the subjects' specific DPF and DSF values, for single distance and dual slope methods respectively, from which changes of the absorption coefficient ($\Delta\mu_a$) have been recovered. In this particular case, for brain measurements and at the two wavelengths considered, under the assumption that the major absorbers are oxyhemoglobin, deoxyhemoglobin and water (no lipid content), the changes of $[\Delta\text{HbO}_2]$ and $[\Delta\text{Hb}]$ can be calculated by inverting Eq. 2, using though a proper relative absorption coefficient $\Delta\mu_{\text{aH}_2\text{O}}$ (see Eq 26):

$$\Delta\mu_{\text{aH}_2\text{O}} = \Delta\mu_a - \epsilon_W \cdot \text{CH}_2\text{Ovf} \quad (26)$$

corrected by the volume fraction of water content (CH_2Ovf), assumed equal to 70 v/v % according to literature [18, 19].

4.2.3 Signal processing

During the experiment, two types of datasets have been recovered: physiological signals provided by FD NIRS and plethysmograph measurements, and behavioral responses data, from two pins of Arduino configured as output. Both datasets were uploaded and analyzed to recover different kind of information, studying the hemodynamic and behavioral response of each subject.

The acquired hemodynamic raw signals with NIRS can be affected by different types of noise, which can be categorized into instrumental and physiological noise. Since they are not related to brain activity, it's important to remove and reduce them, before recovering and analyzing hemoglobin concentration changes from the raw data. To avoid confounding contributions due to instrumental noise, present in hardware or in the surrounding environment, one of the first steps was the minimization of these effects during the acquisition itself [47, 48]. Data were collected in the dark in order to reduce the contribution of external light and to minimize it, between DC and AC intensity data, it was decided to use the second one, since AC data are considered more robust against the environmental light [13]. Phase data were cleaned from phase jumping before proceeding with the signal analysis.

At this point, each pair of time traces (at 690 and 830 nm) were converted into oxy- and deoxyhemoglobin concentration changes, applying the mathematical formula present in Chapter 2.2. These data are still affected by the second type of noise, i.e., the physiological noise, which can be divided in three main contributions, belonging to different frequency bands: the cardiac signal or heartbeat (~ 1 Hz), respiration rate (~ 0.3 Hz) and low frequency oscillations, like the Mayer waves (~ 0.1 Hz), which are related to blood pressure fluctuations and depend on activity state, body posture and age of subjects [6]. To minimize these contributions, a Butterworth bandpass filter of 4 order with high and low cutoff frequencies of 0.01 Hz and 0.1 Hz was applied [49]. The selected frequency band removed a portion of noise including heartbeat, low frequency oscillations and baseline drifts, leaving though contaminations of those signals with frequency band superimposed to the one of interest, as the case of respiration. Hence, a folding average algorithm was applied across sections with the same task (congruent and incongruent), characterized by the same time periods (20 s), to evaluate the hemodynamic response between congruent and incongruent tasks. Averaging across sections with the same task condition helped to evaluate signal reliability [50]. Data without reliable pattern were omitted from further analysis.

4.3 Results

4.3.1 Behavioral response

In order to evaluate the behavioral response of each subject to the cognitive test, comparing congruent and incongruent task, three different parameters were evaluated: the number of answers, the accuracy (as the percentage of correct responses) and time responses. These data were automatically saved in a subject specific folder at the end of each experiment, with the time of trials (Arduino output). The latter was used to find the proper instants corresponding to the beginning and the end of each task section (see Fig. 27).

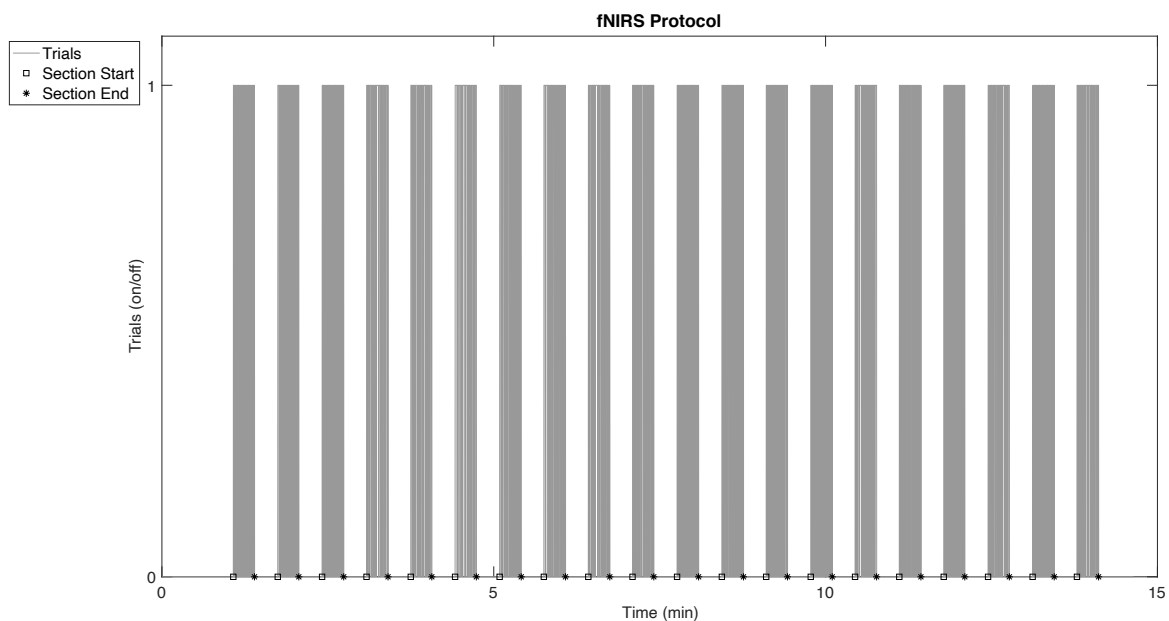


Figure 27: Temporal distribution of single trials within each section provided by a pin of the Arduino configured as an output. Circles and stars highlight sections starts and ends respectively.

Figures 28 and 29 show the mean values and standard deviation of each behavioral parameter recovered for subject 1 and 2 during a representative day trial, averaging results across sections with the same task (congruent and incongruent). The number of answers provided were lower during incongruent task (top left histogram), as expected by the interference effect, which requires to suppress the inappropriate goal (reading the word) and to focus on the task goal (naming the color) at the same time [43]. The same behavior is also reported in the boxplot, in the center. Outliers TR are representative values, corresponding to first trials of sections, which usually require more time since the subject doesn't know exactly

when the following section will start after each recovery period. Bottom plot contains the same information, i.e., time responses higher during incongruent tasks, but representing the mean values (with corresponding standard deviations) for each section, pointing out the difference between congruent and incongruent tasks during the entire protocol, distinguished by red and blue windows respectively.

Across the three parameters, only accuracy shows a small difference between the two tasks, with a lower value and higher variability during incongruent task. This can be explained by the fact that subject could take an unlimited time (till the end of the section) to give an answer, as soon as he/she felt confident about it. Having no time restrictions for each trial, the rate of correct answers resulted similar between the two tasks. Slight differences can be seen across subjects and each behavioral consideration is valid for both.

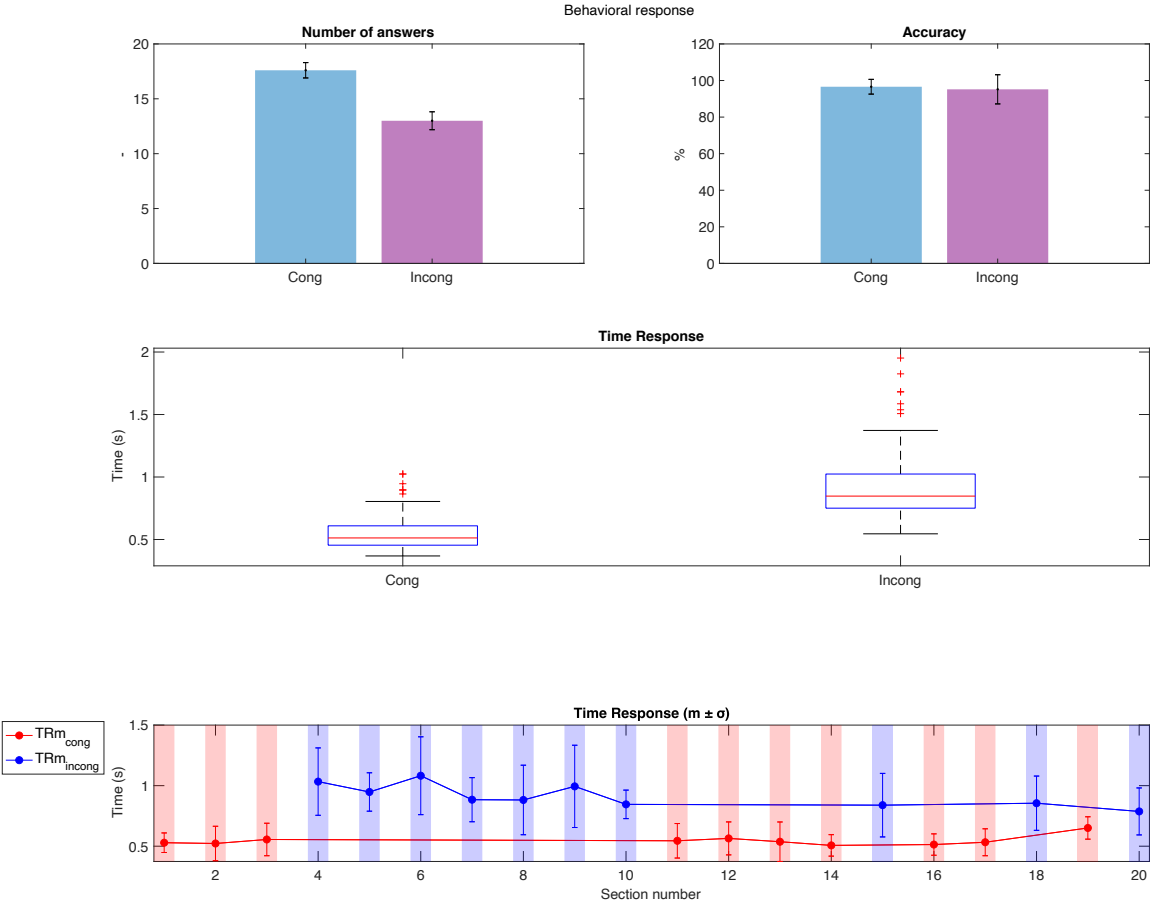


Figure 28: Representative behavioral responses of subject 1 for averaged sections with the same task (congruent against incongruent). Top plots show the number of answers and accuracy expressed with mean values and standard deviations. Boxplot shows the median time responses (with the lower and upper quartiles, outliers, minimum and maximum values) expressed in seconds for each task, averaged across sections. Mean values and standard deviations time responses for each section are also shown in the bottom plot. Red and blue windows refer to congruent and incongruent sections respectively. Acronyms: time response (TR).

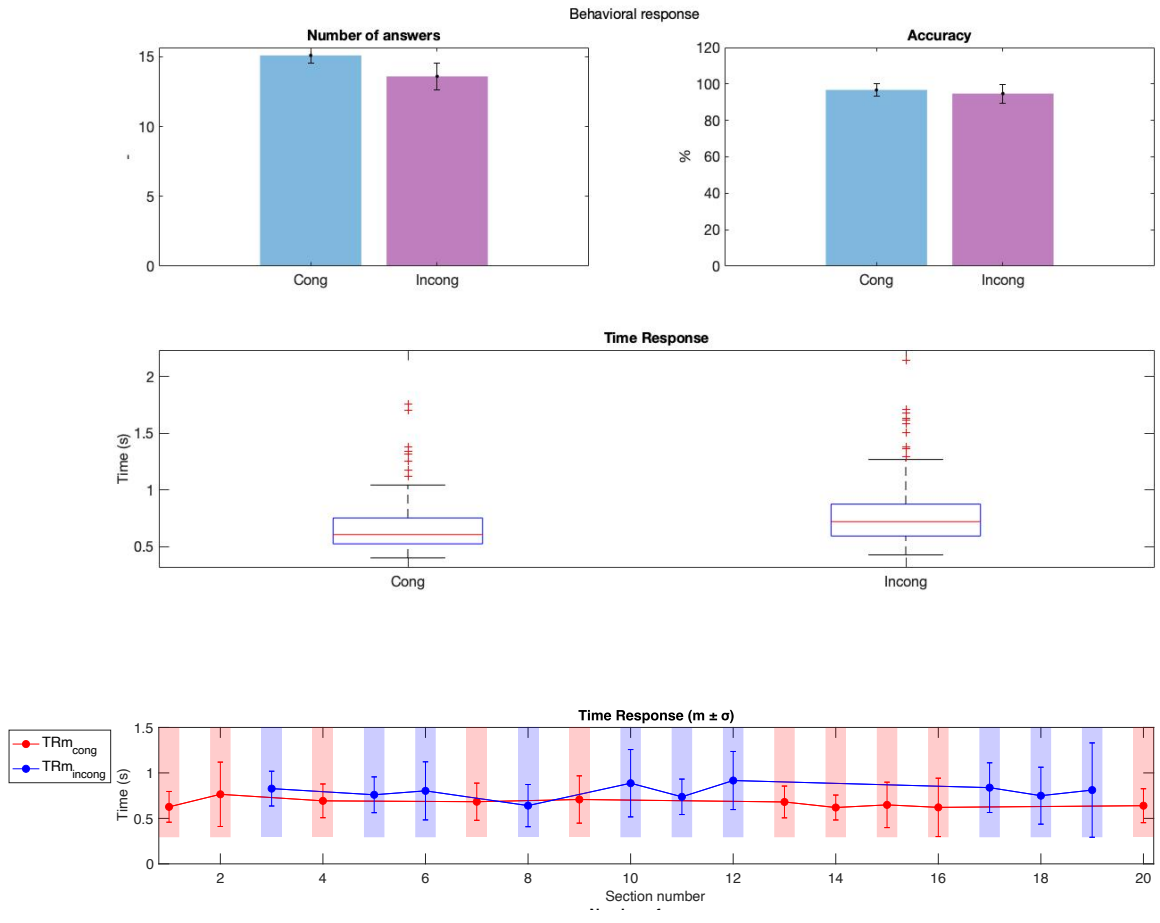


Figure 29: Representative behavioral responses of subject 2 for averaged sections with the same task (congruent against incongruent).

4.3.2 Hemodynamic response

Regarding the hemodynamic response of each subject, dual slope intensity (DSI) and phase ($DS\phi$) data recovered with two probes are reported in Fig. 30 and 31, for a representative case (trial 1 subject 1), as an example of signal processing applied. Each subplot shows the time traces (expressed in minutes) of oxy- (red) and deoxyhemoglobin (blue) concentration changes before (raw signals on top) and after (filtered signals on bottom) the physiological noise removal. Red and blue windows highlight the randomized periods of congruent and incongruent tasks alternated with recovery periods, both lasting 20 s.

Opposite trend of oxy- and deoxyhemoglobin is visible during the entire protocol, as a result of the neurovascular coupling. Looking at each section singularly, it's also possible to visualize the increase of $[\Delta HbO_2]$ and decrease of $[\Delta Hb]$, occurring and lasting some seconds after the beginning and the end of each section [6]. However, some of them don't show the expected trend but highlight an increase in deoxyhemoglobin concentration during part of the task. This can be explained by the time required by the task-evoked response to physiologically occur and return to the base level, since it's not instantaneous with the task beginning/end [39, 49]. However, the best explanation must be sought in the protocol design and particularly attention should be paid when choosing the proper temporal intervals for activation and recovery periods. In fact, the latter are known to be strictly influenced by factors such as mind wandering, physiological fluctuations and the protocol design. In block design protocols, as the one introduced for this study, rest periods are usually chosen of the same length of task periods, since the refraction time lasts almost as the activation one and a certain interval is required to let the response turning back to baseline values. At the same time, this type of protocol can be more easily subjected to mind wandering, compared to event-related protocol where the rest periods are chosen shorter than the activation ones [9].

As concerns the second datatype (ϕ), the recovered phase signals confirmed to suffer from higher levels of noise, compared to intensity data, as shown in Fig 31 [13]. In particular, signal recovered with detector AB are affected by higher level of noise compared to the ones detected with detector CD (placed on LPFC and RPFC respectively). After processing the signals, the same consideration of intensity data can be addressed to phase.

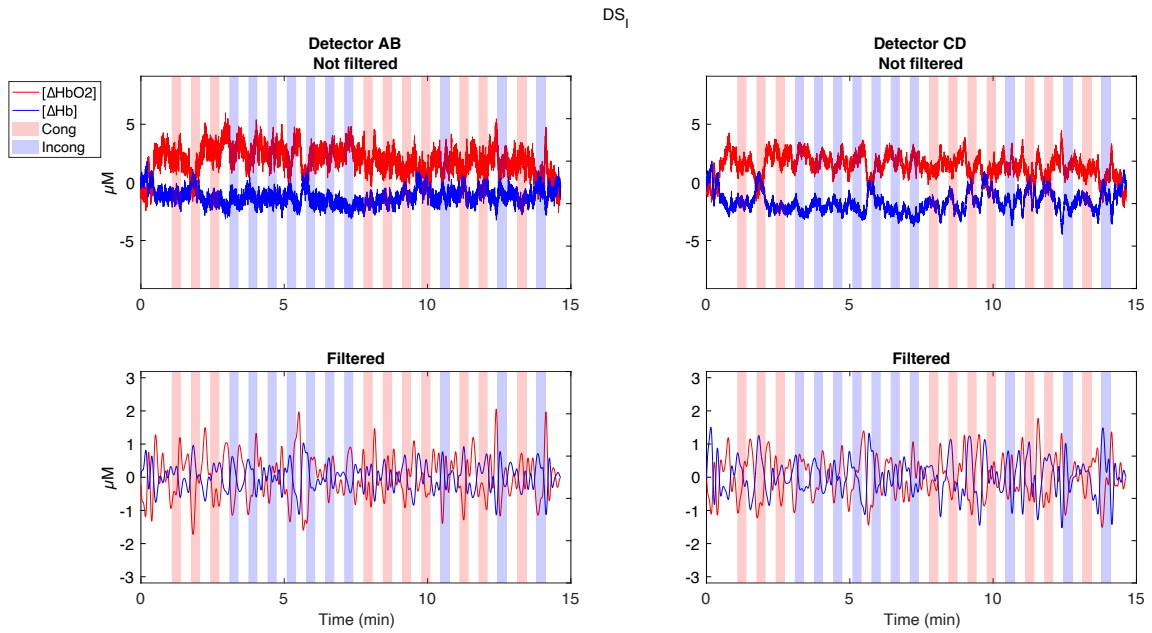


Figure 30: Representative oxy- (red) and deoxyhemoglobin (blue) concentrations changes, expressed in μM , recovered from fNIRS Dual Slope phase (DS_{ψ}) data using two probes (detectors AB on the left, detectors CD on the right) on prefrontal cortex (PFC) of subject 1. Top plots represent raw data whereas bottom plots show filtered signals. Red and blue windows correspond to congruent and incongruent sections, respectively. Acronyms: oxyhemoglobin (HbO_2), deoxyhemoglobin (Hb).

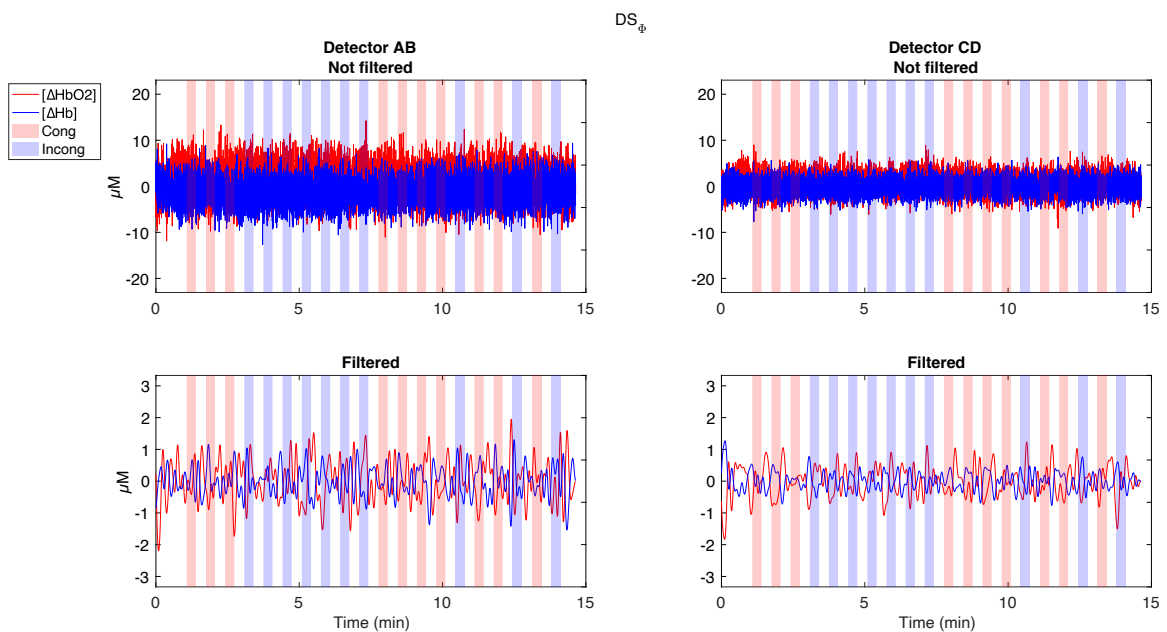


Figure 31: Representative oxy- (red) and deoxyhemoglobin (blue) concentrations changes, expressed in μM , recovered from fNIRS Dual Slope phase (DS_{ϕ}) data using two probes (detectors AB on the left, detectors CD on the right) on prefrontal cortex (PFC) of subject 1.

The following figures show the filtered signals after the application of the folding averaging algorithm across sections with the same task, for each datatype and probe signal. This averaging process was done to compare the hemodynamic response between activation and resting periods and between congruent and incongruent sections, and it could be applied since both intervals were chosen with the same length (20 s). Plots show oxy- and deoxyhemoglobin concentration changes averaged in time (expressed in seconds), with time intervals from 0 to 20 s corresponding to task periods, whereas intervals from 20 to 40 s refer to recovery periods. Hence, typical activation ([HbO₂] increase and [Hb] decrease) and deactivation ([HbO₂] decrease and [Hb] increase) trends should be seen in order in these two 20 s time windows.

Figure 32 shows results obtained by analyzing intensity data on left PFC (detectors A-B). First row subplots refer to mean values without standard deviation (omitted to make the figures less confusing), recovered with four single distances, whereas second row subplots show mean values and standard deviation of hemoglobin changes recovered with dual slope. To evaluate the amplitude and latency of the hemodynamic response, oxy- and deoxyhemoglobin maximum and minimum peaks respectively have been calculated for each functional curve and method and they are shown with dots. According to literature, components change related to functional activity are usually small, with a value of $\sim 0,5 \mu\text{M}$ for oxy-hemoglobin and $\sim -0,2$ for deoxyhemoglobin, with a variability of $1 \mu\text{M}$ due to responses not task-related, whereas as concern peak latency, it is concurrently with the end of the task [6]. In light of this, dual slope and single distances seem to achieve physiological values, except for single distance incongruent case, shown in the upper right subplot. In fact, the highest/ lowest peaks, recovered on one side of the probe, are too high in amplitude to be only due to task response. They are probably related to other physiological contributions occurring for example in more superficial layers. In fact, the highest peak just corresponds to the short single distance (25 mm), characterized by a smaller penetration depth compared to long single distances (35 mm).

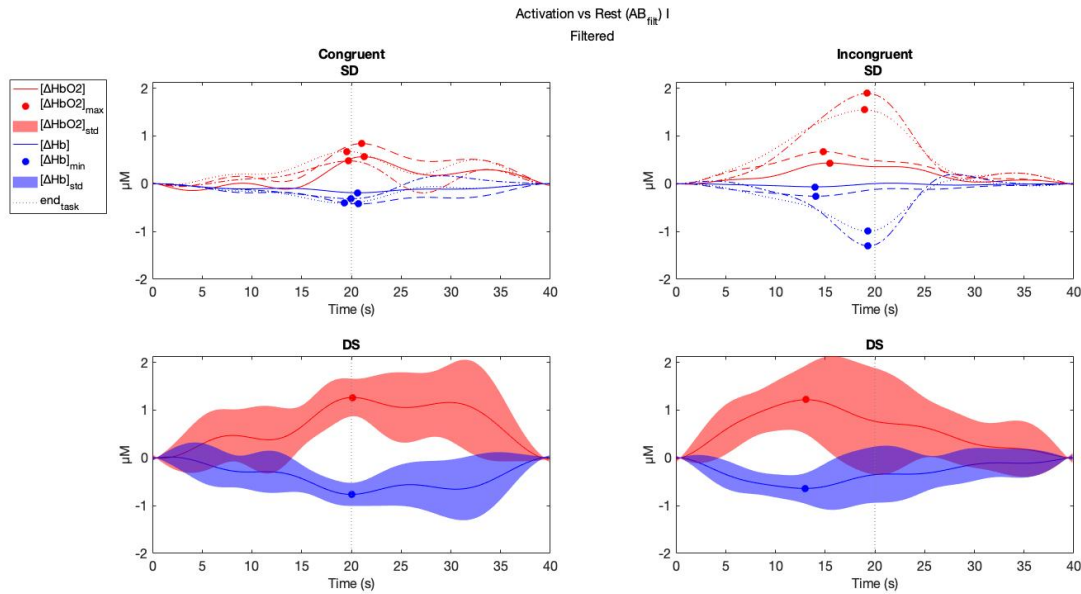


Figure 32: Representative oxy- (red) and deoxyhemoglobin (blue) concentrations changes (expressed in μM) recovered from SDI (top) and DSI (bottom) filtered data on LPFC (detector A-B), after applying a folding averaging algorithm between sections of the same task (congruent, on the left and incongruent, on the right). Grey dashed line at 20 s separates activation periods (from 0 to 20 s) and rest (from 20 to 40 s). Short single distances are represented with solid and dashed-dot line, whereas long SD are represented with dashed and dotted lines. Bottom plots show DSI with overlapped standard deviation. Peaks of oxy- and deoxyhemoglobin recovered are shown with dot points. Acronyms: oxyhemoglobin (HbO_2), deoxyhemoglobin (Hb).

Figure 33 show results obtained by analyzing phase data on the same side of PFC. The same consideration can be applied to phase data, with some differences. The peak present in the upper right subplot (incongruent task measured with single distance) is now disappeared and this can find an explanation with previous simulations studies which proved that phase is characterized by deep layers sensitivity, compared to intensity [13]. However, in general phase signals are more affected by noise levels, resulting in the higher standard deviation obtained. Peak latency recovered during congruent task is not considered physiological, being almost at the middle of rest periods. Moreover, the curve of hemoglobin species achieved is more distant from the expected shape of a task-related hemodynamic response, for this reason phase signals were analyzed for each case and subject, but not considered to draw conclusions about activation or deactivation responses.

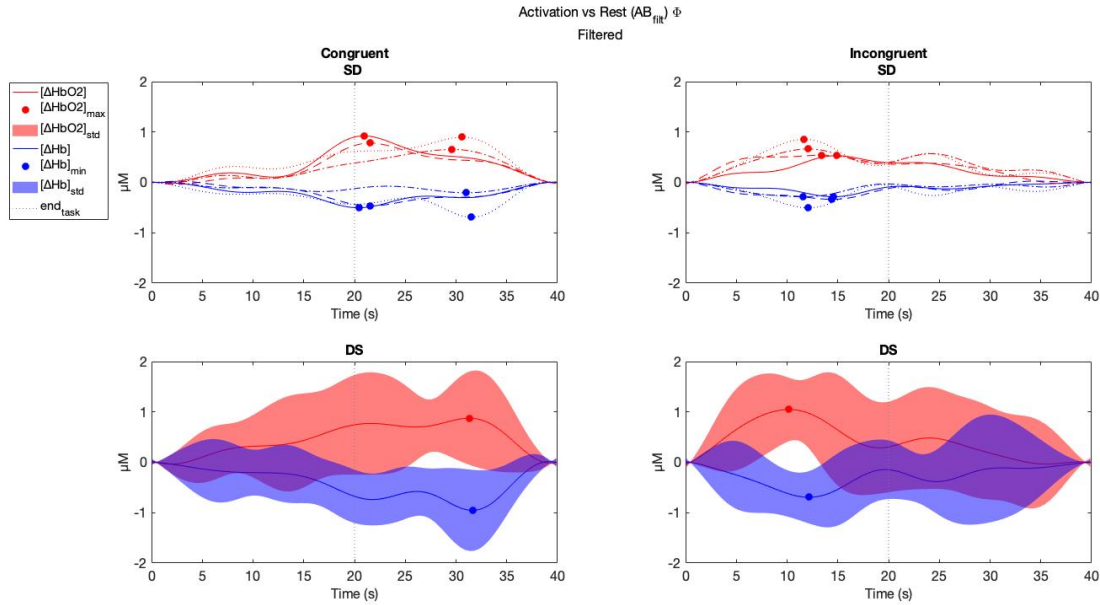


Figure 33: Representative oxy- (red) and deoxyhemoglobin (blue) concentrations changes (expressed in μM) recovered from $\text{SD}\Phi$ (top) and $\text{DS}\Phi$ (bottom) filtered data on LPFC (detector A-B).

The following figure 34 represents averaged intensity data achieved by the second probe, placed on the right PFC (detectors C-D). What is more evident in this case, is the unexpected difference of peaks between congruent and incongruent task. Functional activation signals should have the higher hemodynamic response occurring during incongruent task, since it features the higher interference effect. However, this strange behavior can be explained looking at two aspects: the design of the protocol and the randomized task-order specific for this trial. First, the fact that this protocol usually involved in clinical studies contains only pure blocks, with the same task-trials, proved to be little challenging compared to block mixing congruent and incongruent tasks, since the inappropriate goal is never reinforced [43]. The major difficulty encountered is that the subject doesn't know when the next section starts and what type it will be. However, once it started, the participant is aware that the task will remain the same for the entire section and this contributes to reduce the goal maintenance. On the contrary, mixed blocks protocols, introducing congruent trials within each section, challenge the goal maintenance promoting the goal loss by reinforcing the word reading process. Moreover, looking at this specific trial, it should be noted that randomized order across task-sections provided 7 incongruent sections in a row, reducing the goal maintenance, with the subject getting used to the task. In future experiments, this is something that should be taken into consideration and changed, to see if effectively higher activation due to interference effect and goal maintenance it's visible alternating incongruent and congruent trials.

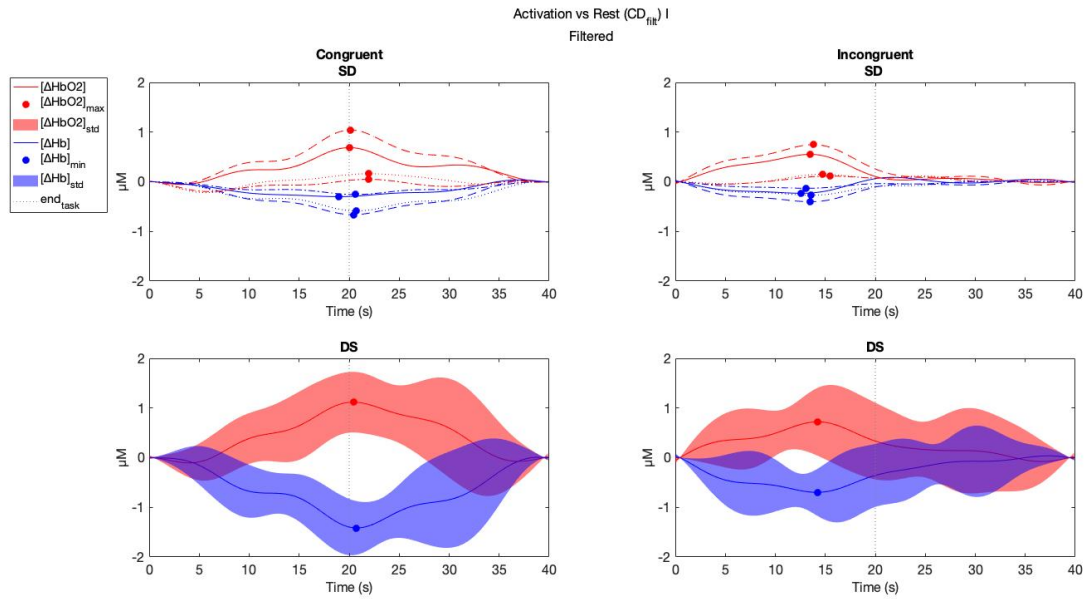


Figure 34: Representative oxy- (red) and deoxyhemoglobin (blue) concentrations changes (expressed in μM) recovered from SDI (top) and DSI (bottom) filtered data on RPF (detector C-D), after applying a folding averaging algorithm between sections of the same task (congruent, on the left and incongruent, on the right).

The following figure (Fig. 35) represents averaged phase data achieved by the second probe, placed on the right PFC (detectors C-D). The same considerations expressed above can apply to this case. As concerns single distances subplots (top) one of the two pairs achieve the highest value with the short single distance, probably related to superficial contributions and it is not representative of the activation response. The fact that peaks latency occurs earlier than the end of task section during incongruent task can find explanation to the randomized order of sections for this trial. The participants got used to the task after 7 consecutive incongruent tasks and the bigger response was achieved earlier. However, as anticipated, phase signals were analyzed for each case and subject, but not considered to draw conclusions about activation or deactivation response.

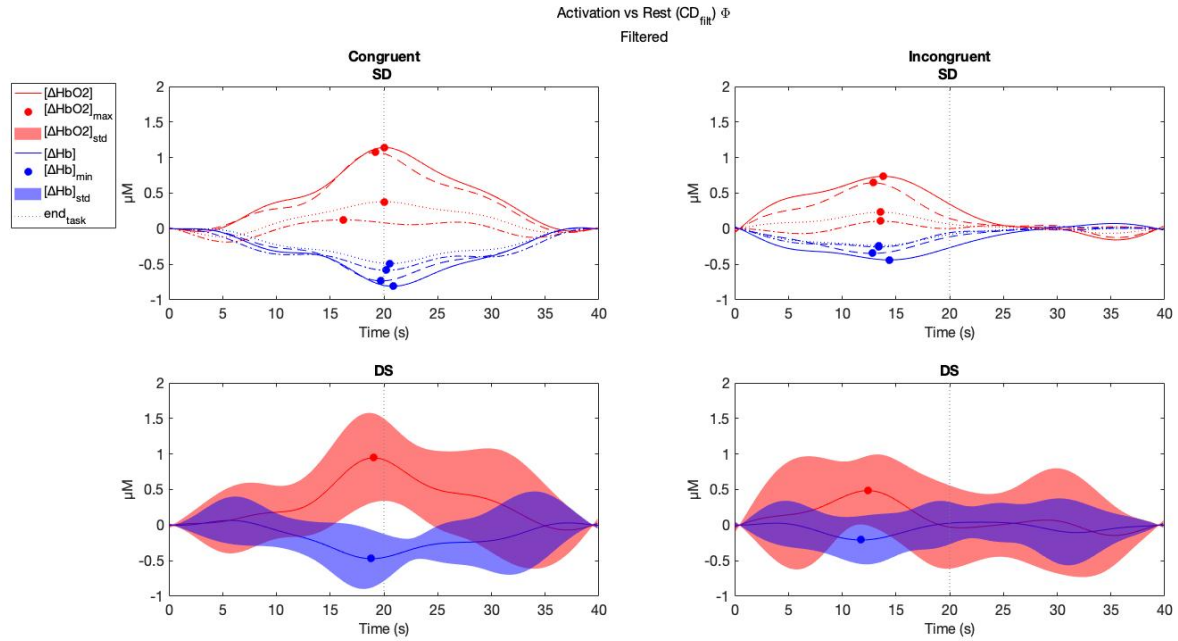


Figure 35: Representative oxy- (red) and deoxyhemoglobin (blue) concentrations changes (expressed in μM) recovered from SD Φ (top) and DS Φ (bottom) filtered data on RPFC (detector C-D).

Figure 36 resumes information about peaks amplitude recovered for subject 1 during a single trial, comparing results obtained with two probes, during congruent and incongruent task. All the cases show positive changes of oxyhemoglobin and negative changes of deoxyhemoglobin representative of the neurovascular coupling. From the point of view of the expected hemodynamic response across different tasks, the fact that congruent peaks are like the incongruent ones can probably find explanation in the block design of the protocol, not reinforcing the interference effect, and in the randomized order of this specific trial. Peaks with almost the same amplitude are recovered on both sides of PFC, showing a comparable activation level.

For phase signals too, the difference in the hemodynamic response between congruent and incongruent task is not visible. No big difference between LPFC and RPFC is elicited. In general, the only expected response is positive and negative changes of oxy- and deoxyhemoglobin respect to the baseline, as a result of the brain activation induced by task (see Fig. 37).

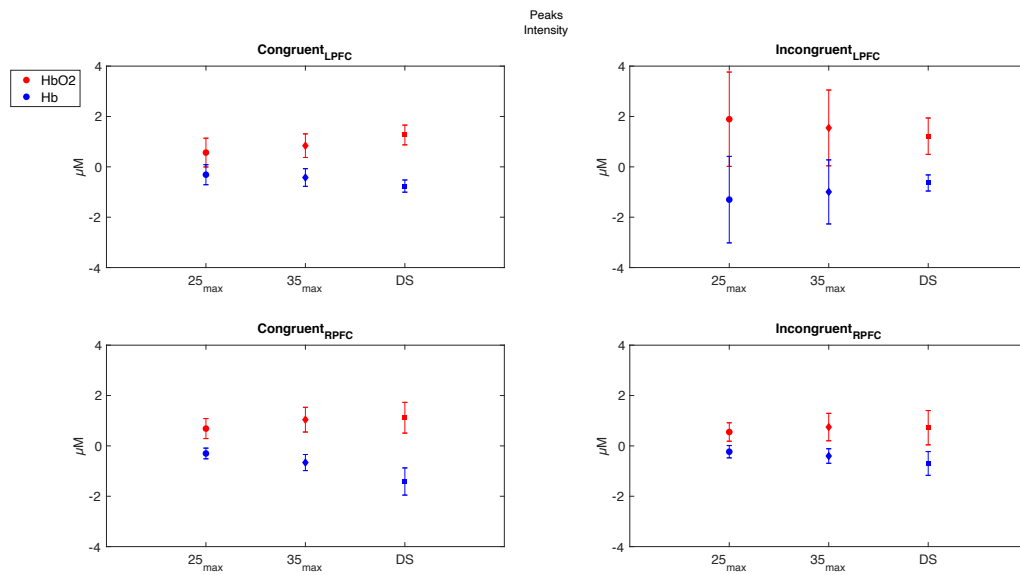


Figure 36: Representative oxy- (red) and deoxyhemoglobin (blue) concentrations changes peaks with standard deviations (expressed in μM) recovered for subject 1 during a single day-trial, with SD and DS intensity for each probe (LPFC on top with detectors A-B, RPFC on bottom with detectors CD), and each task (congruent, on the left and incongruent, on the right). Maximum single distances short and long are represented with circles and diamonds respectively, whereas dual slope peaks are represented by squares.

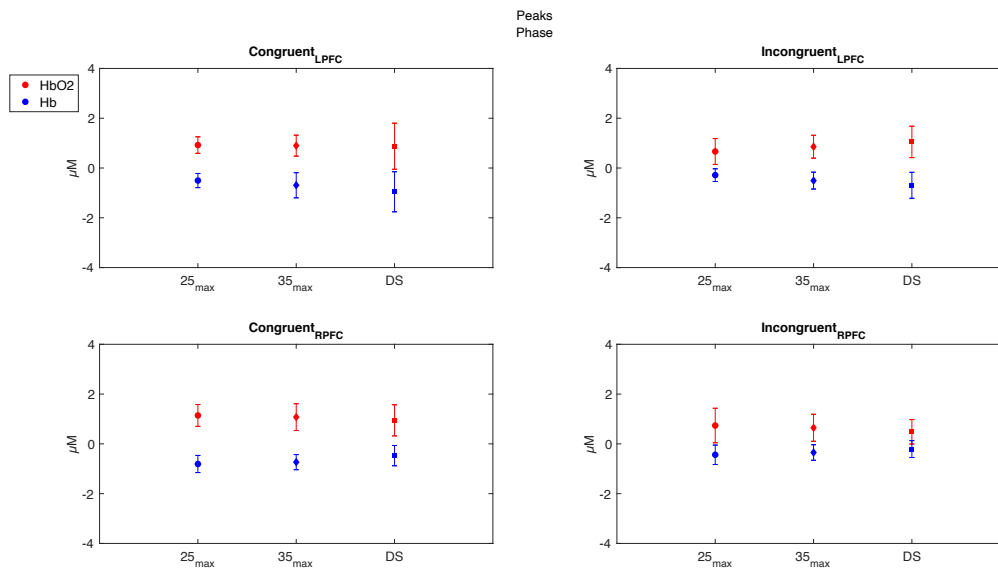


Figure 37: Representative oxy- (red) and deoxyhemoglobin (blue) concentrations changes peaks with standard deviations (expressed in μM) recovered for subject 1 during a single day-trial, with SD and DS phase for each probe (LPFC on top with detectors AB, RPFC on bottom with detectors CD), and each task (congruent, on the left and incongruent, on the right).

The same analysis for subject 2 on a representative trial is proposed in Fig. 38 for intensity data and in Fig. 39 for phase data. Considerations resulting from for the previous subject are valid for the subject 2. The only difference between two subjects is the lower amplitude of peaks achieved by subject 2, this can be explained either with a smaller activation response or with a different contact between the probe and the scalp, which in previous analysis done in the laboratory was demonstrated to affect results.

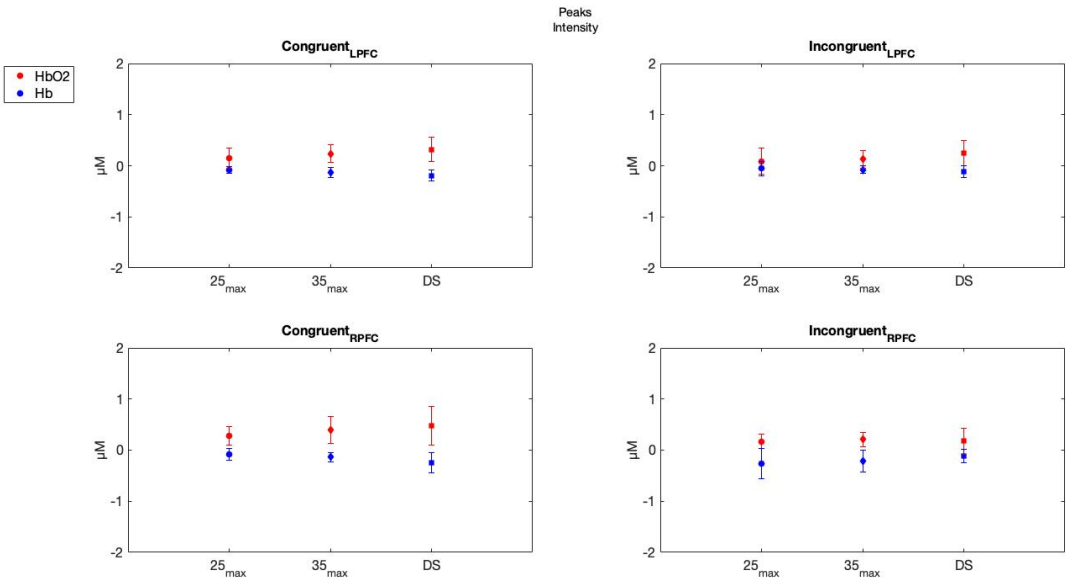


Figure 38: Representative oxy- (red) and deoxyhemoglobin (blue) concentrations changes peaks with standard deviations (expressed in μM) recovered for subject 2 during a single day-trial, with SD and DS intensity for each probe (LPFC on top with detectors A-B, RPFC on bottom with detectors CD), and each task (congruent, on the left and incongruent, on the right).

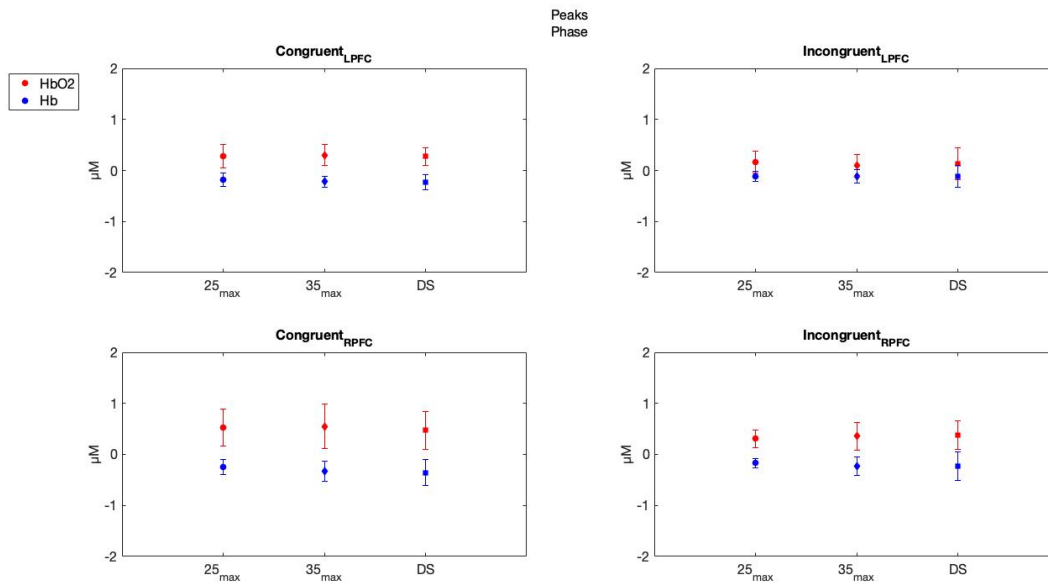


Figure 39: Representative oxy- (red) and deoxyhemoglobin (blue) concentrations changes peaks with standard deviations (expressed in μM) recovered for subject 2 during a single day-trial, with SD and DS phase for each probe (LPFC on top with detectors AB, RPFC on bottom with detectors CD), and each task (congruent, on the left and incongruent, on the right).

4.4 Discussion

The aim of brain measurements was to assess the functional response during a cognitive Stroop Color and Word test on two subjects. Moreover, the collected data were analyzed using single distance and dual slope methods to evaluate the possibility to achieve enhanced sensitivity with the novel approach during *in vivo* applications, as demonstrated in previous simulation studies.

From a cognitive point of view, typical parameters characterizing the behavioral response, such as time response, accuracy and number of answers have been evaluated. Both subjects have shown results coherent with what expected, with higher response times and lower accuracy during the incongruent task, as a result of the conflict between resistance to interference and goal maintenance, induced by the interference effect.

From a functional point of view, oxy- and deoxyhemoglobin concentration changes were analyzed to assess the hemodynamic response and evaluate the presence of activation compared to rest periods, and differences between incongruent and congruent task. Both subjects have shown activation signals during task, characterized by an increase of oxyhemoglobin and a decrease of deoxyhemoglobin levels compared to resting states periods, as a result of the neurovascular coupling. However, no difference between congruent and incongruent task were obtained in terms of peaks amplitude. This is probably related both to the design of the protocol, based on section with the same task, and to the randomized order of same task-sections for the case of subject 1. For the future, a solution could be the introduction of mixed-blocks or even-related protocols which are known to enhance the interference effect, alternating congruent and incongruent task within sections or trials, respectively.

Regarding the comparison between dual slope (more sensitive to deep layers) and single distance methods (more sensitive to superficial layers), the few measurements recovered, and their high level of variability didn't allow to uniquely agree with what expressed in previous simulation studies. However, looking at the two representative cases shown, it is possible to conclude that peaks of changes around $0,5 \mu\text{M}$ for oxy-hemoglobin and $-0,2 \mu\text{M}$ for deoxyhemoglobin are usually considered attributable to the functional response, whereas peaks bigger than $1,5 \mu\text{M}$ are not considered to be representative of the hemodynamic response alone, but they are affected by other contributions. In fact, when they are in the proper range, peaks recovered with dual slope bigger than single distances are considered more representative of

the hemodynamic response, since by theory they are characterized by deep layer sensitivity compared to single distance data. Instead, peaks out of the expected range, usually measured with short single distances, they can be representative not only of the task-related response but also of other confounding contributions, coming from superficial layers.

Hence, a limitation of this study can be found in the small sample of participants and trials, which do not allow further statistical analysis and did not provide sufficient information to establish the goodness of the results obtained in terms of the hemodynamic response. Moreover, since the functional response is a local response, occurring in focal zones of the brain, the use of only two channels to evaluate the bilaterally response of PFC reduces the possibility to detect the localized activation compared to array systems. For future studies it's so suggested to increase the number of volunteers and trials, to better evaluate the functional response, allowing intra and inter subject variability comparison, and to produce array systems which can provide higher information from a spatial point of view, detecting responses occurring in localized positions.

Conclusion

The aim of this study was a further characterization of a novel multi-distance approach developed in our laboratory. For this reason, a theoretical study based on simulations and *in vivo* measurements were carried out in order to investigate the potential use of this method for several applications in the biomedical field.

In general, the simulation study based on diffusion theory contributed to better understand the influence of sensitivity region of the Dual Slope data in two-layer media, demonstrating the importance and influence of the optical properties, mainly scattering, of the upper (surface) layer on the effective concentration's recovery.

Regarding measurements on brain and skeletal muscles, they showed the possibility to extend the use of this method for *in vivo* applications, being capable of recovering tissue oxidative parameters and measuring the hemodynamic response, exploiting protocols specific for each biological tissue and task. Even though the sample of participants was limited, the promising results obtained in both protocols shown the practical applicability and the potential use for research and diagnostics of the new DS NIRS method, paving the way for new *in vivo* applications.

For future studies, the possibility to include a large number of participants will help to better characterize the method, allowing comparisons based on intra and inter subject variability and further statistical analysis, both with absolute and relative measurements. Another future direction would be the development of an array system, increasing the number of sources and detectors. This would help to investigate a larger volume, following spatio-temporal distribution of tissue properties occurring at the same time in localized zones of the probed volume.

Acknowledgements

I would like to express my gratitude to my supervisor Prof. Valentina Agostini, for the support provided and for following me throughout these months.

I also thank my external supervisor Prof. Fantini to have given me trust, allowing to live an unforgettable experience in the DOIT laboratory. I wanna say thank you also to Prof. Sassaroli, Giles and Cristianne for the precious advice and the help provided in this period. I'd really hope to see you soon.

Grazie a mamma e papà per tutto l'amore mostratomi in questi anni, per avermi supportato in ogni mia scelta, nei momenti felici ma soprattutto in quelli più difficili.

Grazie a Paolo, Claudia e tutta la mia famiglia per avermi sostenuta in tutti questi anni, siete stati per me una colonna portante.

Grazie a Silvia per aver sempre creduto in me ed avermi strappato un sorriso anche nei momenti più difficili.

Grazie agli amici che mi hanno accompagnato in tutti questi anni, soprattutto a Cate ed Ele, per avermi regalato alcuni dei momenti più preziosi e per essere sempre il mio porto sicuro. Questo traguardo non sarebbe stato lo stesso senza di voi.

Grazie ad Euge per tutti i momenti memorabili che abbiamo condiviso. Non avrei potuto chiedere un fratellino migliore.

Ma soprattutto grazie a te G. per essere il mio punto di riferimento costante ed avermi insegnato che non esistono distanze per sentirsi a casa. Resterai sempre il regalo più bello.

Bibliography

- [1] D. Contini *et al.*, “Brain and muscle near infrared spectroscopy/imaging techniques,” *Journal of Near Infrared Spectroscopy*, vol. 20, no. 1, pp. 15–27, 2012, doi: 10.1255/jnirs.977.
- [2] F. Lange and I. Tachtsidis, “Clinical brain monitoring with time domain NIRS: A review and future perspectives,” *Applied Sciences*, vol. 9, no. 8, p. 1612, 2019, doi: 10.3390/app9081612.
- [3] G. Blaney *et al.*, “Dual-slope diffuse reflectance instrument for calibration-free broadband spectroscopy,” *Applied Sciences*, vol. 11, no. 4, p. 1757, 2021, doi: 10.3390/app11041757.
- [4] M. Rupawala *et al.*, “Shining a light on awareness: A review of functional near-infrared spectroscopy for prolonged disorders of consciousness,” *Frontiers in Neurology*, vol. 9, p. 350, 2018, doi: 10.3389/fneur.2018.00350.
- [5] I. J. Bigio and S. Fantini, *Quantitative Biomedical Optics: Theory, Methods, and Applications*. Cambridge: Cambridge University Press, 2016. doi: 10.1017/cbo9781139029797.
- [6] F. Scholkmann *et al.*, “A review on continuous wave functional near-infrared spectroscopy and imaging instrumentation and methodology,” *NeuroImage*, vol. 85, pp. 6–27, 2014, doi: 10.1016/j.neuroimage.2013.05.004.
- [7] C. Udina *et al.*, “Functional near-infrared spectroscopy to study cerebral hemodynamics in older adults during cognitive and motor tasks: A review,” *Frontiers in Aging Neuroscience*, vol. 11, p. 367, 2020, doi: 10.3389/fnagi.2019.00367.
- [8] T. Hamaoka *et al.*, “Near-infrared spectroscopy/imaging for monitoring muscle oxygenation and oxidative metabolism in healthy and diseased humans,” *Journal of Biomedical Optics*, vol. 12, no. 6, 2007, doi: 10.1117/1.2805437.
- [9] F. Herold *et al.*, “Applications of functional near-infrared spectroscopy (fNIRS) neuroimaging in exercise–cognition science: A systematic, methodology-focused review,” *Journal of Clinical Medicine*, vol. 7, no. 12, p. 466, 2018, doi: 10.3390/jcm7120466.

- [10] B. Hallacoglu *et al.*, “Absolute measurement of cerebral optical coefficients, hemoglobin concentration and oxygen saturation in old and young adults with near-infrared spectroscopy,” *Journal of Biomedical Optics*, vol. 17, no. 8, 2012, doi: 10.1117/1.jbo.17.8.081406.
- [11] G. Blaney *et al.*, “Broadband absorption spectroscopy in tissue: combining dual-slope continuous-wave and self-calibrating frequency-domain measurements,” *Optical Tomography and Spectroscopy of Tissue XIV*, vol. 11639, 2021, doi: 10.1117/12.2582792.
- [12] S. Fantini and A. Sassaroli, “Frequency-Domain Techniques for Cerebral and Functional Near-Infrared Spectroscopy,” *Frontiers in Neuroscience*, vol. 14, p. 300, 2020, doi: 10.3389/fnins.2020.00300.
- [13] G. Blaney *et al.*, “Phase dual-slopes in frequency-domain near-infrared spectroscopy for enhanced sensitivity to brain tissue: First applications to human subjects,” *Journal of Biophotonics*, vol. 13, no. 1, pp. 1–13, 2020, doi: 10.1002/jbio.201960018.
- [14] A. Sassaroli *et al.*, “Dual-slope method for enhanced depth sensitivity in diffuse optical spectroscopy,” *Journal of the Optical Society of America A*, vol. 36, no. 10, pp. 1743–1761, 2019, doi: 10.1364/josaa.36.001743.
- [15] G. Blaney *et al.*, “Broadband absorption spectroscopy of heterogeneous biological tissue,” *Applied Optics*, vol. 60, no. 25, pp. 7552–7562, 2021, doi: 10.1364/ao.431013.
- [16] J. Choi *et al.*, “Noninvasive determination of the optical properties of adult brain: near-infrared spectroscopy approach,” *Journal of Biomedical Optics*, vol. 9, no. 1, p. 221, 2004, doi: 10.1117/1.1628242.
- [17] L. Gagnon *et al.*, “Double-layer estimation of intra- and extracerebral hemoglobin concentration with a time-resolved system,” *Journal of Biomedical Optics*, vol. 13, no. 5, 2008, doi: 10.1117/1.2982524.
- [18] B. Hallacoglu *et al.*, “Optical characterization of two-layered turbid media for non-invasive, absolute oximetry in cerebral and extracerebral tissue,” *PLOS ONE*, vol. 8, no. 5, 2013, doi: 10.1371/journal.pone.0064095.
- [19] S. L. Jacques, “Optical properties of biological tissues: A review,” *Physics in Medicine and Biology*, vol. 58, no. 14, 2013, doi: 10.1088/0031-9155/58/14/5007.
- [20] T. Hamaoka and K. K. McCully, “Review of early development of near-infrared spectroscopy and recent advancement of studies on muscle oxygenation and oxidative metabolism,” *Journal of Physiological Sciences*, vol. 69, no. 3, pp. 799–811, 2019, doi: 10.1007/s12576-019-00697-2.

- [21] B. Grassi and V. Quaresima, “Near-infrared spectroscopy and skeletal muscle oxidative function *in vivo* in health and disease: a review from an exercise physiology perspective,” *Journal of Biomedical Optics*, vol. 21, no. 9, 2016, doi: 10.1117/1.jbo.21.9.091313.
- [22] M. Ferrari, M. Muthalib, and V. Quaresima, “The use of near-infrared spectroscopy in understanding skeletal muscle physiology: Recent developments,” *Philosophical Transactions of the Royal Society A: Mathematical, Physical and Engineering Sciences*, vol. 369, no. 1955, pp. 4577–4590, 2011, doi: 10.1098/rsta.2011.0230.
- [23] T. J. Barstow, “Understanding near infrared spectroscopy and its application to skeletal muscle research,” *Journal of Applied Physiology*, vol. 126, no. 5, pp. 1360–1376, 2019, doi: 10.1152/jappphysiol.00166.2018.
- [24] S. Jones *et al.*, “Recent developments in near-infrared spectroscopy (NIRS) for the assessment of local skeletal muscle microvascular function and capacity to utilise oxygen,” *Artery Research*, vol. 16, pp. 25–33, 2016, doi: 10.1016/j.artres.2016.09.001.
- [25] C. Casavola *et al.*, “Blood flow and oxygen consumption with near-infrared spectroscopy and venous occlusion: spatial maps and the effect of time and pressure of inflation,” *Journal of Biomedical Optics*, vol. 5, no. 3, pp. 269–276, 2000, doi: 10.1117/1.429995.
- [26] M. C. P. Van Beekvelt *et al.*, “Performance of near-infrared spectroscopy in measuring local O₂ consumption and blood flow in skeletal muscle,” *Journal of Applied Physiology*, vol. 90, no. 2, pp. 511–519, 2001, doi: 10.1152/jappl.2001.90.2.511.
- [27] V. Gerovasili *et al.*, “Utilizing the vascular occlusion technique with NIRS technology,” *International Journal of Industrial Ergonomics*, vol. 40, no. 2, pp. 218–222, 2010, doi: 10.1016/j.ergon.2009.02.004.
- [28] A. A. Sanni and K. K. Mccully, “Interpretation of Near/Infrared Spectroscopy (NIRS) signals in skeletal muscle,” *Journal of Functional Morphology and Kinesiology*, vol. 4, no. 2, p. 28, 2019, doi: 10.3390/jfmk4020028.
- [29] R. Bezemer *et al.*, “Assessment of tissue oxygen saturation during a vascular occlusion test using near-infrared spectroscopy: the role of probe spacing and measurement site studied in healthy volunteers.,” *Critical care*, vol. 13, Suppl 5, 2009, doi: 10.1186/cc8002.
- [30] M. C. P. Van Beekvelt *et al.*, “Adipose tissue thickness affects *in vivo* quantitative near-IR spectroscopy in human skeletal muscle,” *Clinical Science*, vol. 101, no. 1, pp. 21–28, 2001, doi: 10.1042/cs20000247.

- [31] K. S. Hong and M. A. Yaqub, “Application of functional near-infrared spectroscopy in the healthcare industry: A review,” *Journal of Innovative Optical Health Sciences*, vol. 12, no. 6, 2019, doi: 10.1142/S179354581930012X.
- [32] P. Pinti *et al.*, “The present and future use of functional near-infrared spectroscopy (fNIRS) for cognitive neuroscience,” *Annals of the New York Academy of Sciences*, vol. 1464, no. 1, pp. 5–29, 2020, doi: 10.1111/nyas.13948.
- [33] L. Ferreri *et al.*, “The promise of near-infrared spectroscopy (NIRS) for psychological research: A brief review,” *Année Psychologique*, vol. 114, no. 3, pp. 537–569, 2014, doi: 10.4074/S0003503314003054.
- [34] H. Zohdi *et al.*, “Color-dependent changes in humans during a verbal fluency task under colored light exposure assessed by SPA-fNIRS,” *Scientific Reports*, vol. 11, no. 1, 2021, doi: 10.1038/s41598-021-88059-0.
- [35] V. Toronov *et al.*, “Study of local cerebral hemodynamics by frequency-domain near-infrared spectroscopy and correlation with simultaneously acquired functional magnetic resonance imaging,” *Optics Express*, vol. 9, no. 8, pp. 417-427, 2001, doi: 10.1364/oe.9.000417.
- [36] M. Causse *et al.*, “Mental workload and neural efficiency quantified in the prefrontal cortex using fNIRS,” *Scientific Reports*, vol. 7, no. 1, 2017, doi: 10.1038/s41598-017-05378-x.
- [37] N. E. Adleman *et al.*, “A developmental fMRI study of the Stroop color-word task,” *NeuroImage*, vol. 16, no. 1, pp. 61–75, 2002, doi: 10.1006/nimg.2001.1046.
- [38] A. Yennu *et al.*, “Prefrontal responses to Stroop tasks in subjects with post-traumatic stress disorder assessed by functional near infrared spectroscopy,” *Scientific Reports*, vol. 6, no. 1, 2016, doi: 10.1038/srep30157.
- [39] M. L. Schroeter *et al.*, “Near-infrared spectroscopy can detect brain activity during a color-word matching stroop task in an event-related design,” *Human Brain Mapping*, vol. 17, no. 1, pp. 61–71, 2002, doi: 10.1002/hbm.10052.
- [40] R. Goenarjo *et al.*, “Cerebral oxygenation reserve: The relationship between physical activity level and the cognitive load during a stroop task in healthy young males,” *International Journal of Environmental Research and Public Health*, vol. 17, no. 4, 2020, doi: 10.3390/ijerph17041406.
- [41] Y. Yuan *et al.*, “Effect of light on cognitive function during a Stroop task using functional near-infrared spectroscopy,” *Phenomics*, vol. 1, pp. 54–61, 2021, doi: 10.1007/s43657-021-00010-5.

- [42] H. Yanagisawa *et al.*, “Acute moderate exercise elicits increased dorsolateral prefrontal activation and improves cognitive performance with Stroop test,” *NeuroImage*, vol. 50, no. 4, pp. 1702–1710, 2010, doi: 10.1016/j.neuroimage.2009.12.023.
- [43] S. Bélanger *et al.*, “Inhibition impairments in Alzheimer’s disease, mild cognitive impairment and healthy aging: Effect of congruency proportion in a Stroop task,” *Neuropsychologia*, vol. 48, no. 2, pp. 581–590, 2010, doi: 10.1016/j.neuropsychologia.2009.10.021.
- [44] T. J. Huppert *et al.*, “Functional imaging of cognition in an old-old population: A case for portable functional near-infrared spectroscopy,” *PLOS ONE*, vol. 12, no. 10, 2017, doi: 10.1371/journal.pone.0184918.
- [45] P. Plenger *et al.*, “fNIRS-based investigation of the Stroop task after TBI,” *Brain Imaging and Behavior*, vol. 10, no. 2, pp. 357–366, 2016, doi: 10.1007/s11682-015-9401-9.
- [46] B. Grässler *et al.*, “Multimodal measurement approach to identify individuals with mild cognitive impairment: Study protocol for a cross-sectional trial,” *BMJ Open*, vol. 11, no. 5, 2021, doi: 10.1136/bmjopen-2020-046879.
- [47] N. Naseer and K. S. Hong, “fNIRS-based brain-computer interfaces: A review,” *Frontiers in Human Neuroscience*, vol. 9, no. 3, 2015, doi: 10.3389/fnhum.2015.00003.
- [48] P. Raggam *et al.*, “NICA: a novel toolbox for near-infrared spectroscopy calculations and analyses,” *Frontiers in Neuroinformatics*, vol. 14, no. 26, 2020, doi: 10.3389/fninf.2020.00026.
- [49] G. Pfurtscheller *et al.*, “Focal frontal (de)oxyhemoglobin responses during simple arithmetic,” *International Journal of Psychophysiology*, vol. 76, no. 3, pp. 186–192, 2010, doi: 10.1016/j.ijpsycho.2010.03.013.
- [50] J. Gervain *et al.*, “Near-infrared spectroscopy: A report from the McDonnell infant methodology consortium,” *Developmental Cognitive Neuroscience*, vol. 1, no. 1, pp. 22–46, 2011, doi: 10.1016/j.dcn.2010.07.004
- [51] G. Blaney *et al.*, “Dual-slope imaging in highly scattering media with frequency-domain near-infrared spectroscopy,” *Optics Letters*, vol. 45, no. 16, pp. 4464–4467, 2021, doi: 10.1364/OL.394829.

